

STORAGE OF HEPARAN SULPHATE IN NEUROLOGICAL
MUCOPOLYSACCHARIDOSIS IS ASSOCIATED WITH SECONDARY DEFICIENCY OF
NEURAMINIDASE 1

Tianmeng Xu
Integrated Program in Neuroscience
McGill University, Montreal
March 2023

A thesis submitted to McGill University in partial fulfillment of the requirements of the degree
Master of Science

TABLE OF CONTENTS

LIST OF FIGURES.....	IV
LIST OF TABLES	VI
LIST OF ABBREVIATIONS.....	VII
ABSTRACT.....	X
RÉSUMÉ.....	XII
ACKNOWLEDGEMENTS	XIII
CONTRIBUTION OF AUTHORS.....	XVI
CHAPTER 1.....	1
INTRODUCTION AND LITERATURE REVIEW	1
1. LYSOSOMES	1
1.1 Lysosome formation.....	1
1.2 Lysosomal storage disorders	3
1.3 Pathological consequences of lysosomal storage	4
1.4 Classification of LSD	5
1.5 Diagnosis and therapeutic options.....	6
1.5.1 Enzyme replacement therapy (ERT).....	6
1.5.2 Hematopoietic stem cell transplantation (HSCT)	7
1.5.3 Enzyme enhancement therapy (EET)	8
1.5.4 Substrate reduction therapy (SRT).....	9
2. MUCOPOLYSACCHARIDOSES	9
2.1 Mucopolysaccharidosis type III (MPS III).....	10
2.1.1 MPS IIIA.....	11
2.1.2 MPS IIIB.....	11
2.1.3 MPS IIIC.....	11
2.1.4 MPS IIID.....	13
2.1.5 MPS IIIE	13
2.1.6 Lysosomal catabolism of Heparan sulfate (HS).....	13
2.1.7 CNS pathology and neuronal dysfunction in MPS III.....	16
3. NEURAMINIDASE 1 (NEU1).....	17
3.1 Lysosomal multienzyme complex of NEU1	18
3.2 Sialidosis.....	18
4. RATIONALE AND OBJECTIVES	19
CHAPTER 2.....	22
MATERIALS AND METHODS	22
1. Animals	22
2. Enzyme activity.....	23
A) NEU1 Activity measurements.....	23
B) β -galactosidase activity.....	24
C) β -hexosaminidase activity measurement	24
3. Perfusion and tissue fixation	24
4. Immunohistochemistry	25
5. Immunocytochemistry.....	26
6. Preparation of bone marrow-derived macrophages (BMDM)	26
7. Extraction of HS from patients' urine	27
8. Treatment of cultured BMDM with HS.....	28
9. Stereotaxic injections of the lentiviral vector.....	28
10. Behavioral tests	30
A) Y-maze.....	30

B)	Novel object recognition test (NOR)	31
C)	Open field (OF)	32
11.	Cultures of iPSC-derived neurons	33
A)	Generation and establishment of iPSC lines	33
B)	Induction of cortical neuronal progenitor cells (NPC) and cortical neurons	33
C)	Cortical neuronal differentiation.....	34
12.	Intracranial injection of AAV.....	34
13.	Acquisition of images and Statistical analysis.....	35
CHAPTER 3	36
RESULTS	36
Aim 1. HS storage is associated with NEU1 deficiency		36
A)	NEU1 is deficient in tissues of MPS IIIC mouse models.....	36
B)	NEU1 is deficient in the brain of MPS IIIC mice.....	38
C)	HS storage is related to NEU1 deficiency in MPS IIIC	41
Aim 2. NEU1 deficiency can be rescued by reducing HS storage		44
Aim 3. Treatment of cultured cells with exogenous HS induces NEU1 deficiency.....		46
Aim 4. Stereotaxic injection of LV-CTSA-NEU1-GFP in the brain of MPS IIIC mice ameliorates behaviour abnormalities and CNS pathology.....		47
A) <i>Hgsnat</i> ^{P304L} mice show partial rescue of behavior abnormalities after stereotaxic injection with LV-CTSA-NEU1-GFP		50
B) Distribution of the NEU1-GFP expression in the mouse brain six months post-injection.....		55
C) Stereotaxic injection of LV-CTSA-NEU1-GFP partially rescues reduction of synaptic protein markers in the hippocampus of <i>Hgsnat</i> ^{P304L} mice.		58
Aim 5. No amelioration of synaptic defects in human iPSC-derived cultured cortical MPS IIIA neurons transduced with LV-CTSA-NEU1-GFP.		62
CHAPTER 4	66
DISCUSSION	66
CHAPTER 5	74
CONCLUSION.....		74
CHAPTER 6	76
BIBLIOGRAPHY		76

LIST OF FIGURES

FIGURE 1. DISTRIBUTION OF 20 REPORTED MISSENSE VARIANTS IN HGSNAT PROTEIN	12
FIGURE 2. DEGRADATION PATHWAY OF HS	15
FIGURE 3. NOVEL OBJECT RECOGNITION TEST	32
FIGURE 4. INCREASED LYSOSOMAL BIOGENESIS IN TISSUES OF MPS IIIC MOUSE MODELS	37
FIGURE 5. NEU1 ACTIVITY IS REDUCED IN TISSUES OF MPS IIIC MICE.....	38
FIGURE 6. X-GAL STAINING OF <i>Neu1</i> ^{-/-} BRAIN SECTIONS.	39
FIGURE 7. NEU1 ACTIVITY IN DISTINCT BRAIN REGIONS.....	40
FIGURE 8. HS IS ACCUMULATED IN THE BRAIN OF MPS IIIC MICE.....	42
FIGURE 9. NEU1 IS DEFICIENT IN THE BRAIN OF MPS IIIC mice.....	43
FIGURE 10. HS STORAGE IS REDUCED AND NEU1 LEVELS INCREASED IN MPS IIIC MICE RECEIVING GENE THERAPY WITH AAV-HGSNAT VECTOR	45
FIGURE 11. TREATMENT OF BMDM WITH EXOGENOUS HS.....	47
FIGURE 12. OPTIMIZATION OF INJECTION COORDINATES AND VIRAL VOLUMES.....	48
FIGURE 13. GFP EXPRESSION IN THE MOUSE BRAIN ONE MONTH AFTER STEREOTAXIC INJECTIONS OF LV-GFP.....	49
FIGURE 14. GFP EXPRESSION IN THE MOUSE BRAIN ONE MONTH AFTER STEREOTAXIC INJECTIONS OF LV-CTSA-NEU1-GFP	49
FIGURE 15. NEU1 ACTIVITY IN THE BRAIN OF MICE ONE MONTH AFTER STEREOTAXIC INJECTION OF LV-CTSA-NEU1-GFP.....	50
FIGURE 16. Y-MAZE TEST DOES NOT REVEAL A SIGNIFICANT DIFFERENCE IN THE BEHAVIOUR OF WT AND MPS IIIC MICE AT THE AGE OF 6 MONTHS.....	51
FIGURE 17. IMPROVEMENT OF THE SHORT-TERM MEMORY IN <i>Hgsnat</i> ^{P304L} MICE INJECTED WITH LV-CTSA-NEU1-GFP.....	52

FIGURE 18. TRAJECTORY TRACES	53
FIGURE 19. <i>Hgsnat</i> ^{P304L} MICE INJECTED WITH LV-CTSA-NEU1-GFP SHOW A TREND FOR NORMALIZATION OF REDUCED ANXIETY AS REVEALED BY OF TEST.	54
FIGURE 20. GFP EXPRESSION IN THE MOUSE BRAIN SIX MONTHS AFTER STEREOTAXIC INJECTIONS OF LV-GFP.	56
FIGURE 21. NEU1-GFP EXPRESSION IN THE MOUSE BRAIN SIX MONTHS AFTER STEREOTAXIC INJECTIONS OF LV-CTSA-NEU1-GFP.	57
FIGURE 22. LEVELS OF PROTEIN MARKERS OF GLUTAMATERGIC SYNAPSE ARE INCREASED IN THE BRAINS OF <i>Hgsnat</i> ^{P304L} MICE INJECTED WITH LV-CTSA-NEU1-GFP	59
FIGURE 23. LEVELS OF SYNAPSTIC VESICLE PROTEIN MARKER SYN1 SHOW A TREND FOR INCREASE IN THE BRAINS OF <i>Hgsnat</i> ^{P304L} MICE INJECTED WITH LV-CTSA-NEU1-GFP	60
FIGURE 24. <i>Hgsnat</i> ^{P304L} MICE TREATED WITH LV-CTSA-NEU1-GFP SHOW AMYLOID PROTEIN ACCUMULATION IN LEVEL 4 AND 5 PYRAMIDAL CORTICAL NEURONS SIMILAR TO THAT IN <i>Hgsnat</i> ^{P304L} AND SHAM-TREATED <i>Hgsnat</i> ^{P304L} MICE	61
FIGURE 25. <i>Hgsnat</i> ^{P304L} MICE TREATED WITH LV-CTSA-NEU1-GFP SHOW GM2 GANGLIOSIDE ACCUMULATION IN PYRAMIDAL HIPPOCAMPAL NEURONS SIMILAR TO THAT IN <i>Hgsnat</i> ^{P304L} AND SHAM_TREATED <i>Hgsnat</i> ^{P304L} MICE	62
FIGURE 26. NEU1 ACTIVITY IS SIGNIFICANTLY REDUCED IN HUMAN MPS IIIA NPC.....	63
FIGURE 27. LV-CTSA-NEU1-GFP-TRANSDUCED HUMAN CULTURED MPS IIIA NEURONS DO NOT SHOW AMELIORATION OF SYNAPTIC DEFECTS.	65

LIST OF TABLES

TABLE 1. CLASSIFICATION OF MPS	10
TABLE 2. ANTIGENS AND DILUTIONS USED FOR IMMUNOHISTOCHEMISTRY	25
TABLE 3. ANTIGENS AND DILUTIONS USED FOR IMMUNOCYTOCHEMISTRY	26

LIST OF ABBREVIATIONS

AAV	Adeno-associated virus
Ab	Antibody
A/P	Anterior/posterior
APP	Amyloid precursor protein
BBB	Blood-brain barrier
BDNF	Brain-derived neurotrophic factor
BMDM	Bone marrow-derived macrophages
BSA	Bovine serum albumin
CLEAR	Coordinated lysosomal expression and regulation
CNS	Central nervous system
CPC	Cetylpyridinium chloride
CTSA	Cathepsin A
DI	Discrimination index
DMEM	Dulbecco's Modified Eagle Medium
D/V	Dorsal/Ventral
ECM	Extracellular matrix
EET	Enzyme enhancement therapy
ER	Endoplasmic reticulum
ERT	Enzyme replacement therapy
FBS	Fetal bovine serum
FGF-2	Fibroblast growth factor 2
GAGs	Glycosaminoglycans

GALNS	N-acetylgalactosamine 6-sulfatase
GBL1	β -galactosidase
GCL	Granule cell layer
GDNF	Glial cell-derived neurotrophic factor
GFP	Green fluorescent protein
HGSNAT	Heparan sulfate acetyl-CoA: α -glucosaminide N-acetyltransferase
HS	Heparan sulphate
HSCT	Hematopoietic stem cell transplantation
HSPGs	Heparan sulfate proteoglycans
IDUA	α -iduronidase
iPSCs	Induced pluripotent stem cells
LTP	Long-term potentiation
LV	Lentivirus
LMC	Lysosomal multienzyme complex
LSD	Lysosomal storage disorders
M6P	Mannose-6-phosphate
mEPSC	Miniature excitatory postsynaptic current
M/L	Medial/lateral
MOI	Multiplicity of infection
MPS	Mucopolysaccharidosis
MTORC1	Master growth regulator mTOR complex
NB	Neurobasal
NEAA	Non-essential amino acids

NEU	Neuraminidase
NOR	Novel-object recognition
NPC	Neuronal progenitor cell
OF	Open field
PBS	Phosphate-buffered saline
PC	Pharmacological chaperones
PFA	Paraformaldehyde
PSA	Polysialic acid
PSD-95	Postsynaptic density protein 95
RBC	Red blood cell
ROS	Reactive oxygen species
sgRNA	Single guide nucleotide RNA
SGSH	N-Sulfoglucosamine Sulfohydrolase
SRT	Substrate reduction therapy
SSC	Somatosensory cortex
Syn1	Synapsin 1
TFEB	Transcription factor EB
TGN	<i>Trans</i> Golgi network
TLR4	Toll like receptor 4
VGLUT1	Vesicular glutamate transporter 1
X-GAL	5-bromo-4-chloro-3-indolyl- β -D-galactopyranoside

ABSTRACT

Mucopolysaccharidoses (MPS) are a group of rare genetic diseases caused by deficiencies of lysosomal enzymes required to degrade glycosaminoglycans (GAG). Seven MPS subtypes, MPS I, II, IIIA, IIIB, IIIC, IIID, and VII, are associated with heparan sulfate (HS) accumulation and severe neurological decline. Although different pathogenic mechanisms have been investigated, it remains unclear if HS is directly responsible for the changes observed in the brain of neurological MPS patients and mouse models. Since there is currently no curative treatment for most of these disorders, it is vital to understand the mechanism underlying the neuropsychiatric symptoms and neurodegeneration in MPS patients to provide new routes for therapeutic interventions.

We report two MPS IIIC mouse models generated in our lab, a constitutive HGSNAT KO (knockout) mouse, *Hgsnat-Geo*, and an *Hgsnat*^{P304L} mouse, expressing misfolded HGSNAT Pro304Leu variant, present a secondary deficiency of neuraminidase 1 (NEU1). Importantly, low levels of NEU1 activity were also observed in patients and mouse models of neurological MPS that store HS but not in other neurological lysosomal diseases that do not store this specific GAG [52, unpublished]. This suggests that secondary NEU1 deficiency is associated with the accumulation of HS. Since NEU1 plays a significant role in maintaining normal levels of sialylation of brain glycoproteins essential for synaptogenesis, we hypothesize that the secondary deficiency of NEU1 leads to defects in synaptic transmission. To address the first hypothesis, we investigated the relationship between HS accumulation and NEU1 protein levels in the brains of MPS IIIC mice by immunohistochemical analysis. Our experiments demonstrated that increased HS storage is linked to a more severe NEU1 deficiency. Importantly, NEU1 levels were rescued in the brains of MPS IIIC mice that received a bilateral injection of an adeno-associated virus

(AAV) expressing HGSNAT, which also reduced the accumulation of HS. To investigate the causative relationship between HS accumulation and NEU1 activity, we cultured bone marrow-derived mouse macrophages in different concentrations of exogenous HS. These experiments revealed that treating cells with increasing doses of HS resulted in a proportional decrease in NEU1 activity levels. Finally, to study the relationship between secondary NEU1 deficiency and defects in synaptic transmission and neurodegeneration, we rescued NEU1 activity in the hippocampi and somatosensory cortices of *Hgsnat*^{P304L} mice by performing a bilateral stereotaxic injection of a lentivirus (LV) expressing Cathepsin A (CTSA) and GFP-tagged-NEU1 (LV-CTSA-NEU1-GFP). We found that treated mice showed improved short-term memory and a trend for normalization of anxiety. Furthermore, mice injected with the LV-CTSA-NEU1-GFP also had an increase in neuronal synaptic markers, including postsynaptic density protein 95 (PSD-95) and vesicular glutamate transporter (VGLUT1), when compared to control mice.

Altogether, our results provide strong evidence that storage of HS in the neurons of neurological MPS patients and mouse models leads to the secondary deficiency of NEU1, which in turn causes widespread over-sialylation in brain glycans, potentially leading to common pathological processes such as synaptic defects and neurodegeneration. Thus, our research identifies a novel pathophysiological mechanism in the diseases of the MPS spectrum linking the synaptic defects with a secondary deficit of NEU1 in the neurons.

RÉSUMÉ

Les mucopolysaccharidoses (MPS) sont un groupe de maladies génétiques rares causées par des mutations chez les enzymes lysosomales nécessaires à la dégradation des glycosaminoglycannes. Sept sous-types de MPS, MPS I, II, IIIA, IIIB, IIIC, IIID et VII, sont associés à une accumulation d'héparane sulfate (HS) et à un déclin neurologique sévère. Bien que différents mécanismes pathologiques aient été étudiés, il n'est toujours pas clair si l'HS est directement responsable des changements observés dans le système nerveux des patients atteints de MPS et des modèles murins. Puisqu'il n'existe actuellement aucun traitement pour la plupart des MPS, il est important de mieux comprendre le mécanisme causant les symptômes neuropsychiatriques et la neurodégénérescence chez les patients atteints de MPS afin de trouver un moyen de traiter ces maladies.

Deux modèles de souris MPS IIIC ont été générés dans notre laboratoire, *Hgsnat-Geo* (KO), et *Hgsnat*^{P304L}. Ces deux modèles présentent tous un déficit secondaire en neuraminidase 1 (NEU1). Ce phénomène est aussi observé chez les patients et les modèles murins d'autres types de MPS neurologiques où l'HS est accumulé, mais pas dans les maladies lysosomales neurologiques qui ne stockent pas ce GAG spécifique [52, non publié]. Cela suggère donc que le déficit en NEU1 est associé à une accumulation d'HS. Étant donné que NEU1 joue un rôle majeur dans le maintien d'un niveau normal de sialylation des glycoprotéines cérébrales essentiel pour la synaptogénèse, notre hypothèse est que le stockage d'HS contribue au déficit secondaire de NEU1 entraînant ainsi des défauts dans la transmission synaptique. Notre premier objectif est d'étudier la relation entre l'accumulation d'HS et le niveau de NEU1 dans le cerveau de nos souris MPS IIIC par analyse immunohistochimique. Nos résultats montrent qu'un stockage accru d'HS est lié à une déficience plus sévère en NEU1. Cependant, le niveau de NEU1 peut être augmenté après avoir réduit

l'accumulation d'HS chez les souris ayant reçu une injection bilatérale d'un vecteur du type AAV exprimant HGSNAT. Pour étudier l'effet causatif de l'HS sur l'activité de NEU1, nous avons aussi cultivé des macrophages de souris dérivés de la moelle osseuse en présence de différentes concentrations d'HS et nous avons pu montrer qu'une hausse de concentration d'HS entraînait une diminution proportionnelle des niveaux d'activité de NEU1. Finalement, nous avons également étudié la relation entre le déficit en NEU1 et les défauts de transmission synaptique et la neurodégénérescence. Pour cela, nous avons effectué une injection stéréotaxique bilatérale d'un lentivirus (LV) exprimant la cathepsine A (CTSA), NEU1 et GFP (LV-CTSA-NEU1-GFP) dans l'hippocampe et le cortex de nos souris *Hgsnat*^{P304L}. Nous avons constaté que les souris traitées présentaient une amélioration de la mémoire à court terme et une normalisation de l'anxiété. De plus, les souris injectées avec le LV-CTSA-NEU1-GFP ont également une augmentation des marqueurs synaptiques, y compris la protéine de densité postsynaptique 95 (PSD-95) et le transporteur vésiculaire du glutamate (VGLUT1).

En résumé, nos résultats fournissent une preuve solide que l'accumulation d'HS dans les neurones des patients atteints de MPS neurologiques et des modèles murins cause une déficience secondaire de NEU1. La réduction de cette neuraminidase provoque alors une sur-sialylation des glycanes dans les cerveaux de nos souris MPS IIIC conduisant potentiellement à des processus pathologiques courants tels que des défauts synaptiques et la neurodégénérescence. Notre recherche identifie un nouveau mécanisme physiopathologique dans les maladies du spectre MPS reliant ainsi les défauts synaptiques à un déficit secondaire de NEU1 dans les neurones.

ACKNOWLEDGEMENTS

Foremost, I would like to express my deep and sincere gratitude to my research supervisor, Dr. Alexey V. Pshezhetsky, for accepting me as an undergraduate student in his lab in 2018, for giving me the opportunity to do research and for constantly providing invaluable guidance throughout my projects and in the writing of this thesis. I am very lucky as I was given the opportunity to work in your lab and grow as a research scientist. Thank you for your patience, motivation, and your invaluable advice. Working and studying under your guidance was a great privilege and honor.

I also want to thank Dr. Xuefang Pan for teaching me the techniques and answering all my questions when I started in the lab. She was always there with her support and encouragement whenever I needed it. I learned so many things from you, and this project would not be possible without your help. Thank you for your time, assistance, and advice.

I want to thank my supervisor, my advisory committee members, and my mentor for their insightful feedback and comments, Dr. Thomas Durcan, Dr. Nathalie Lamarche-Vane, Dr. Christian Beauséjour, and Dr. David Ragsdale. A particular word of gratitude is due to Dr. Bénédicte Amilhon and Dr. Guillaume Ducharme for showing me how to perform stereotaxic brain surgeries and giving me advice on how to increase mice's survival rate.

My sincere thanks also go to the Canadian *MPS Society* for giving me two scholarships, allowing me to work on the gene therapy project. These summer internships allowed me to learn more about MPS and work on diverse, exciting projects. My research is only possible with the

help of our collaborators, Dr. Brian Bigger, for providing us with brain samples of mice injected with AAV expressing HGSNAT, and Dr. Monty McKillop, for producing the lentiviruses used in this project.

I am also grateful to all those with whom I had the pleasure to work during this and other related projects. I thank my former and current lab members, Rachel Héon-Roberts, Annie Nguyen, Gustavo Monteiro Viana, Afitz Da Silva, Antoine Caillon, Mahsa Taherzadeh, and Kalley Kho for your help and for all the fun we had in the last four years. A special thanks to Camila De Britto Pará De Aragão for showing me how to collect and purify stem cells from bone marrow and helping me during my summer projects. I would also like to thank Travis Moore for teaching me how to culture iPSCs and differentiate them into neurons.

I thank all the CHU Sainte-Justine animal facility personnel, especially Eugénie Lacas and Sonja Lesperance, for setting up breeding cages for my stereotaxic injections and for taking care of the mice after the surgeries.

Lastly, I am incredibly grateful to my parents for their endless love, support, and sacrifices in educating and preparing me for my future. I am also very thankful to my sister and my friends for their understanding and continuous support in completing this research work.

CONTRIBUTION OF AUTHORS

Tianmeng Xu: Performed stereotaxic brain injections, performed behavioral tests, collected and prepared brain tissues, performed immunofluorescence analyses of brain samples, cultured bone marrow-derived macrophages, isolated heparan sulfate from patients' urine, measured enzyme activities in cells and mouse tissues, cultured iPSC-derived neurons with the help of Travis Moore, performed all statistical tests and confocal imaging.

Dr. Monty McKillop: Produced the lentiviruses

Dr. Brian Bigger: Provided us with the fixed brain tissues of mouse injected with AAV expressing HGSNAT and appropriate controls

Dr. Alexey Pshezhetsky and Dr. Thomas Durcan: Guided the project, provided advice, proofread, critically evaluated, and revised this thesis

Travis Moore: Helped to culture iPSC-derived neurons

Rachel Héon-Roberts and Annie Nguyen: measured NEU1, β -galactosidase, and β -hexosaminidase enzyme activities in some tissues, stained brain tissues with 5-bromo-4-chloro-3-indolyl- β -D-galactopyranoside (X-GAL) substrate.

CHAPTER 1

INTRODUCTION AND LITERATURE REVIEW

1. LYSOSOMES

Lysosomes are membrane-bound organelles that participate in numerous biological processes in the cell, including catabolism, autophagy, antigen presentation, intracellular pathogen destruction, plasma membrane repair, exosome release, apoptosis, and cell adhesion and migration. Lysosomes were first discovered by Christian de Duve in 1955 and were termed “suicide bags” because of their ability to break down multiple types of biomolecules. These acidic compartments contain more than 60 hydrolytic enzymes, including proteases, glycosidases, lipases, nucleases, phospholipases, phosphatases, and sulfatases [1]. Lysosomal enzymes generally require an acidic environment for optimal activity, and the lysosome maintains a pH of 5.0-5.2 in its interior due to the activity of H⁺ ATPases [1]. In their simplest form, lysosomes are described as dense spherical vacuoles. Still, they can be extraordinarily diverse in shape and size depending on the stage, position inside the cell, and the materials taken up for digestion [2].

1.1 Lysosome formation

Genes encoding for lysosomal protein are transcribed in the nucleus, controlled by the Transcription Factor EB (TFEB). TFEB induces the transcription of various lysosomal genes by binding to the promoter type known as the coordinated lysosomal expression and regulation (CLEAR) network [3]. TFEB activity and its nuclear translocation are regulated at various levels, including post-translational modification and protein-protein interactions [3]. Under normal circumstances and in resting cells, TFEB is largely cytosolic (attached to an outer surface of the lysosomal membrane), phosphorylated, and inactive [3]. Regulator, Rag GTPases, and v-ATPases form a complex that recruits the master growth regulator mTOR complex 1 (mTORC1) to the

lysosomal surface [3]. mTORC1 then becomes activated and phosphorylates TFEB, preventing the translocation of TFEB to the nucleus. When the physiological and nutritional status of the cell is perturbed, mTORC1 becomes inactive and can no longer phosphorylate TFEB [80]. The dephosphorylation of TFEB by calcineurin then promotes its nuclear translocation to activate transcriptional target genes [81]. After being synthesized in the rough endoplasmic reticulum (ER), lysosomal soluble proteins are packaged into COPII vesicles and transported to the *trans*-Golgi network (TGN), where they are further modified and tagged with the mannose-6-phosphate (M6P) marker. The M6P tag is recognized by transmembrane M6P receptor proteins, which bind to lysosomal hydrolases on the luminal side of the membrane [1]. M6P receptor proteins also bind to adaptins, which help package the hydrolases into clathrin-coated vesicles that bud from the TGN and are directed to the late endosomes [1]. Because the binding between the M6P tag and its receptor is pH dependent, the acidic internal pH of late endosomes causes the hydrolases to dissociate from the M6P receptors. Consequently, the M6P receptors are recycled, while the enzymes remain in the lysosome to perform their functions.

Lysosomal transmembrane proteins are also synthesized in the rough endoplasmic reticulum. However, while most lysosomal hydrolases are tagged with the M6P marker for vesicular transport to the endosomes, lysosomal transmembrane proteins contain consensus targeting motifs (tyrosine or dileucine-based) in their cytosolic regions [5]. After passage through the Golgi apparatus, these proteins can either be delivered via a direct route or indirectly, where they first reach the cell surface before entering the endocytic pathway [5]. Other mechanisms by which proteins are targeted to lysosomes involve *N*-glycosylation, covalent lipid attachment, or M6P alternatives such as MPRs, LIMP2, and Sortilin [5].

At least three different pathways deliver materials to be digested by lysosomes. Endocytosis is the best-studied of these pathways and involves the formation of vesicles containing internalized molecules. These vesicles then fuse with small intracellular organelles called early endosomes. While some endocytosed materials are retrieved and recycled back to the plasma membrane via recycling endosomes, others remain in the early endosomes, which gradually mature into late endosomes (multivesicular bodies), the precursors of lysosomes. The second pathway involves the phagocytosis of large particles and microorganisms by specialized phagocytic cells such as macrophages and neutrophils. These phagocytic cells take up large particles by the formation of phagosomes, which then fuse with lysosomes, forming phagolysosomes. The third mechanism delivering materials for lysosomal catabolism is autophagy, which allows the clearing of old cytoplasmic proteins and cell components such as mitochondria and the reusing of nutrients such as amino acids and fatty acids, nucleic acids, and sugars for the synthesis of macromolecules. Macroautophagy, the most prevalent type of autophagy, begins with the enclosure of the cytosolic component by a double membrane, forming an autophagosome. Once the autophagosome fuses with the lysosome, thereby forming an autolysosome, lysosomal hydrolases will then degrade its content.

1.2 Lysosomal storage disorders

Lysosomal storage disorders are a group of more than 70 morphologically similar genetically inherited metabolic conditions caused by a failure in the biogenesis, lysosomal targeting, or function of lysosomal enzymes, activators, or transporters. The prevalence of LSD is estimated to be one in every 5000 live births, with certain populations having a higher incidence of specific types of LSD [6]. LSDs are characterized by the accumulation of various undegraded substrates in cells of different tissues and organs of the body, eventually compromising their functions. Most

patients with LSDs are non-symptomatic at birth, although some are affected in utero and present a fetal swelling (hydrops fetalis). Depending on the disease and severity of mutation, clinical symptoms can develop after birth (infantile form), at the age of several years (juvenile form), or even in adulthood [7]. The severity within the same genetic subtype mainly depends on the degree to which the enzymatic activity is compromised. Complete, or near-complete, deficiency of enzymatic activity is typically associated with earlier onset and death. In contrast, a relatively high residual enzymatic activity generally causes less severe pathology. Still, drastically different severity and progression of the diseases are often recorded in patients with the same genotype or even siblings, delineating the existence of genetic, epigenetic, and environmental modifies [82].

Although the majority of LSD is caused by defects in the genes encoding lysosomal hydrolases, genetic defects of activator/transporter proteins, lysosomal membrane channels and transporters, or dysfunction of proteins involved in vesicular traffic and the biogenesis of lysosomes can also lead to the accumulation of undegraded substrates in endosomes and lysosomes and development of LSDs [7].

1.3 Pathological consequences of lysosomal storage

Accumulation of primary storage material generally contributes to the disruptions of multiple biochemical and cellular functions. For instance, it has been shown that in mucopolysaccharidoses (MPS), undegraded GAG, such as heparan-, dermatan- or chondroitin sulfate, can cause non-physiologic activation of signal transduction receptors such as the Toll-like receptor 4 (TLR4) [reviewed in 8]. This leads to a widespread release of proinflammatory cytokines and activation of the innate immune system [56]. As a consequence, storage of GAG increases the release of IL-1 β , TNF- α , and TGF- β in MPS I, MPS II, MPS III, MPS VI, and MPS

VII animal models [reviewed in 8, 83, 84]. The expression of these cytokines is thought to be a direct factor causing cartilage degeneration in MPS VI and MPS VII patients. Besides the activation of signal transduction receptors, accumulated substrates can also modify the response of these receptors. In Hurler syndrome, the accumulation of HS oligosaccharides interferes with the binding of fibroblast growth factor 2 (FGF-2) to its receptor and, impairs the downstream signaling cascade [9]. Since FGF-2 is also involved in the protection and development of neurons and neuronal precursor cells, impairment of its signaling may explain the increased neuronal apoptosis and neurodegeneration seen in Hurler patients [9]. Numerous data also indicate that lysosomal storage may interfere with autophagic processes as the accumulation of protein aggregates, lipids, and dysfunctional mitochondria, all autophagy substrates, is detected in the cells of animal models of LSD [10]. The reduction of autophagic flux also contributes to the accumulation of polyubiquitinated proteins and progressive mitochondrial dysfunction, all of which increase the levels of reactive oxygen species (ROS) and render cells more sensitive to apoptosis and inflammatory stimuli [11]. Furthermore, recent reports have also suggested increased alterations of intracellular calcium homeostasis, lipid biosynthesis, and protein trafficking, as well as peroxisomal dysfunction and ER stress in multiple LSD [reviewed in 12].

1.4 Classification of LSD

LSD are usually classified according to the biochemical type of stored materials and include sphingolipidoses, oligosaccharidosis, mucopolipidoses, mucopolysaccharidoses, lipoprotein storage disorders, lysosomal transport defects, and neuronal ceroid lipofuscinoses among others. Even though most LSD are inherited in an autosomal recessive pattern, Fabry, Danon, and Hunter syndromes are X-linked disorders [13].

1.5 Diagnosis and therapeutic options

Multiple treatments are being investigated for LSD. They include, for instance, enzyme replacement therapy (ERT), hematopoietic stem cell transplantation (HSCT), enzyme enhancement therapy (EET), and substrate reduction therapy (SRT), among others. These methods are now approved for several diseases. For instance, ERT has been used to treat some non-neurological forms of LSD, while HSCT has been approved for some neuropathic LSD where the deficient enzyme can be secreted by donor cells. However, only a fraction of LSD can be treated safely and efficiently, and symptomatic treatment remains the only option for most of them [7]. Even for those disorders for which specific therapy is available, early diagnosis and initiation of treatment are critical. In LSD with skeletal malformation, screening can be performed via skeletal radiography to look for evidence of dysostosis multiplex. Abdominal ultrasonography and echocardiography can be used to identify organomegaly, and cardiac abnormalities, respectively [13]. Urine can also be screened for high levels of oligosaccharides in oligosaccharidoses or GAGs in disorders of the MPS spectrum. Direct measurement of enzyme activity, either by tandem mass spectrometry or digital microfluidics fluorometric assays, is also used to screen for lysosomal diseases [7]. Currently, most LSD can also be rapidly identified through next-generation sequencing [15].

1.5.1 Enzyme replacement therapy (ERT)

ERT has been approved for six LSD, including Gaucher disease, Fabry disease, Pompe disease, and MPS I, II, and VI. This approach delivers the deficient enzyme intravenously at a controlled dosage and frequency. Despite multiple examples of successfully commercialized enzymes for LSD, ERT also has its limitations. Most ERTs used for treating LSD produced antidrug antibody (ADA) responses, which can result in hypersensitivity and inhibition of enzyme activity and

require immunosuppression [16]. Thus far, ERT has been largely unsuccessful in treating neurological LSD due to the problem with the enzyme crossing the blood-brain barrier (BBB). Several methods were then explored to solve this issue. For instance, intrathecal infusion of human heparan-*N*-sulfatase was performed in MPS IIIA and IIIB patients to bypass the BBB [17]. Furthermore, enzymes can also be modified to cross the BBB. This method was tried in MPS I, where the deficient enzyme α -iduronidase (IDUA) is fused with a monoclonal antibody against the human insulin receptor HIRMAb, enhancing the transport of IDUA [18]. Patients receiving the HIRMAb-IDUA fusion protein showed improved neurological and cognitive function and stabilization of urinary GAG levels [18]. A similar approach has also been developed for MPS II [85]. However, further studies are necessary to fully assess the efficacy of these approaches.

Despite its limitations, ERT may be safer than other treatments, such as cell and gene therapy. For example, previous experiments have shown that integrating foreign DNA into the host genome could cause neoplasia, hepatotoxicity, and dorsal root ganglion toxicity in some LSD patients [19].

1.5.2 Hematopoietic stem cell transplantation (HSCT)

Another way to circumvent the BBB is to use donor-derived myeloid cells as a source of enzymes that can be taken up by enzyme-deficient host cells. These donor-derived myeloid cells can migrate across the BBB and differentiate into microglia, which can secrete functional enzymes and improve neurocognitive outcomes. Hematopoietic stem progenitor cells (HSPC) can also be genetically modified to constitutively express supra-physiological levels of the missing enzyme. LV-mediated HSPC gene therapy has already been approved for metachromatic leukodystrophy patients. Additionally, several AAV-mediated gene therapies are currently in clinical trials for MPS IIIA, MPS IIIB, and GM1 gangliosidosis, among others [reviewed in 86]. In Krabbe disease

and MPS I, II, and VII, HSCT was shown to prevent the progression of CNS symptoms in some patients [20, 21]. However, the success of the transplantation depends on the ability of the deficient enzyme to be effectively secreted from the myeloid cells and the stage of the disease. For optimal results, HSCT must be performed in the early phase of the disease and only in patients capable of tolerating the conditioning and transplantation regimen.

1.5.3 Enzyme enhancement therapy (EET)

All cells have mechanisms that control the proper folding of newly synthesized enzymes. Whereas appropriately folded and stable proteins leave the ER, progress to the Golgi apparatus, and then to their final cellular destination, misfolded and mutant proteins cannot be appropriately trafficked and are usually retained in the ER and degraded. This process is regulated by the quality control system of the ER, which rely on chaperone proteins and folding factors such as the heat shock proteins, immunoglobulin-binding protein (BiP), calnexin, and calreticulin [22]. These chaperones recognize misfolded proteins due to the exposure of usually hidden hydrophobic domains or specific sequences [23]. In the case of many LSD, missense mutations result in the failure of the lysosomal proteins to fold correctly, thus preventing them from reaching the lysosome and carrying their normal function [reviewed in 24]. To solve this issue, small molecules known as pharmacological chaperones (PC) have been developed to rescue misfolded or unstable mutant enzymes. The use of PC was shown to be successful in animal models for several LSD such as Fabry, Gaucher, and Pompe diseases [reviewed in 24, 25], and the PC Galafold has been clinically approved for the treatment of Fabry patients affected with amendable mutations [87]. However, one of the major disadvantages of EET is that PC are mutation-specific, and some mutations are not responsive to the treatment [26].

1.5.4 Substrate reduction therapy (SRT)

SRT is a therapeutic approach aiming to decrease levels of accumulating substrates by inhibiting corresponding biosynthetic pathways. SRT has been used to treat patients with Gaucher disease using Miglustat (Zavesca), a commercial formulation of aminosugar N-butyldeoxynojirimycin [27]. This compound strongly inhibits ceramide glucosyltransferase and, thereby, decreases glucosylceramide synthesis, which is accumulated in Gaucher disease [27]. Another drug, called Eliglustat (Cerdelga), is an even more potent inhibitor of ceramide glucosyltransferase and was recently approved to treat non-neurologic types of Gaucher disease in the USA and Europe [28]. In MPS patients, Genistein, a natural isoflavone, was shown to reduce GAG synthesis and reduce levels of accumulating/secreted GAGs. However, placebo-controlled clinical trials in MPS III patients showed no significant clinical benefits [29]. Some complications could also result from lowering the production of substrates, and alteration of other biological processes is the possible consequence of SRT. For example, Miglustat also inhibits intestinal lactase resulting in diarrhea and weight loss in the treated patients [88].

2. MUCOPOLYSACCHARIDOSES

Mucopolysaccharidoses (MPS) are a group of lysosomal diseases caused by deficiencies of lysosomal enzymes required to degrade GAG. The various forms and subtypes of MPS have been studied (Table 1), and the enzyme deficiencies underlying each disease have been identified and extensively analyzed. All seven MPS described to date are heterogeneous and progressive disorders characterized by various somatic and neurological manifestations depending on the type of GAG accumulated [reviewed in 30].

MPS	Name	Deficient Enzyme	GAG Accumulated	Pattern of inheritance
I	Hurler/Scheie/Hurler-Scheie	α -L-iduronidase	HS + DS	AR
II	Hunter	Iduronate-2-sulfatase	HS + DS	XR
III A	Sanfilippo A	Heparan-N-sulfatase	HS	AR
III B	Sanfilippo B	α -N-acetylglucosaminidase	HS	AR
III C	Sanfilippo C	Acetyl CoA α -Glucosaminide N-actyltransferase	HS	AR
III D	Sanfilippo D	N-acetylglucosamine 6-sulfatase	HS	AR
III E	Sanfilippo E	Arylsulfatase G	HS	NA
IV A	Morquio A	N-acetylgalactosamine-6-sulfatase	KS + CS	AR
IV B	Morquio B	β -galactosidase	KS + CS	AR
VI	Maroteaux-Lamy	N-acetylgalactamine 4-sulfatase	DS + CS	AR
VII	Sly	β -glucuronidase	HS + DS + CS	AR
IX	Natowicz	Hyaluronidase-1	Hyaluronic acid	AR

Table 1. Classification of MPS

DS, dermatan sulphate; HS, heparan sulphate; KS, keratan sulphate; CS, chondroitin sulphate; AR, autosomal recessive; XR, X-linked recessive, NA, non-applicable.

2.1 Mucopolysaccharidosis type III (MPS III)

In mucopolysaccharidosis type III (MPS III), or Sanfilippo syndrome, patients mainly present with neurobehavioral deficits and early-onset cognitive declines, while somatic signs of the disease are absent or mild. There are four subtypes of MPS III (A to D), all caused by the genetic deficiencies of lysosomal enzymes involved in the breakdown of heparan sulfate. MPS III patients generally do not display clinical features at birth [reviewed in 33]. However, deficiency of HGSNAT eventually leads to progressive lysosomal accumulation of HS, giving rise to severe

neurological symptoms such as developmental delay, speech and hearing loss, impaired cognition, childhood dementia, hyperactivity, aggressiveness, and autistic features [34].

2.1.1 MPS IIIA

MPS IIIA is caused by mutations in the *SGSH* gene leading to the deficiency of the enzyme Heparan-N-sulfatase. Although there are no significant clinical differences between the four types of MPS III, type A has been suggested to have an earlier onset of disease, rapid progression of symptoms, and shorter lifespan [31]. It is also the most frequent of all Sanfilippo subtypes and accounts for about 2/3 of all cases [reviewed in 89].

2.1.2 MPS IIIB

MPS IIIB is caused by mutations in the *NAGLU* gene encoding the α -N-acetylglucosaminidase (NAGLU) enzyme. MPS IIIB is the second most common subtype of MPS III and is slightly less aggressive than MPS IIIA [90].

2.1.3 MPS IIIC

MPS IIIC subtype is caused by mutations in the gene encoding heparan sulfate acetyl-CoA: alpha-glycosamide N-acetyltransferase (HGSNAT) enzyme, which is involved in HS catabolism. HGSNAT acetylates the non-reducing terminal alpha-glucosamine residues of HS. This modification is critical for their cleavage by N-acetyl-alpha-glycosaminidase in the lysosomal degradation process of HS. More than 70 disease-causing HGSNAT mutations were identified in MPS IIIC patients. The mutations span the entire *Hgsnat* gene and include splice-site mutations, nonsense mutations, insertions, deletions, and 35 missense mutations (Fig.1) [32].

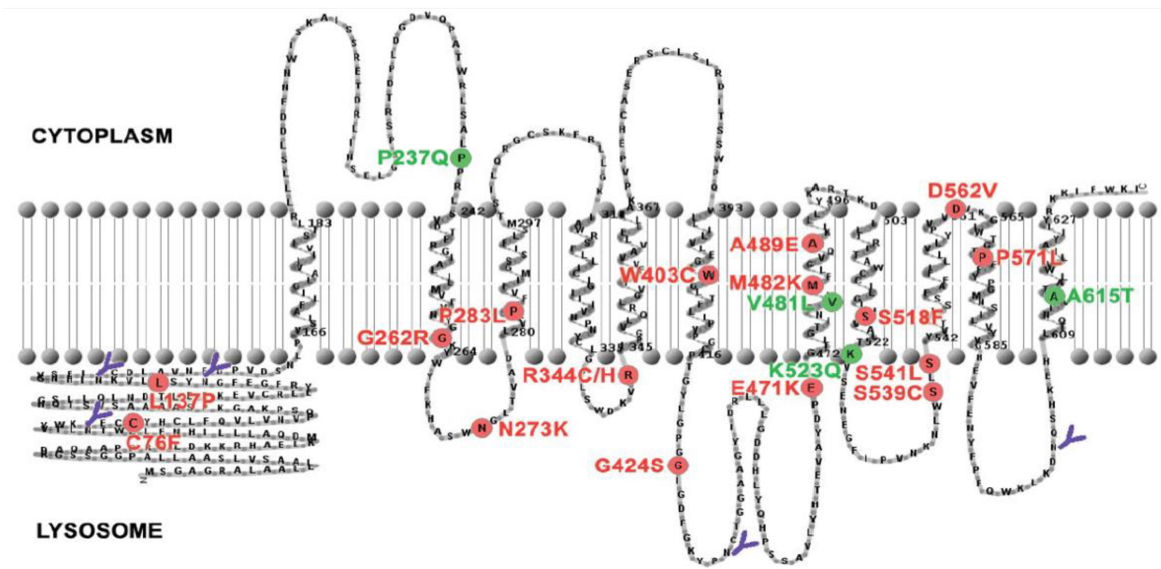


Figure 1. Distribution of 20 reported missense variants in HGSNAT protein.

Visual representation of HGSNAT membrane topology using the TMRPres2D software. There are 11 predicted transmembrane domains and five potential N-glycosylation sites oriented toward the lysosomal lumen (shown in blue). Mutations causing misfolded proteins are shown in red. Polymorphisms are shown in green [35].

Although several therapeutic approaches for treating MPS IIIC are under investigation, no clinically approved specific therapies exist, and only symptomatic treatment is possible. For instance, ERT is ineffective for MPS IIIC due to the inability of the enzyme to cross the BBB. Delivering replacement enzyme intrathecally or intravitreally to bypass the BBB is potentially invasive and cannot be easily achieved because the enzyme is an insoluble transmembrane protein. Moreover, due to insufficient evidence of neurologic benefit, HSCT and umbilical cord blood cell transplantation are not currently considered effective treatments for MPS III [reviewed in 36]. Studies on pharmacologic chaperones capable of increasing residual enzyme activity in the mutant variants, where amino acid substitutions cause HGSNAT misfolding [reviewed in 35], suggest that some patients could be treated with this approach. However, the efficacy of this strategy is still being explored in MPS IIIC. Another method being studied is *in vivo* gene therapy using HGSNAT-encoding viral vectors. Intracerebral gene therapy is well tolerated in children with MPS

IIIA or MPS IIIB, with some patients showing ameliorations in neurocognitive abilities and moderate improvements in sleep and behavior [reviewed in 35]. Yet, gene therapy for MPS IIIC is still in the pre-clinical stage. Therefore, there is currently no curative treatment for MPS IIIC, and most patients die before adulthood [34].

2.1.4 MPS IIID

MPS IIID is caused by mutations in the gene encoding the enzyme *N*-acetylglucosamine 6-sulfatase. MPS IIID is the rarest subtype of MPS III.

2.1.5 MPS IIIE

The deficiency of the lysosomal arylsulfatase G (*ARSG*) enzyme causes the incomplete degradation of HS. MPS IIIE has not been discovered in humans, but dog and mouse models of the subtype have been generated. *Asrg*-deficient mice show pronounced accumulation of HS in visceral organs and the CNS, neuronal death, and behavioral deficits [91]. In humans, a homozygous founder missense variant in *ARSG* has been instead associated with an atypical form of Usher syndrome [92].

2.1.6 Lysosomal catabolism of Heparan sulfate (HS)

HS proteoglycans play essential roles in various physiological functions such as cell signaling, distribution of growth factors, cell motility, and adhesion [37]. Degradation of HS is a tightly regulated process and involves multiple lysosomal enzymes that act sequentially to fully break down the oligosaccharide chains (Fig.2) [38]. There are, in fact, eight lysosomal enzymes that catabolize HS once it is brought to the lysosomes via endocytic mechanisms [39]. Deficiencies of four distinct enzymes in this catabolic pathway are responsible for causing individual subtypes of

MPS III: heparan-N-sulphatase deficiency for MPS IIIA, α -N-acetylglucosaminidase deficiency for MPS IIIB, HGSNAT for MPS IIIC, and N-acetylglucosamine 6-sulfatase for MPS IIID [40].

The accumulation of HS oligosaccharides in cells may cause cell, tissue, and organ dysfunction. For instance, previous reports have shown that lysosomal storage of heparan sulfate is associated with mitochondrial defects, altered autophagy, and neuronal death [41]. Furthermore, the severity of neurodegeneration can be predicted based on the level of HS accumulation. In contrast, clearance of this GAG in the brains of MPS II mice was shown to reverse neuronal cell damage and neurologic symptoms [42]. These findings, therefore, point to an association between HS accumulation in the CNS, neurodegeneration, and neurocognitive impairment [42].

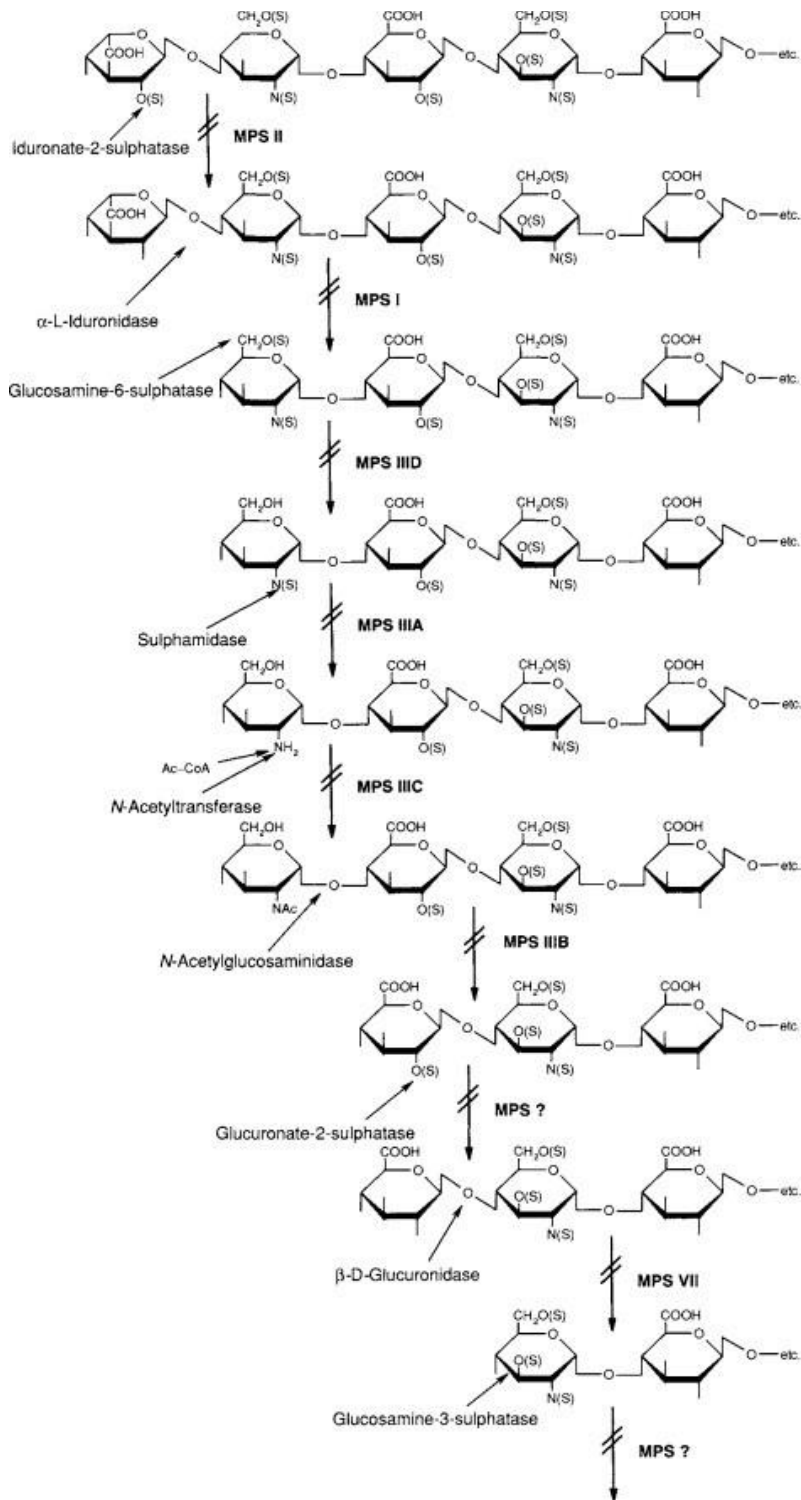


Figure 2. Degradation pathway of HS

Deficiency of any of the eight enzymes involved in the degradation of HS is responsible for causing one of the subtypes of MPS depicted in the diagram [40].

2.1.7 CNS pathology and neuronal dysfunction in MPS III

In animal models of MPS III, behavioral abnormalities often precede significant neuronal loss and brain atrophy [43]. This observation suggests that changes in neuronal circuit function may contribute to functional pathological changes within neurons at disease onset [43]. Dwyer *et al.* showed that in MPS IIIA mice, alteration of the synaptic architecture appears as early as postnatal day 21 (P21) [43]. In particular, they revealed a significant difference in the levels of the excitatory postsynaptic marker PSD-95 in P21 somatosensory cortices. They also evaluated total miniature excitatory postsynaptic current (mEPSC), which demonstrated fewer large events in the mutant mice when compared to WT [43]. Similar results were also found in MPS IIIC mouse models, where the frequency and amplitude of mEPSC were reduced by 43% compared to WT mice [44]. Furthermore, an abnormal distribution and reduction of multiple synaptic proteins, including PSD-95, VGLUT1, synaptophysin, and Syn1, were also observed in cultured hippocampal and CA1 pyramidal MPS IIIC neurons [44]. More specifically, densities of VGLUT1+ (the presynaptic transporter of glutamate in synaptic vesicles) and PSD-95+ puncta, as well as the juxtaposition of these two synaptic markers, were significantly decreased in MPS IIIC neurons, suggesting a reduction in the number of functional excitatory synapses [44].

Both immunocytochemical and transmission electron microscopy analyses showed a reduction of synaptic vesicles *in vivo* and *in vitro* [44]. Additionally, when the authors analyzed post-mortem cortical tissues of neurological MPS I, II, IIIA, IIIC, and -IIID patients, they found that PSD-95 was one of the most affected biomarkers in the human brain [44]. Importantly, PSD-95 defects and behavioral deficits were rescued by restoring the primary HGSNAT deficiency and reducing HS storage through the intracranial injection of AAV vectors (AAV9 and AAV2 true type [TT] expressing the codon-optimized human HGSNAT in MPS IIIC mice) [44, 45]. These results

further suggest a causative relationship between HS storage and synaptic dysfunction in MPS III. Therefore, it is tempting to speculate that defects in neural circuits could be targeted to correct behavioral and cognitive impairments in neurological MPS patients [44].

3. NEURAMINIDASE 1 (NEU1)

NEU1 is a lysosomal enzyme that cleaves terminal sialic acids from glycan chains of glycoproteins. NEU1 is part of a larger family of neuraminidases in mammals, including NEU2, NEU3, and NEU4. These enzymes' expression patterns, intracellular localization, and substrate specificity are different but can overlap significantly [reviewed in 46,100]. For instance, the kidney, liver, pancreas, skeletal muscle, lungs, and placenta show high levels of NEU1 [100]. NEU3 is highly expressed in the adrenal gland, skeletal muscle, testis, thymus, and heart, whereas NEU4 is mainly found in the heart, skeletal muscle, placenta, spleen, and liver [48,49]. On the contrary, NEU2 expression is generally very low in tissues except for the placenta and testis [47]. Only NEU1, NEU3, and NEU4 show high expression in the brain.

NEU1 is the most abundant of all mammalian neuraminidases [50]. It is localized on the inner membrane of lysosomes, where it participates in the catabolism of sialylated glycopeptides and oligosaccharides. NEU1 is also present on the outer cellular membranes, where it regulates cellular processes and intracellular interactions by desialylation of multiple classes of receptors. Several studies also proposed that NEU1 plays a critical role in the CNS by removing polysialic acid (PSA) content on neuronal surfaces during neuronal proliferation, differentiation, migration, and long-term potentiation [reviewed in 46]. Additionally, NEU1 is responsible for the proper migration of immature hippocampal granule cells by regulating the amount of PSA on the surface of these cells

[51]. Loss of NEU1 activity also leads to increased amyloidogenic processes, as seen in sialidosis, a neurosomatic lysosomal storage disorder caused by mutations in the *NEU1* gene [93].

3.1 Lysosomal multienzyme complex of NEU1

NEU1 is part of a lysosomal multienzyme complex (LMC) with Cathepsin A (CTSA), β -galactosidase (GBL1), and N-acetylgalactosamine 6-sulfatase (GALNS). NEU1 activity is intrinsically linked to CTSA, a protective protein required for the activation, stability, and normal function of NEU1 [reviewed in 46]. In the cells of galactosialidosis patients carrying mutations in the *CTSA* gene, LMC is disrupted, leading to a secondary loss of NEU1 activity, a drastic decrease of GBL1, and a partial reduction of GALNS activity [52, unpublished]. Both sialidosis and galactosialidosis clinically manifest with pathological changes in the CNS.

3.2 Sialidosis

Sialidosis is an autosomal recessive LSD caused by a genetic deficiency of NEU1, which results in the accumulation of sialic acid-rich glycopeptides and oligosaccharides in most body tissues [53]. Two types of sialidosis, type I and type II, are described based on the onset of the disease and the severity of symptoms. Sialidosis type I, also called cherry-red spot myoclonus, is less severe than type II of the disease. Patients with type I usually develop symptoms in their teens or twenties. Common disease manifestations include progressive myoclonus, ataxia, and macular cherry-red spots [54]. The symptoms worsen over time, and patients with sialidosis type 1 usually require wheelchair assistance later in life. Sialidosis type II can be further subdivided into congenital, infantile, and juvenile forms. Affected patients can have widespread swelling, organomegaly, abnormal bone development, intellectual disabilities, and coarse, distinctive facial

feature [54]. Patients with the congenital form have such severe health problems that they are usually stillborn or die soon after birth [55].

4. RATIONALE AND OBJECTIVES

Various hypotheses were proposed to explain how the primary storage of HS in neurological MPS diseases leads to prominent neurodegeneration. In particular, extracellular HS oligosaccharides have been shown to induce neuroinflammation in MPS III mouse models by activating microglia through interaction with the TLR4 receptors [56]. Widespread neuroinflammatory response and increased release of inflammatory cytokines could, then, lead to impaired cognition and neuronal loss observed in both patients and MPS IIIC mouse models [57]. Another proposed mechanism includes oxidative stress and altered mitochondrial functioning. Accumulation of HS has been associated with abnormal mitochondrial numbers and morphology and compromised energy metabolism detected in the brain of MPS IIIC mice [reviewed in 30]. Since mitochondria produce a significant amount of ROS that contribute to oxidative stress, mitochondrial damage could, therefore, change intracellular processes and neurotransmission, affecting CNS functioning [58]. Although different mechanisms have been investigated, it remains unclear if HS is directly responsible for the changes observed in the brain of neurological MPS patients and mouse models or if they result from secondary effects of lysosomal storage in general, such as autophagy block and neuronal accumulation of simple gangliosides and misfolded proteins [30]. To elucidate this question, we propose investigating whether HS accumulation directly contributes to neurodegeneration seen in MPS patients through inducing secondary enzyme deficits.

The recent unpublished data obtained in our laboratory demonstrate that NEU1 activity is significantly reduced in the brain tissues of MPS IIIA, C, and D patients and MPS IIIA, B, and C mouse models. However, the mechanism causing this secondary deficiency and its pathological consequences are unknown [52, unpublished]. When measuring the activities of lysosomal enzymes in the brain tissues of our MPS IIIC mouse models, we have previously detected a 50% reduction in total neuraminidase activity measured at acidic pH [52, unpublished]. NEU2 has a neutral pH and a very low expression in the brain, suggesting that our results reflected a reduction in the activity of one of the three remaining neuraminidases, NEU1, 3, and 4. The assays repeated in the presence of the NEU3/NEU4 specific inhibitor, C9-4BPT-DANA, revealed an even more drastic decline of the neuraminidase activity to less than 10% of the levels detected in the normal mice, demonstrating that NEU1 is the enzyme showing the secondary deficiency in the brain tissues of MPS IIIC patients and mice.

Importantly, we only observed a reduction of NEU1 activity in patients and mouse models of neurological MPS that store HS [52, unpublished]. NEU1 levels were normal or even increased in the brain tissues of mouse models of other neurological lysosomal diseases, including Tay-Sachs, Niemann-Pick type C1, and mucopolidosis IV [52, unpublished]. These results suggest that the accumulation of a specific GAG, HS, is associated with decreased NEU1 levels. Importantly, *Neu1* mRNA levels in the brains of MPS IIIC mice are normal [52, unpublished], suggesting that the reduction occurs at the post-translational level.

Since NEU1-mediated cleavage of sialic acids from glycans attached to glycoproteins was proposed to be critical for proper brain development and function, it is essential to study the link

between the secondary NEU1 deficiency and cognitive decline and neurodegeneration occurring in MPS IIIC mice.

Our main hypothesis is that the storage of HS contributes to the dissociation of the LMC, thus causing the secondary deficiency of NEU1 at the protein level. We also hypothesize that the reduction of NEU1 activity significantly contributes to the CNS pathology, previously detected in MPS IIIC patients and mouse models, by inducing amyloidogenesis and defects in synaptic transmission [4].

Our specific aims are:

1. To investigate the relationship between HS accumulation and NEU1 protein levels in the brains of MPS IIIC mice.
2. To study if levels of NEU1 activity can be rescued in MPS IIIC mice that have received a bilateral injection of AAV expressing the codon-optimized human WT *Hgsnat* transgene.
3. To investigate the effect of exogenous HS on NEU1 activity in cultured macrophages derived from MPS IIIC and WT mice.
4. To test if an increase of NEU1 activity in hippocampi and somatosensory cortices of MPS IIIC mice by stereotaxic brain injection of a lentivirus overexpressing human WT CTSA and NEU1-GFP (LV-CTSA-NEU1-GFP) could correct synaptic defects and reduce the formation of amyloid plaques potentially associated with NEU1 deficiency.
5. To test if synaptic defects are rescued in MPS IIIA iPSC-derived neurons by transduction with the LV-CTSA-NEU1-GFP virus.

CHAPTER 2

MATERIALS AND METHODS

1. Animals

1.1.1 *Hgsnat-Geo* (KO) mouse strain

Hgsnat-Geo mice were generated from C57Bl6 mice by a targeted disruption of the *Hgsnat* gene at the Texas Institute for Genomic Medicine using the gene trap technology [57]. The generation of this MPS IIIC mouse model was previously described by Zambrowicz *et al.* and Hansen *et al.* [59,60]. Briefly, a selectable marker β -geo, containing a functional fusion between the β -galactosidase-encoding gene and the *neo* gene from Tn5, was inserted into intron 7 of the *Hgsnat* gene [57]. This insertion led to the splicing of exon 7 into the β -geo cassette to generate a fusion protein containing *Hgsnat* amino acid sequence encoded by exons 1-7, followed by aminoglycoside 3'-phosphotransferase and β -galactosidase [57]. The *Btk* exon in the trap construct contained termination codons in all reading frames, thereby preventing the translation of the downstream *Hgsnat* exons [57].

1.1.2 *Hgsnat*^{P304L} (KI) mouse strain

Hgsnat^{P304L} mice with a C57Bl/6J background were generated by targeting exon 9 of the *Mus musculus* gene *Hgsnat* using CRISPR-Cas9 technology at the McGill Transgenic Core Facility Animal Modeling [61]. Briefly, a single guide nucleotide RNA (sgRNA) was designed to target a genomic site on the murine *Hgsnat* locus with minimal potential off-target effects [61]. sgRNA and Cas9 mRNA were then microinjected into zygotes with single-stranded oligodeoxynucleotide, barring a c.911C>T mutation encoding for the P304L change [61]. The zygotes were cultured overnight in EmbryoMax KSOM drops and covered with mineral oil [61]. At the 2-cell stage, the embryos were transferred to pseudo-pregnant female oviducts to generate chimeric mouse litters

[61]. Heterozygous mice were then bred with C57Bl/6J WT, and their pups were genotyped by PCR using DNA extracted from tails. Heterozygotes were then crossed to obtain homozygotes [61].

All the mice were maintained and housed according to the Canadian Council on Animal Care (CCAC) guidelines. The animals were kept in a fixed temperature and humidity environment with a 12 h light/dark cycle and continuous access to food and water. All the animal experimentations were approved by the Animal Care and Use Committee of the Sainte-Justine Hospital Research Center.

2. Enzyme activity

Different brain regions were micro-dissected and homogenized in 100 μ L of water using a sonic dismembrator (Artek Systems Corporation). For organs, such as the liver, spleen, kidney, whole brain, and lungs, approximately 50 mg of the tissue was homogenized in 300 μ L of water.

A) NEU1 Activity measurements

To assay NEU1 activity specifically, we prepared a reaction mixture containing 5 μ L of homogenate with 12.5 μ L of 0.1 M sodium acetate buffer, pH 4.6, 12.5 μ L of 0.8 mM fluorogenic substrate 4-methylumbelliferone-N-acetyl-neuraminic acid (Sigma-Aldrich), and 10 μ L of 250 μ M NEU3/NEU4 inhibitor, C9-4BPT-DANA. After 60 minutes of incubation at 37°C, the reaction was stopped by adding 960 μ L of 0.4 M glycine buffer, pH 10.4. Then, 250 μ L of the final reaction mixture was transferred to a black 96-well plate (CoStar), and the concentration of 4-methylumbelliferone was measured using a ClarioStar plate reader (BMG Labtech).

The total neuraminidase activity was also measured using the same method but replacing the inhibitor C9-4BPT-DANA with an equal amount of water.

B) β -galactosidase activity

Homogenates (10 μ L) were prepared as described previously, diluted (1:10), and mixed with 12.5 μ L of buffer (0.4 M sodium acetate and 0.2 M NaCl, pH 4.2) and 12.5 μ L of 1.5 mM fluorogenic substrate 4-methylumbelliferyl β -D-galactoside (Sigma-Aldrich). The reaction mixture was then incubated for 15 min at 37°C. After stopping the reaction with 964 μ L of 0.4 M glycine buffer, pH 10.4, 250 μ L of the reaction mixture was transferred to a black 96-well plate which was then analyzed with the fluorometer.

C) β -hexosaminidase activity measurement

To measure β -hexosaminidase activity, 2.5 μ L of diluted (1:10) homogenate was added to 15 μ L of 0.1 M sodium acetate buffer, pH 4.2, and 12.5 μ L of 3 mM 4-methylumbelliferyl N-acetyl- β -D-glucosaminide (Sigma-Aldrich). The reaction mixture was then incubated for 15 min at 37°C and the reaction stopped by adding 970 μ L of 0.4 M glycine buffer, pH 10.4. 250 μ L of the reaction mixture was transferred to a black 96-well plate, then analyzed with the fluorometer.

Total protein concentration was determined using the Quick Start™ Bradford Protein Assay (Cat. #5000201, Bio-Rad Hercules, CA).

3. Perfusion and tissue fixation

Mice were anesthetized using a pentobarbital solution and transcardiacally perfused with phosphate-buffered saline (PBS) to remove blood, followed by 4% paraformaldehyde (PFA). Organs were left overnight in 4% PFA at 4°C and then transferred to a 30% sucrose solution for

two days before being embedded in Tissue-Tek® Optimum Cutting Temperature (OCT compound) and stored at -80°C.

4. Immunohistochemistry

Perfused brain sections of WT, *Hgsnat-Geo*, and *Hgsnat^{P304L}* mice were cut sagittally at a thickness of 40 µm with a cryostat and stored in cryopreservation buffer (0.05 M sodium phosphate buffer, pH 7.4, 15% sucrose, and 40% ethylene glycol) at -20°C until labeling. The samples were stained with primary antibodies diluted in 1% bovine serum albumin (BSA), 0.3% Triton X-100 and PBS after being permeabilized and blocked using 0.3% Triton X-100 in 5% BSA solution. After adding the primary antibodies, the samples were incubated overnight at 4 °C. The next day, mouse brain sections were washed three times with PBS and counterstained with Alexa Fluor-labeled secondary antibodies (dilution 1:400, Life Technologies) for two hours at room temperature. Finally, the slides were mounted using Prolong Gold Antifade Reagent with DAPI (Thermo Fisher Scientific) and analyzed using Leica TCS SPE inverted confocal microscope. A list of primary antibodies used during experiments is described in Table 2.

Antigen	Host/Target Species	Dilution	Manufacturer
Heparan sulphate (HS)	Mouse anti-mouse	1:200	Amsbio (370255-S)
LAMP2	Rat anti-mouse	1:100	DSHB (ABL-93-s)
Neuraminidase (NEU1)	Rabbit anti-mouse	1:200	Abcam (ab233119)
vGLUT1	Rabbit anti-mouse	1:200	Abcam (ab104898)
PSD-95	Mouse anti-mouse	1:200	Abcam (ab99009)
Synapsin-1 (Syn1)	Rabbit anti-mouse	1:200	Abcam (ab64581)
B-amyloid (D54D2)	Rabbit anti-mouse	1:200	Cell Signaling (8243S)
G _{M2}	Mouse humanized	1:300	KM966

Table 2. Antibodies and dilutions used for immunohistochemistry

5. Immunocytochemistry

The PFA-fixed cells were washed three times with PBS and permeabilized with 0.1% Triton-X-100 in PBS for 5 minutes. After permeabilization, cells were washed with PBS and blocked in 5% BSA in PBS for one hour. Primary antibodies diluted with 1% BSA-PBS, as described in Table 3, were added to the cells. Cells were then incubated overnight at 4°C with light shaking. Cells were further washed three times with PBS and incubated with the secondary antibodies (dilution of 1:1000) for two hours. Cells were washed twice and dipped into double-distilled water before being mounted onto microscope slides with Prolong Gold Antifade Reagent containing DAPI.

Antigen	Host/Target Species	Dilution	Manufacturer
MAP2	Chicken anti-mouse	1:500	Abcam (ab5392)
BDNF	Mouse anti mouse	1:2000	DSHB (#9-S)
Neurofilament Medium Chain	Rat anti-mouse	1:200	DSHB (2H3)
vGLUT1	Rabbit anti-mouse	1:1000	Abcam (ab104898)
PSD-95	Mouse anti-mouse	1:1000	Abcam (ab99009)
Synapsin-1 (Syn1)	Rabbit anti-mouse	1:200	Abcam (ab64581)

Table 3. Antibodies and their dilutions used for immunocytochemistry

6. Preparation of bone marrow-derived macrophages (BMDM)

Bone marrow cells were collected from the tibia, femur, and iliac bones of WT and *Hgsnat*^{P304L} mice. After washing with 70% alcohol and three times with ice-cold PBS with 1% penicillin and streptomycin, the bones were flushed with ice-cold Dulbecco's Modified Eagle Medium (DMEM) at both sides to extract bone marrow cells. Then, the cell suspension was centrifuged (450 g, 10 min, 4°C), and the supernatant was removed. To remove red blood cells, the cell pellet was resuspended in a red blood cell (RBC) lysis buffer (155 mM NH₄Cl, 12 mM NaHCO₃, and 0.1 M

EDTA) for 30 seconds. Ice-cold complete DMEM was added to the cell suspension to stop the lysis. After the second round of centrifugation (450 g, 10 min, 4°C), cells were filtered using a 40 µm Nylon cell strainer. Bone marrow cells were then cultured in 10 cm petri dishes in DMEM supplemented with 10% fetal bovine serum (FBS) and containing granulocyte-stimulating factor obtained from cultured L929 cells [62].

7. Extraction of HS from patients' urine

HS oligosaccharides were isolated from urine samples of MPS IIIC patients, obtained from the families with informed research consent. Thirty mL of patients' urine was adjusted to a pH of 5-6 with acetic acid. After 10 min centrifugation at 1050 g, the supernatant was collected and mixed with 600 µl of 5% cetylpyridinium chloride (CPC). The mixture was then incubated overnight at 4°C and centrifuged for 30 min at 1050 g and 4°C to collect the HS-CPC precipitate. The residue was washed twice with 12 mL of ethanol saturated with NaCl. Each washing step was followed by 10 min centrifugation at 1050 g and 4°C. After removing the supernatant, 12 mL of 100% ethanol was added to the samples. After centrifugation, the precipitate was allowed to dry before adding 3 mL of diethyl ether. The supernatant was removed after centrifugation, and the residue dried for another 30 min by a flow of N₂. Six mL of 0.6 M NaCl was then added to the precipitate, and the mixture was incubated for 3 hours at 4°C. After incubation, the samples were centrifuged again to obtain supernatant, to which 24 mL of 100% ethanol was added. After incubation overnight at 4°C, all steps were repeated; but after drying the precipitate for 30 min following the addition of 3 mL of diethyl ether, the residue was resuspended with water and freeze-dried for storage at -20°C. Typically, from 4 to 5 mg of purified HS oligomers were obtained with this protocol.

8. Treatment of cultured BMDM with HS

BMDM obtained from WT and MPS IIIC mice were cultured in a six-well plate at a density of 5×10^6 cells/well in the presence (50, 100, or 300 μg of HS/mL of medium) or absence (control) of HS for seven days. HS was added to the wells 24 h after seeding and after three days of culture, when the medium was replaced. After seven days, the cells were washed with ice-cold PBS and harvested. The total neuraminidase activity and NEU1 activity were measured in cell homogenates as described previously.

9. Stereotaxic injections of the lentiviral vector

Postnatal days 18 and 19 (P18, P19) mice were anesthetized with 5% isoflurane and oxygen in an induction chamber. During the surgery, the mice remained on a heating pad to prevent hypothermia, and the mouse's head was secured in an induction cone with a flow of 2 L of oxygen-containing 2% isoflurane per min. The mouse was immobilized by fixing its head with ear bars and injected subcutaneously with a non-steroidal anti-inflammatory drug Carprofen/Rimadyl (Zoetis, DIN 02255693, 0.1 mL of Carprofen mixed with 9.9 mL of 0.9% Sodium Chloride, 0.15 mL per mouse). A small amount of an eye lubricant OptixCare was applied to protect the eyes and prevent the formation of cataracts. Then, the fur on top of the head was shaved to expose the underlying skin, and the remaining hair was removed using the Nair hair removal cream. The cream was removed with saline (0.9% sodium chloride, Baxter Corporation) after hair started falling off to avoid skin irritation. An iodine solution (10% povidone-iodine, Laboratoire Atlas) was applied to disinfect the surgical area before cutting the skin, starting from the back of the head. The flaps of the skin were then spread apart using a Q-tip saturated with saline solution to expose the underlying skull. Next, the two reference points, bregma and lambda, were localized and

marked. The entomological needle was first moved to bregma, where it touched the skull without pushing into it, and the coordinate display was then reset to zero.

The stereotaxic arm was then moved to lambda and, subsequently, to both sides of the skull to ensure that the skull was well aligned. While some natural variations exist between skulls, a well-positioned head should have lambda at the following coordinates after setting bregma at zero: 0 mm on the medial/lateral (M/L) axis, approximately 4.4 mm along the anterior/posterior (A/P) axis, and 0 mm on the dorsal/ventral (D/V) axis in P18 mice. Regarding each side of the skull, the coordinates should be 2.5 mm M/L, 2.5 mm A/P, and less than 0.1 mm D/V. One hole was made on each side of the brain using a microdrill (Foredom, K.1070 Micromotor kit). The coordinates were 1.5 mm on each hemisphere's M/L axis and 2.2 mm on the A/P axis. The holes were less than 1 mm in diameter and deep enough to pierce the skull without damaging the dura mater. To remove bone fragments around the holes, a saline solution was used to flush the surrounding areas.

The glass capillary needles used for injections of the vector were made by melting and stretching glass capillaries (3.5" Drummond #3-000-203-G/X) using the micropipette puller (Sutter Instrument Company). After filling the glass capillary needles with mineral oil (Sigma BioReagent, #MKCM5718), the needles were fixed onto the Nanoliter Injector (Drummond Scientific Company, Nanoject III #3-000-207) and half-emptied by letting the mineral oil flow out of the needle. Then, the needles were filled with 1.8 μ L of the viral vector solution. After resetting the coordinate display using bregma, the Nanoliter micropipette was moved to the injection site (1.5 mm M/L, 2.2 mm A/P). For each hemisphere, the micropipette was first lowered to a depth of 2.2 mm to target the hippocampus and then to 1.2 mm to target layers IV and V of the cortex.

These coordinates have been determined previously by injecting Indian ink or a lentivirus expressing GFP (LV-GFP) in mice of similar age.

The virus was injected at a speed of 2 nL/second using the Nanoliter injector, and each injection lasted about seven minutes. After injecting 900 nL of the virus into the hippocampus, we waited six minutes for the viral solution to set down before moving the needle to the cortex. This step was performed to avoid the vacuum effect that could aspirate the virus upward. After all the injections were completed, the wound was sutured with ethilon nylon suture (Ethicon, PMP346), and a pea-sized amount of an antibiotic cream (Polysporin, Jonhson & Jonhson inc, DIN 02237227) was applied to the surgical zone. Finally, another dose of diluted Carprofen (0.15 mL) was injected subcutaneously into the mouse, which was then removed from the stereotaxic frame and returned to its cage. All the injected mice were put on a wet diet, and their condition was observed daily following the surgery.

10. Behavioral tests

A) Y-maze

Spontaneous alternations were measured in the Y-maze behavioral test to assess the spatial working memory of mice. The Y-maze consists of three identical white Plexiglas arms, measuring 40 x 10 x 20 cm and placed at an angle of 120° apart. Printouts with different colors and patterns were placed on the walls of the testing room to serve as visual cues. This behavioral test was conducted under dim lighting conditions and always at the same time of the day to avoid circadian bias. Mice were placed at the center at the beginning of the experiment. Each session, during which the mouse will freely explore the three arms, lasted 8 minutes and was video recorded by the Smart video tracking software. Then, the number of arm entries and the number of triads were measured

to calculate the number of successful alternations. An entry was counted when all four limbs of the mouse were within an arm. We used the following equation to calculate the percentage of alternation: $[\text{number of alternations}/\text{total number of arm entries} - 2] \times 100$.

B) Novel object recognition test (NOR)

NOR test (Fig. 3) was used to measure short-term recognition memory. One day before the experiment, mice were habituated to a white box of plexiglass (45 cm length x 45cm width x 40 cm height) for 10 min and returned to their home cages. The next day, mice were placed individually in the testing chamber on the opposite side of the objects, facing the wall. The animals were allowed to explore two identical toys (T25 flasks) for 10 min before returning to their home cages. One hour after the initial exposure to the objects, the mouse was placed back into the testing chamber, containing one of the original toys and a new object, a red and blue plastic toy measuring 6.5 x 6.5 x 7.5 cm. Each trial with the novel object lasted 10 min. Between each session, the testing chambers and the objects were washed with 70% ethanol to eliminate any olfactory cue bias. Each session was video-recorded and analyzed manually to determine the discrimination index (DI). The exploration time was counted when the head of the mouse was within a 3 cm radius around the object, but only when the animal was looking at the object, sniffing the object, or touching the object with its snout. Exploration time was not counted when the mouse was within the exploration zone but not actively exploring the objects or if the animal was grooming itself or sitting on top of the toys. All the objects were placed 15 cm away from the right or left walls and 15 cm from the bottom of the box.

The DI was calculated as the difference in time spent exploring the new and original objects divided by the total exploration time. A positive discrimination index indicates a preference for a novel object, whereas a negative discrimination index suggests a preference for familiar objects.

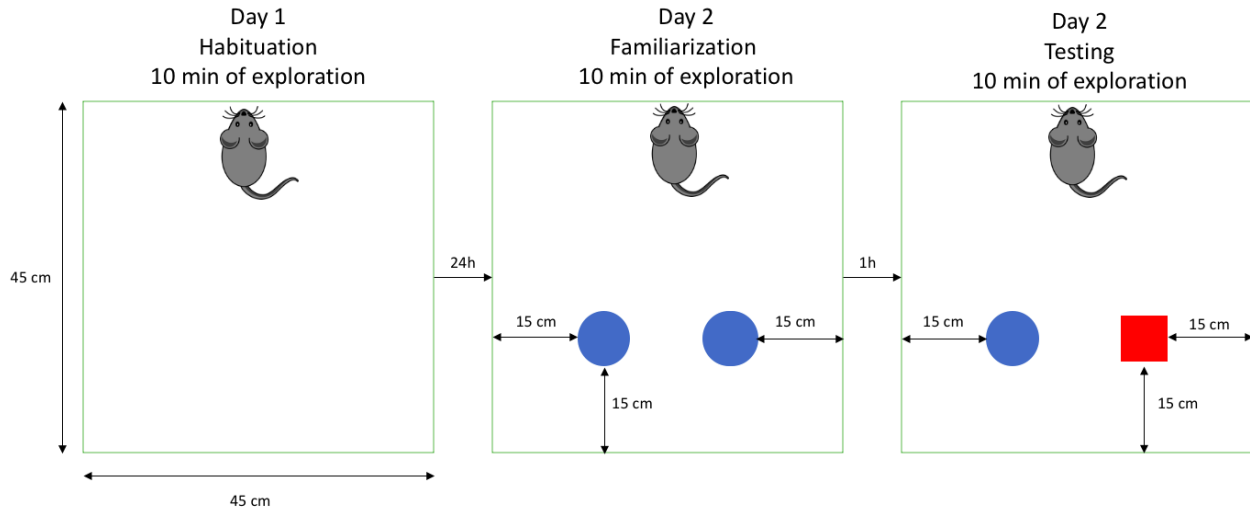


Figure 3. Novel object recognition test

C) Open field (OF)

Mice were habituated to the testing room 30 min before the start of the experiment. Mice were then placed in the center of an open-field arena (45 cm length x 45 cm width x 40 cm height) and allowed to explore for 20 min. Each session was recorded and analyzed by the Smart 3.0 software. The following parameters were measured between the different groups of mice: the number of entries in the center, the total distance traveled, the percent of time spent in the center zone, and the distance traveled in the center zone. The arena was cleaned with 70% ethanol between each trial.

11. Cultures of iPSC-derived neurons

A) Generation and establishment of iPSC lines

Skin fibroblast line of an MPS IIIA patient and healthy control were obtained from the Coriell Institute for Medical Research (NJ, USA) and propagated in Dulbecco's Modified Eagle Medium (DMEM, ThermoFisher) with 10% fetal bovine serum (FBS) and 1% Antibiotic-Antimycotic (15240062, ThermoFisher). All cell lines were tested for mycoplasma before further experiments. The cell lines were reprogrammed into iPSCs using a non-integrating CytoTune-Sendai viral reprogramming kit (A16517, Thermo Fisher Scientific) at the CHU Sainte-Justine iPSC Platform. Cells were cultured in six-well plates coated with Matrigel at 37°C with 5% CO₂ and 5% O₂ atmosphere in the mTeSR™ Plus medium and maintained according to the NeuroEDDU protocol [63]. To assess the pluripotency, each iPSC line was grown with the STEMdiff™ Trilineage Differentiation Kit (Stemcell). The markers for mesoderm, SMA, endoderm, CXCR4, ectoderm, Nestin, and PAX6 were used to identify differentiation into each germline using immunofluorescence.

B) Induction of cortical neuronal progenitor cells (NPC) and cortical neurons

Following the protocol from Chen *et al.*, iPSCs were differentiated into forebrain-committed NPC by dual SMAD inhibition [64]. NPC induction was performed in a monolayer with DMEM/F12 medium (Gibco™, #10565-018) supplemented with N-2 (Gibco™, #17502048), B27 (Gibco™, #17504044), non-essential amino acids (NEAA) (Stem Cell, #07600), FGF-8 growth factor (PeproTech, #100-25), and DMH1. An 80% media change was performed every two days for a period of three weeks. Neuronal markers such as NeuN, transcription factor PAX6, type VI intermediate filament Nestin, and Tuj1 were used to assess the quality of the induction by immunocytochemistry.

C) Cortical neuronal differentiation

After three weeks in culture, NPCs were differentiated into cultured cortical neurons as described [65]. On the first day, cells were resuspended in a 1/1 mixture of DMEMF-12/neurobasal (NB) media containing B27, N-2, NEAA, brain-derived neurotrophic factor (BDNF) (PeproTech, #450-02), glial cell-derived neurotrophic factor (GDNF) (PeproTech, #450-10), laminin, dbCAMP, Compound E, TGF-B3, and rock inhibitor (RI). On the second day, the medium was replaced with 100% NB media. Neurons were then cultured for 28 days until fully differentiated and mature. Before immunocytochemical analysis, neurons were washed with ice-cold PBS twice before being fixed in 4% PFA for 15 min. After fixation, cells were washed three times and stored in PBS at 4°C until labeling. Images containing ten z-stacks separated by 0.5 µm were taken with the Leica SP8 confocal microscope and further processed using the LAS-X or Fiji-ImageJ software.

12. Intracranial injection of AAV

Tordo et al. described a novel AAV, AAV-TT, engineered by substituting 14 amino acids in the AAV2 capsid [45]. These modifications abolished the heparan sulfate proteoglycan (HSPG) binding, which was previously shown to be detrimental to the spread of AAV2 in the CNS [45]. Compared to other AAV serotypes, such as AAV9 or AAVrh10, AAV-TT has provided greater transduction levels of neurons throughout the brain [45]. To evaluate whether this novel vector could correct MPS IIIC pathologies, they engineered it to contain the codon-optimized human HGSNAT (coHGSNAT) transgene. Using stereotaxic brain injection, Tordo et al. administered the AAV-TT-HGSNAT vector through a bilateral intracranial delivery of the virus into the striatum of eight-week-old female MPS IIIC and WT mice [45]. The AAV was delivered in 2.6 x

10^9 viral genomes (vg) in each hemisphere [45]. Sham-treated mice received 3 μ L per hemisphere of either PBS or AAV-GFP [45].

13. Acquisition of images and Statistical analysis

Fixed brain tissues were cut using a cryostat at 40 μ M and mounted with ProLong Gold antifade mounting reagent with DAPI. Slides were then analyzed using the Leica TCS SPE inverted confocal microscope. Confocal images were generated by combining 10 Z-stacks, taken at a distance of 0.5 μ m. The percentage of the stained area (for HS, NEU1, PSD95, VGLUT1, Syn1, APP, and GM2) between different groups was compared using the ImageJ 1.50i software for immunohistochemical analysis of the brain. Densities of PSD-95, VGLUT1 and BDNF positive puncta were estimated by manually counting puncta along the axon at 30 μ m increments starting from 10 μ m away from the soma. The results were expressed as a mean number of puncta/10 μ m. Quantification was blinded for all behavioral data. All statistical analyses were performed using Prism GraphPad 9.0 software (GraphPad Software, San Diego, California, USA). All data were tested for normal distribution by D'Agostino and Pearson test, and the significance of results was determined by using t-tests when comparing two groups or a One-way ANOVA test followed by Tukey's multiple comparison test when comparing more than two groups. A p-value of 0.05 or less was considered significant.

CHAPTER 3 RESULTS

Aim 1. HS storage is associated with NEU1 deficiency

A) NEU1 is deficient in tissues of MPS IIIC mouse models

When we measured the activities of several lysosomal enzymes in our MPS IIIC mouse models, we found that in contrast to most lysosomal enzymes, NEU1 activity was significantly reduced in several organs of our *Hgsnat-Geo* and *Hgsnat^{P304L}* mice. More specifically, the activities of β -galactosidase and β -hexosaminidase were shown to be increased in almost all tissues of our MPS IIIC mice, which is consistent with increased biogenesis of lysosomes and TFEB-driven expression of lysosomal genes (Fig.4). However, when we measured the total acidic neuraminidase activity (NEU1, NEU3, and NEU4 combined), we detected a reduction of approximately 50% of total NEU activity in the brains of MPS IIIC mice when compared to WT mice. Except for the kidney of both MPS IIIC mice and the spleen of *Hgsnat^{P304L}* mice, the total neuraminidase activity was also significantly reduced in the peripheral organs of MPS IIIC mice (Fig.5A).

To determine if the reduction in total neuraminidase activity is due to a deficiency of NEU3, NEU4, or NEU1, we used the NEU3/NEU4 inhibitor, C9-4BPT-DANA, which completely inhibits both NEU3 and NEU4 but not NEU1 at the concentration of 125 μ M. While the levels of NEU3 and NEU4 were similar in the tissues of WT and MPS IIIC mice, the specific NEU1 activity was shown to be significantly reduced in the brain, liver, and lungs but not in the spleen, and kidney of MPS IIIC mice (Fig.5B). These results suggest that NEU1 is the only neuraminidase affected in both MPS IIIC mouse models. Furthermore, there is a trend for *Hgsnat^{P304L}* mice to show a more drastic reduction of NEU1 activity than the *Hgsnat-Geo* mice (Fig.5B).

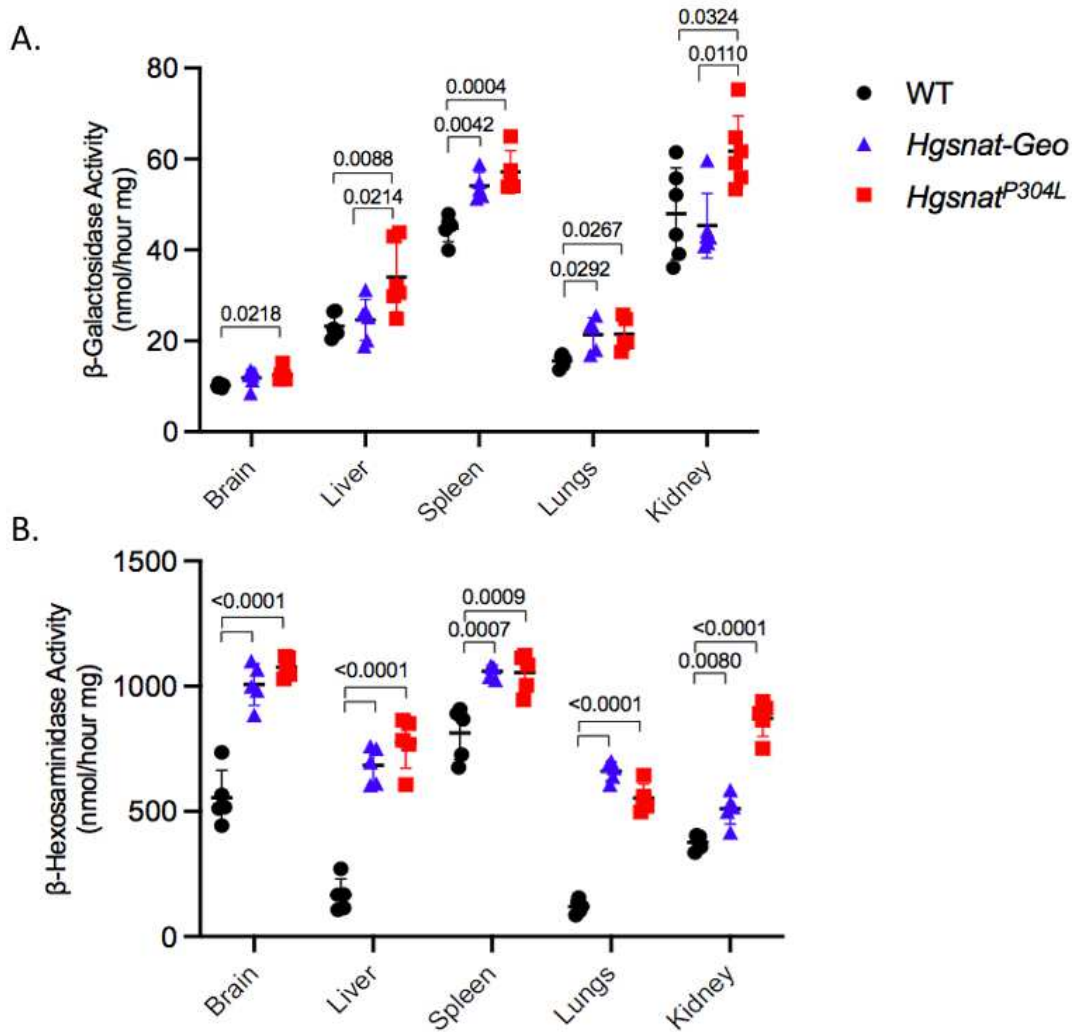


Figure 4. Increased lysosomal biogenesis in tissues of MPS IIIC mouse models

Specific activities of β -galactosidase and β -hexosaminidase were measured in 4-month-old WT, *Hgsnat-Geo*, and *Hgsnat*^{P304L} mice as described previously. **A)** The β -galactosidase activity is significantly increased in all visceral organs of *Hgsnat*^{P304L} mice when compared to their WT counterparts. *Hgsnat-Geo* mice showed an increase of β -galactosidase activity in the spleen and lungs and a trend for an increase in the brain and liver but not in the kidney. **B)** β -hexosaminidase activity is increased in all visceral organs of MPS IIIC mice. Data are represented as mean \pm SD, n=5, with significance determined by the One-way ANOVA test followed by Tukey's multiple comparison test.

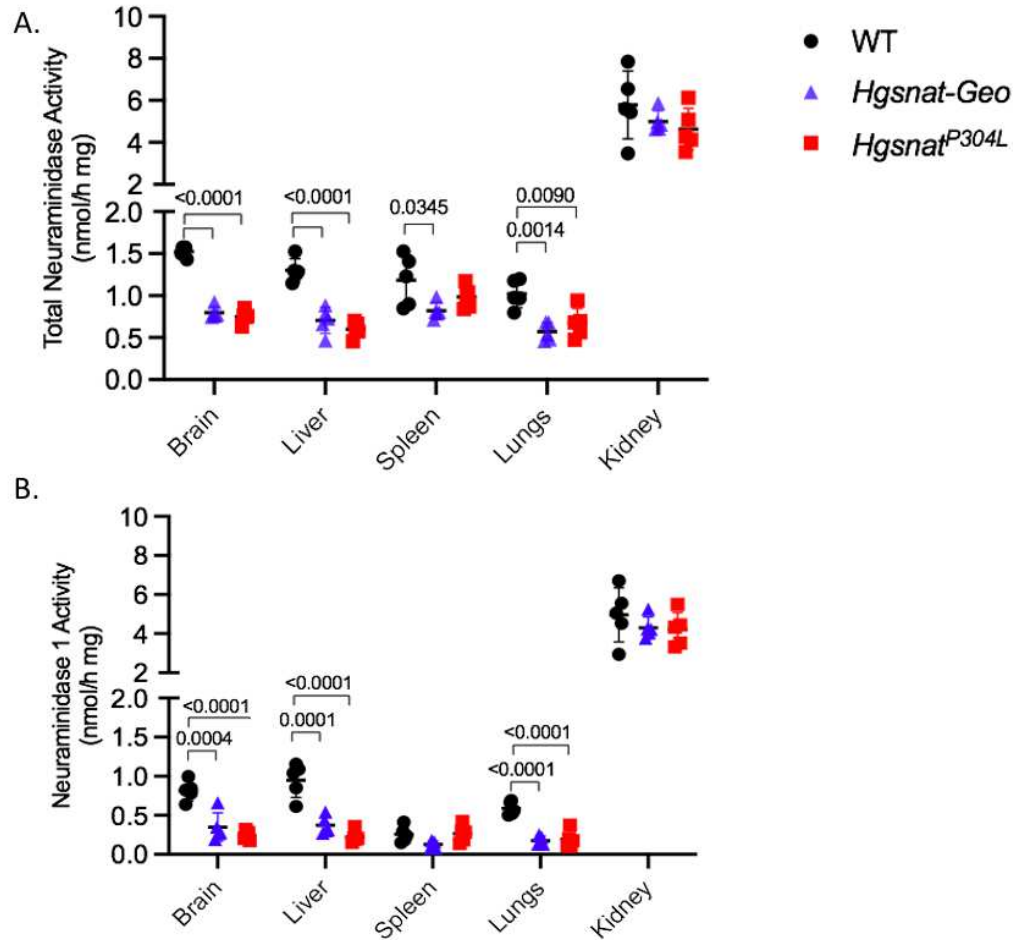


Figure 5. NEU1 activity is reduced in tissues of MPS IIIC mice.

Activity was measured in **A**) the absence (total NEU activity) or **B**) the presence of the NEU3/NEU4 inhibitor, C9-4BPT-DANA (NEU1-specific activity) in the homogenized visceral tissues and brain of 4-month-old WT, *Hgsnat-Geo*, and *Hgsnat^{P304L}* mice. Total neuraminidase activity was reduced in the brain, liver, and lungs of both MPS IIIC mouse models but not in the kidney. While the *Hgsnat-Geo* mice showed a reduction of total NEU activity in the spleen, *Hgsnat^{P304L}* mice only showed a trend for reduction. Similar results were obtained for NEU1-specific activity, where NEU1 deficiency was observed in all organs measured except for the spleen and kidney of MPS IIIC mice. Data are represented as mean \pm SD, n=5, with significance determined by the One-way ANOVA test followed by Tukey’s multiple comparison test.

B) NEU1 is deficient in the brain of MPS IIIC mice

To further determine if NEU1 is reduced in all brain regions of MPS IIIC, we analyzed the levels of NEU1 in five different brain regions: the olfactory bulb, hippocampus, paleocortex,

somatosensory cortex (SSC), and cerebellum. We previously determined that these regions were expressing high levels of *Neu1* transcript by studying brain tissues of NEU1 KO (*Neu1*^{-/-}) mouse model expressing the bacterial LacZ/ β -galactosidase reporter gene in the endogenous *Neu1* locus. The tissues were stained with a LacZ substrate, 5-Bromo-4-Chloro-3-indolyl- β -D-galactopyranoside (X-GAL). The X-GAL substrate is cleaved by bacterial LacZ/ β -galactosidase at neutral pH producing an insoluble blue pigment, allowing to visualize the brains areas with higher *Neu1* expression (Fig. 6). The hippocampus, cerebellum, olfactory bulb, deep layers of SSC and paleocortex were all stained with X-GAL suggesting a strong LacZ expression (Fig.6). We, therefore, selected these regions for further analysis of NEU1 activity in WT and MPS IIIC mice.

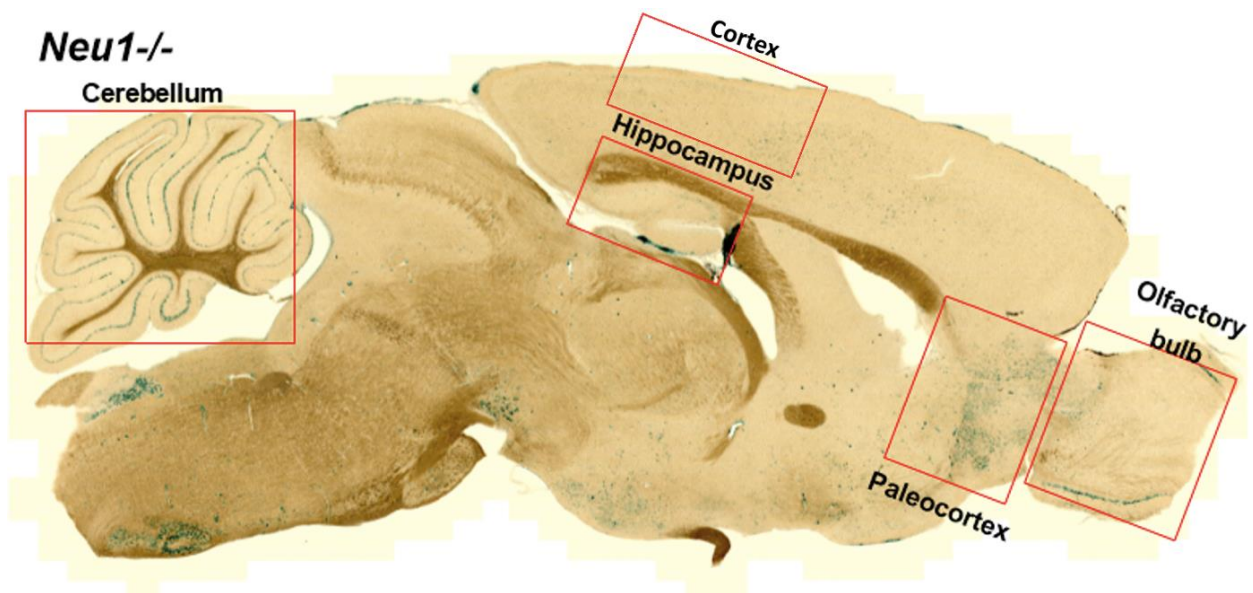


Figure 6. X-GAL staining of *Neu1*^{-/-} brain sections.

Cortical brain sections from 2-month-old *Neu1*^{-/-} mice were stained using the X-GAL substrate (blue) to visualise areas with high expression of *Neu1*. The red boxes indicate the regions that were micro-dissected for Neu1 enzyme activity assays. Images were taken at 10x with the Axioscan.

While measuring the NEU1 activity in each of the selected regions, we found a significant deficiency of NEU1 in the hippocampus, paleocortex, somatosensory cortex, and cerebellum of

both MPS IIIC mouse models as compared to WT mice. However, there was no difference between the NEU1 activity levels measured in olfactory bulbs of WT, *Hgsnat-Geo*, and *Hgsnat^{P304L}* mice (Fig. 7).

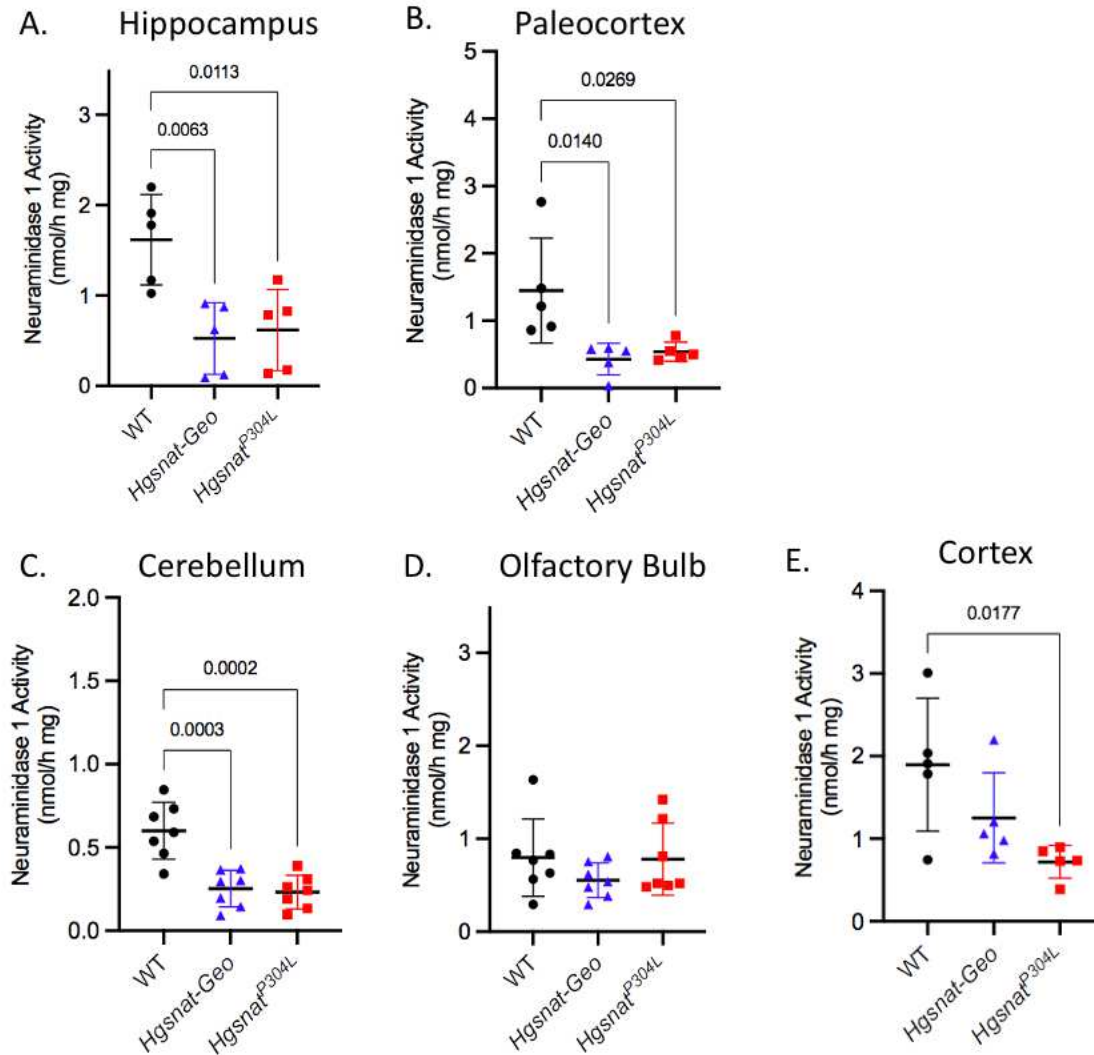


Figure 7. NEU1 activity in distinct brain regions

Specific NEU1 activity was measured in the **A)** hippocampus, **B)** paleocortex, **C)** cerebellum, **D)** olfactory bulb, and **E)** somatosensory cortex of 6-month-old WT, *Hgsnat-Geo*, and *Hgsnat^{P304L}* mice. Each brain region was micro-dissected, and enzyme activity was measured as previously described in the presence of the NEU3/NEU4 inhibitor. NEU1 activity was reduced in the hippocampus, paleocortex, cerebellum, and somatosensory cortex but not in the olfactory bulb. The data show means \pm SD, n=5 mice per genotype or 7 for the cerebellum and olfactory bulb, with significance determined by the One-way ANOVA test followed by Tukey’s multiple comparison test.

C) HS storage is related to NEU1 deficiency in MPS IIIC

Given that NEU1 activity is reduced in the brains of our MPS IIIC mice, we wanted to determine if this deficiency is associated with an accumulation of HS. We performed IHC analysis of brain sections of 6-month-old WT, *Hgsnat-Geo*, and *Hgsnat^{P304L}* mice using anti-NEU1 antibodies to estimate the level of Neu1 protein and antibodies against HS to estimate the level of its accumulation. These results demonstrated that the levels of HS were increased in the hippocampus, paleocortex, cerebellum, and somatosensory cortex but not in the olfactory bulb of MPS IIIC mice (Fig. 8). In almost all brain regions, *Hgsnat^{P304L}* mice tend to show more severe storage of HS than *Hgsnat-Geo* mice (Fig.8).

On the other side, NEU1 expression was significantly reduced only in the hippocampus, somatosensory cortex, and paleocortex but not in the other brain areas. Consistent with the enzymatic NEU1 activity assay results, we saw no significant decrease in Neu1 protein in the olfactory bulbs. In the cerebellum, the NEU1-specific activity decreased, but IHC analysis showed only a trend for reduction of the Neu1 protein (Fig.9).

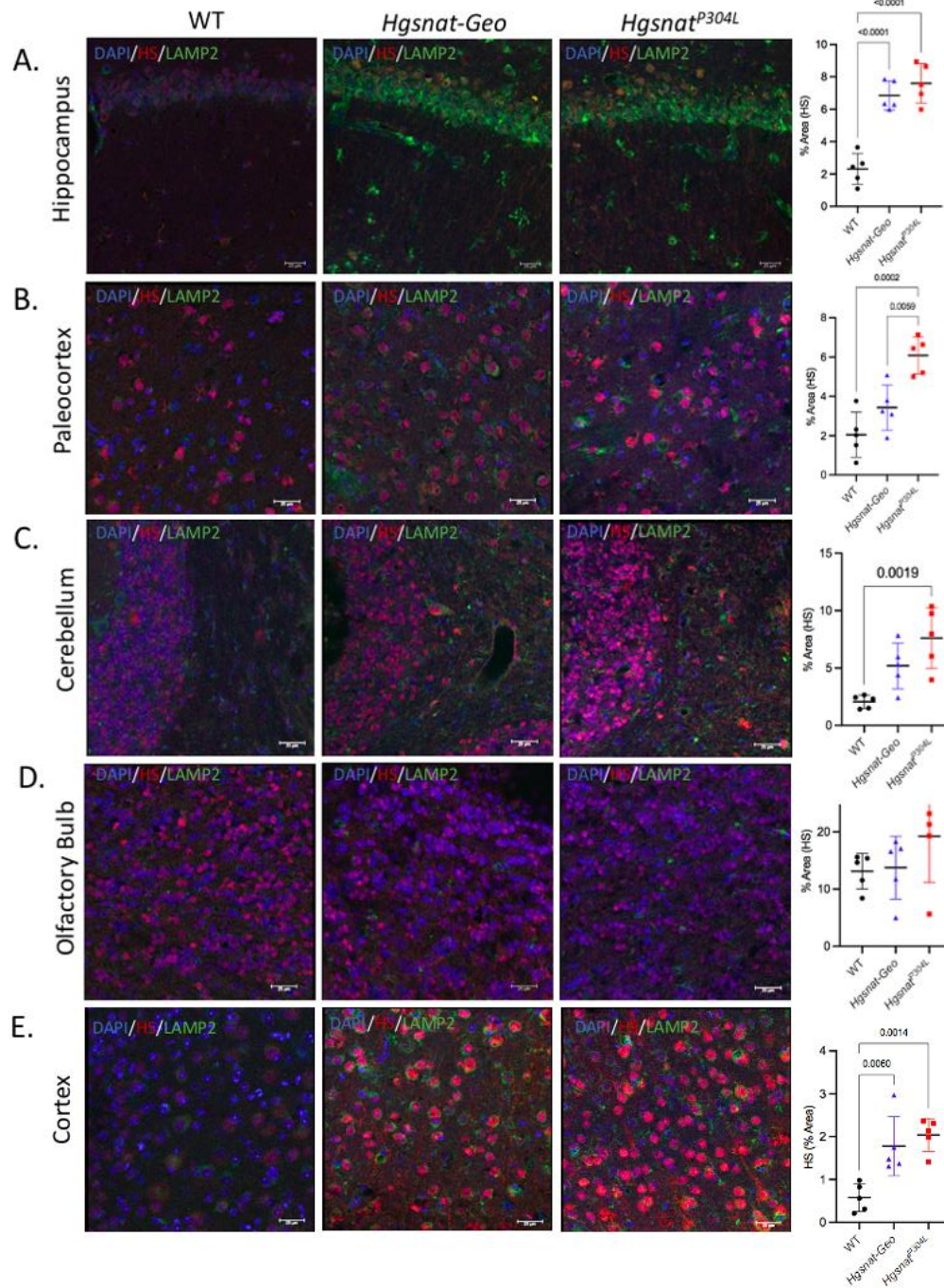


Figure 8. HS is accumulated in the brain of MPS IIIC mice

Brain tissues of 6-month-old WT, *Hgsnat-Geo*, and *Hgsnat*^{P304L} mice were stained against HS (red), LAMP2 (green), and DAPI (blue) in **A)** the hippocampus, **B)** paleocortex, **C)** cerebellum, **D)** olfactory bulb, and **E)** somatosensory cortex. HS storage is increased in the hippocampus, paleocortex, and somatosensory cortex of MPS IIIC mice. Compared to WT, *Hgsnat*^{P304L} mice also showed a higher accumulation of HS in the cerebellum, although *Hgsnat-Geo* mice did not show such a significant increase. The level of HS was similar in the olfactory bulb for different groups of mice. *Hgsnat*^{P304L} mice tend to have more severe storage of HS than *Hgsnat-Geo* mice.

Images were taken with the Leica TCS SPE inverted confocal microscope, with an objective of 40x (scale bar equals 25 μ m). Data on the graph represent the percentage of area stained for HS, and are shown as mean \pm SD, n=5, with significance determined by the One-way ANOVA test followed by Tukey's multiple comparison test.

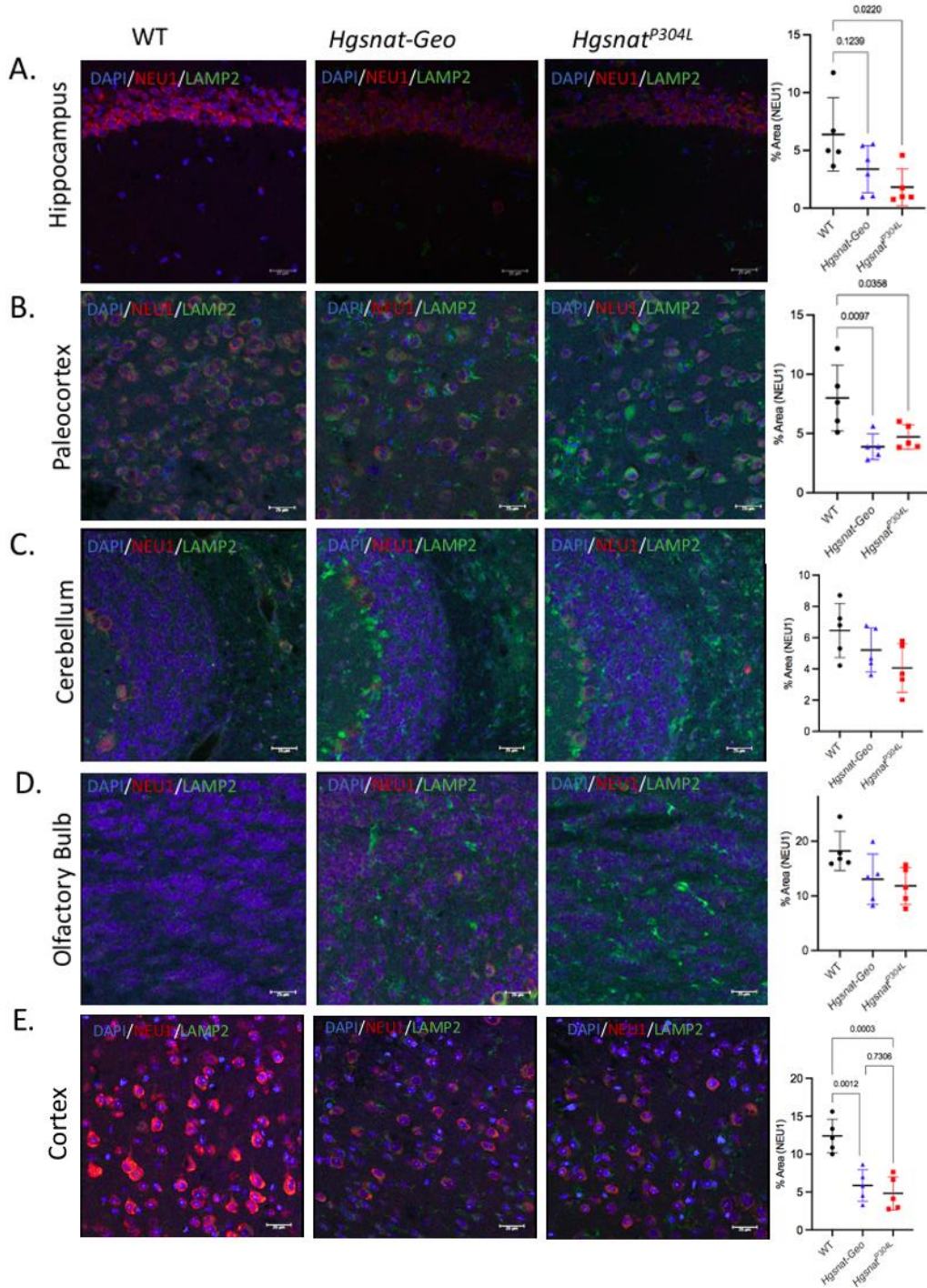


Figure 9. NEU1 is deficient in the brain of MPS IIIC mice

Brain tissues of 6-month-old WT, *Hgsnat-Geo*, and *Hgsnat^{P304L}* mice were stained against NEU1 (red), LAMP2 (green), and DAPI (blue) in A) the hippocampus, B) paleocortex, C) cerebellum,

D) olfactory bulb, and **E)** somatosensory cortex. Immunohistochemical staining of NEU1 is significantly decreased in the hippocampus, paleocortex, and somatosensory cortex of MPS IIIC mice but not in the cerebellum and olfactory bulb. *Hgsnat*^{P304L} mice tend to show a more severe decrease of NEU1 than *Hgsnat-Geo* mice. Images were taken with the Leica TCS SPE inverted confocal microscope, with an objective of 40x (scale bar equals 25 μ m). Data on the graph represent the percentage of area stained for HS, and are showing as mean \pm SD, n=5, with significance determined by the One-way ANOVA test followed by Tukey's multiple comparison test.

Altogether, our results suggest that the accumulation of HS in the brain is associated with a deficiency of NEU1 protein and activity. Furthermore, they show that *Hgsnat*^{P304L} mice typically present a more severe phenotype than *Hgsnat-Geo* mice, showing a higher level of accumulated HS and a more severe deficiency of NEU1. In contrast, in the brain areas with HS levels similar to WT mice, such as the olfactory bulb, NEU1 activity and protein levels are not reduced. These results suggest (but do not prove) that the accumulation of HS may cause the deficiency of NEU1.

Aim 2. NEU1 deficiency can be rescued by reducing HS storage

To further test if the storage of HS causes NEU1 deficiency, we analyzed the brains of *Hgsnat-Geo* mice that were treated with an AAV vector expressing human WT codon-optimized HGSNAT. These experiments, conducted in the laboratory of our collaborator, Dr. Brian Bigger, University of Manchester, UK, demonstrated that in treated mice, HGSNAT deficiency was rescued and HS levels significantly reduced (on average by ~46%) as compared to untreated mice [45]. Four months after the delivery of the AAV, working memory and hyperactivity in AAV-HGSNAT-treated and sham (either PBS or AAV-GFP)-treated *Hgsnat-Geo* mice and in WT mice of matching age and sex were analyzed using Y-maze and Open Field (OF) tests, respectively. AAV-treated *Hgsnat-Geo* mice had significantly improved spatial memory and corrected hyperactivity compared with the sham group [45]. Six months post-treatment, CNS pathology was evaluated in

8-month-old mice by IHC, which revealed a significant decrease in neuroinflammation [45]. We received several perfused frozen brains of AAV-TT-HGSNAT-treated and untreated *Hgsnat-Geo* mice (n=3 for each group) from our collaborators. We measured levels of HS and NEU1 in these samples by immunohistochemistry to test whether the treatment also rescued secondary NEU1 deficiency.

Our results demonstrated that the treatment reduced the storage of HS in the cortex, which was consistent with the results reported by Tordo *et al.* (Fig. 10A). Moreover, the levels of NEU1 also showed a non-significant trend for increase when compared to the untreated *Hgsnat-Geo* mice (Fig. 10B).

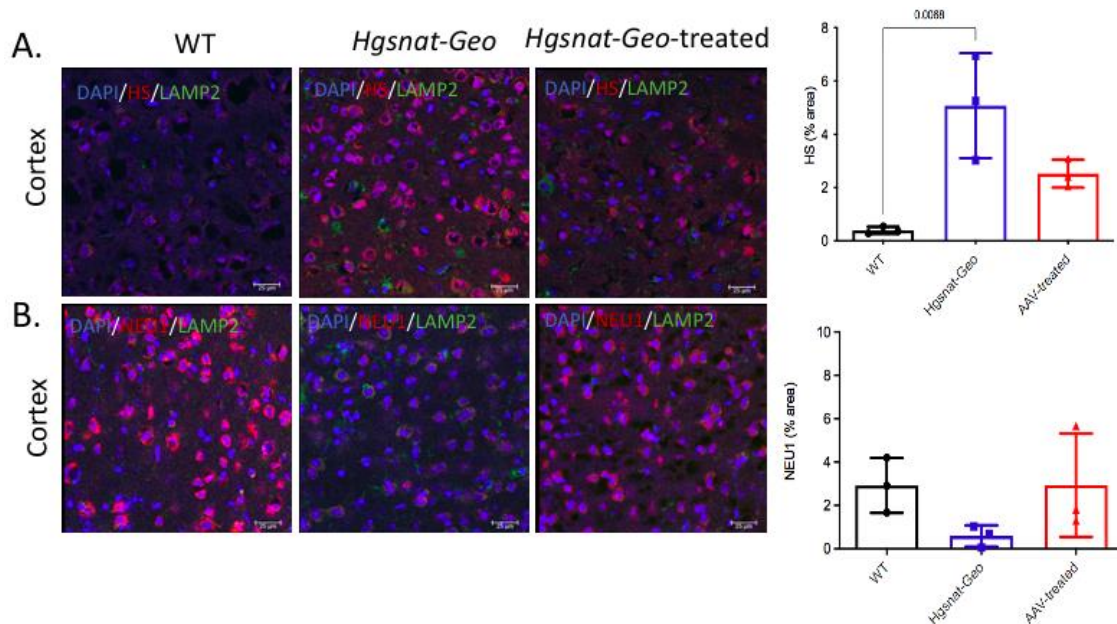


Figure 10. HS storage is reduced and NEU1 levels increased in MPS IIIC mice receiving gene therapy with AAV-TT-HGSNAT vector.

Brain sections of 6-month-old WT, untreated *Hgsnat-Geo* mice, and *Hgsnat-Geo* mice treated with AAV-HGSNAT were stained for **A**) HS (red) and LAMP2 (green) or **B**) NEU1 (red) and LAMP2 (green). Nuclei were counterstained with DAPI (blue). There is a trend for decrease in HS storage and increase in NEU1 levels in the brains of *Hgsnat-Geo* mice receiving the treatment. Images were taken in the SS cortex with a 40x objective; scale bar equals 25 μ m. Data on graphs are presented as means \pm SD, n=3, with significance determined by the One-way ANOVA test followed by Tukey's multiple comparison test.

Aim 3. Treatment of cultured cells with exogenous HS induces NEU1 deficiency

To determine whether an increase in HS storage in lysosomes of cultured cells results in a decrease in NEU1 activity, we treated cultured bone marrow-derived macrophages (BMDM) from WT and *Hgsnat*^{P304L} mice with various concentrations (0, 50, 100, or 300 µg per mL of medium) of HS. After seven days of treatment, cells were harvested and NEU1 activity was measured in the cell homogenates. IHC experiments showed that by treating macrophages from *Hgsnat*^{P304L} mice incapable of degrading HS in the lysosomes, we further increased the concentration of HS in the lysosomal lumen (Fig. 11A and B). The NEU1 activity was reduced in the homogenates of macrophages from both *Hgsnat*^{P304L} and WT mice treated with HS when compared to the levels measured in untreated cells (Fig. 11C and D). For both WT and *Hgsnat*^{P304L} macrophages, higher level of HS caused a more severe decrease in NEU1 specific activity, with the highest NEU1 reduction observed after adding the maximal concentration of HS (300 µg HS/mL of medium) (Fig. 11C). However, in control WT cells, the activity of NEU1 was reduced to the level higher than that in *Hgsnat*^{P304L} macrophages perhaps because some of the endogenously added HS could still be catabolized (Fig. 11C). These data establish a negative causal relationship between HS storage and NEU1 deficiency.

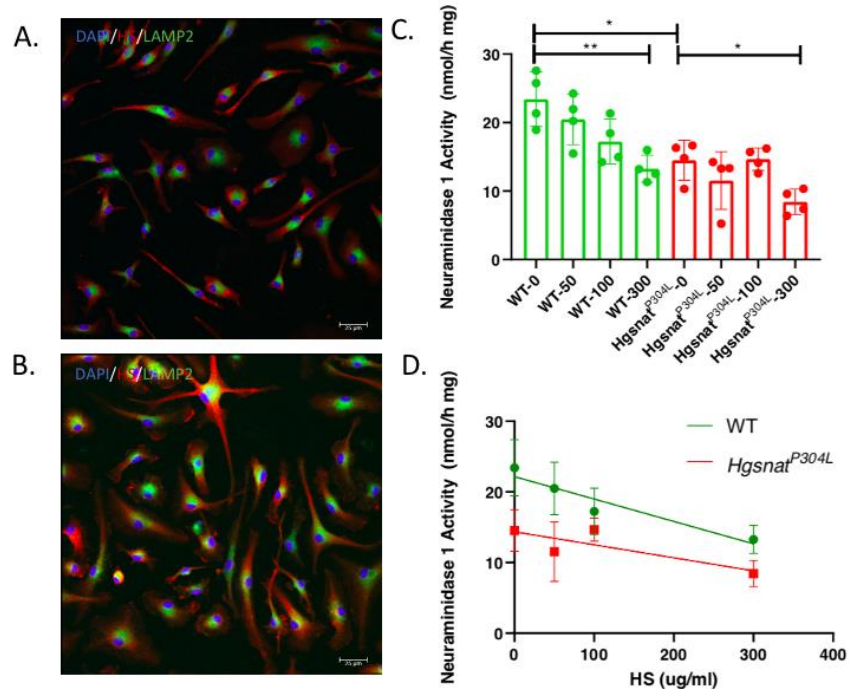


Figure 11. Treatment of BMDM with exogenous HS.

Staining for HS was performed in *Hgsnat*^{P304L} BMDM **A)** untreated or **B)** treated with the exogenous HS (300 µg/mL of media). **C, D)** NEU1 activity was progressively reduced in the presence of increasing concentrations of HS. Confocal images were taken using a 40x objective, scale bar equals 25 µm. Data on graphs are shown as means ± SD, n=4, with significance determined by the unpaired t-test analysis.

Aim 4. Stereotaxic injection of LV-CTSA-NEU1-GFP in the brain of MPS IIIC mice ameliorates behaviour abnormalities and CNS pathology.

Our second hypothesis was that the secondary deficiency of NEU1 in MPS IIIC patients and mice triggers the formation of amyloid plaques and synaptic defects observed in their brains. To test this, we performed a bilateral injection of a lentivirus expressing GFP-tagged-NEU1 and its protector/activator protein, CTSA (LV-CTSA-NEU1-GFP), in the hippocampi and cortices of P18-P19 MPS IIIC mice. In our experience at this age, mice recover well after surgery but still do not show most pathological changes in the CNS, including the formation of amyloid plaques. To optimize the experimental setup, we first injected several WT mice with LV-GFP or LV-CTSA-

NEU1-GFP using different injection coordinates and volumes of the viral vector. We then analyzed the brains one month after the surgery (Fig.12 and 13). In all mice, the GFP-positive areas were measured to assess the diffusion of LV-CTSA- NEU1-GFP in the brain (Fig.14). Based on the obtained results, we set injection coordinates as 1.5 mm M/L, 2.2 mm A/P, 2.2 mm D/V-, and 1.2-mm D/V to better target the CA1 area of the hippocampus and the layers IV and V of the SS cortex. We also conducted enzymatic NEU1 assays in the brain tissues and confirmed that *Hgsnat*^{P304L} mice injected with LV-CTSA- NEU1-GFP tend to show a higher level of NEU1 activity (Fig.15).

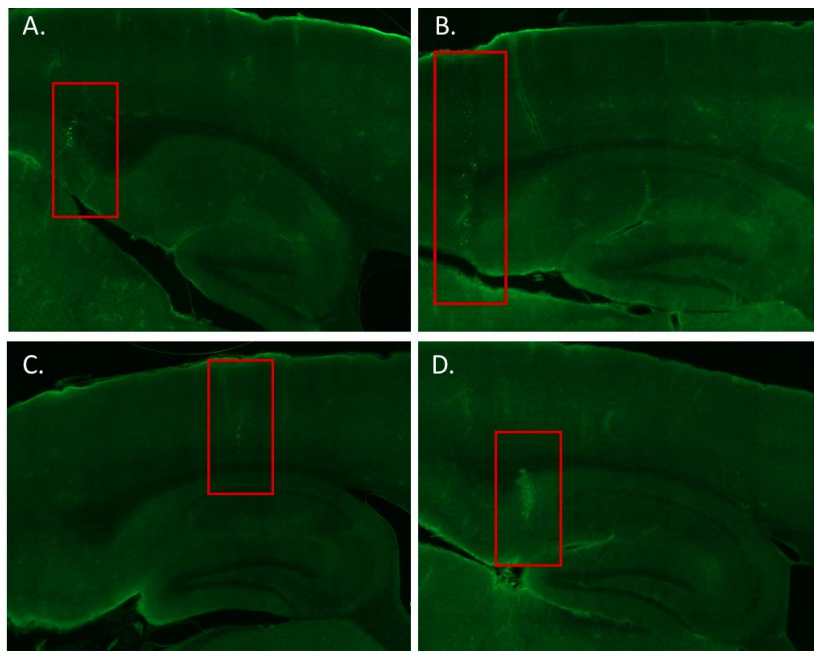


Figure 12. Optimization of injection coordinates and viral volumes

Using the LV-GFP virus, we tested different injection coordinates and viral volumes in four P18 and P19 WT mice. The coordinates were **A)** 1.4 mm M/L, 2.75 mm A/P, 1.2 mm, and 0.8 mm D/V, 300 nL of virus injected, **B)** 1.35 mm M/L, 2.45 mm A/P, 1.5 mm, and 1.0 mm D/V, 350 nL, **C)** 1.7 mm M/L, 2.0 mm A/P, 1.5 mm and 1.3 mm D/V, 400 nL, and **D)** 1.6 mm M/L, 2.5 mm A/P, 1.4 mm and 1.0 mm D/V, 400 nL. Fluorescent images were taken using the Axioscan; red boxes indicate injection sites.

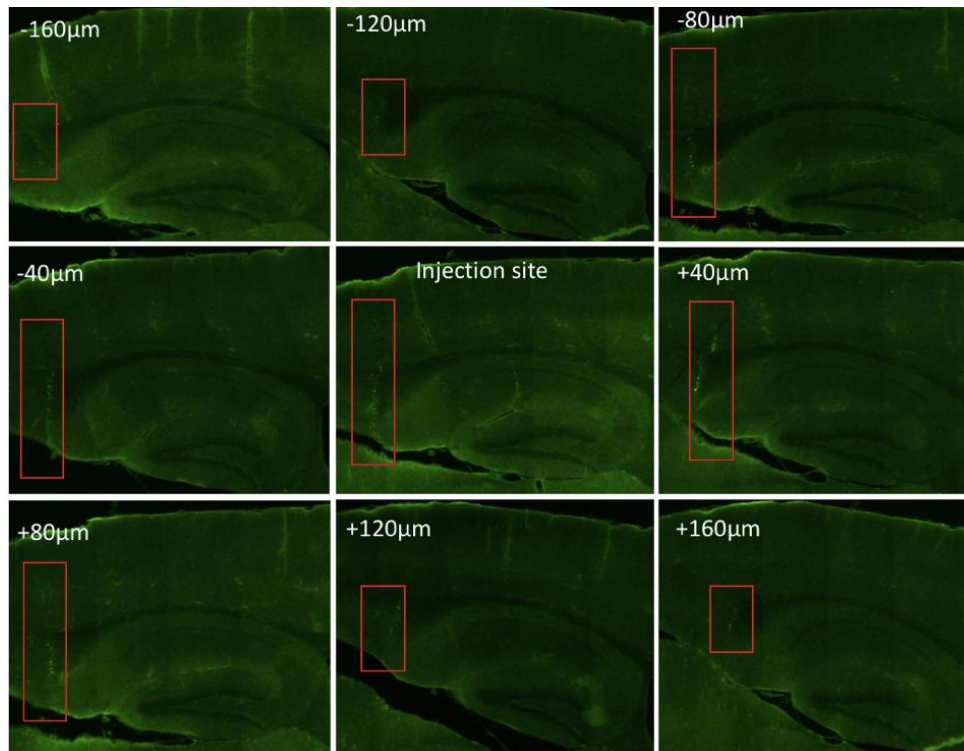


Figure 13. GFP expression in the mouse brain one month after stereotaxic injections of LV-GFP.

GFP expression in the brain slices adjacent to the injection site was assessed one month after the injection of WT P18-P19 mice with 350 nL of the LV-GFP virus at the following coordinates: 1.35 mm M/L, 2.45 mm A/P, 1.5 mm, and 1.0 mm D/V. Red boxes indicate the area of the virus diffusion. Fluorescent images were taken using the Axioscan.

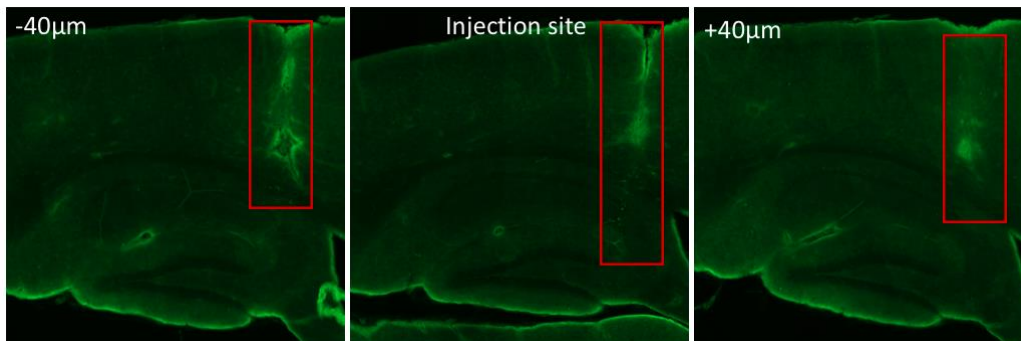


Figure 14. GFP expression in the mouse brain one month after stereotaxic injections of LV-CTSA-NEU1-GFP

GFP expression in the brain slices adjacent to the injection site was assessed one month after the injection of WT P18-P19 mice with 350 nL of the LV-CTSA-NEU1-GFP virus at the following coordinates: 1.35 mm M/L, 2.0 mm A/P, 1.1 mm, and 0.8 mm D/V. Red boxes indicate the area of the virus diffusion. Fluorescent images were taken using the Axioscan.

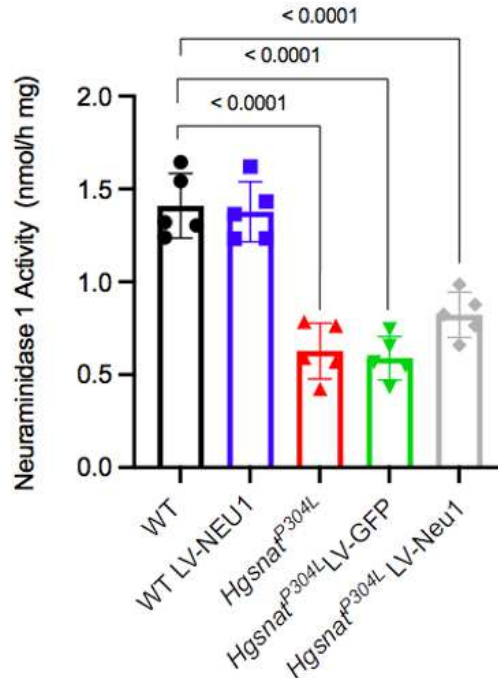


Figure 15. NEU1 activity in the brain of mice one month after stereotaxic injection of LV-CTSA-NEU1-GFP

Hgsnat^{P304L} mice injected with LV-CTSA-NEU1-GFP tend to show a higher level of NEU1 activity when compared to control and sham (LV-GFP)-injected *Hgsnat*^{P304L} mice. Data are shown as means \pm SD, n=5, with significance determined by the One-way ANOVA test followed by Tukey's multiple comparison test.

A) *Hgsnat*^{P304L} mice show partial rescue of behavior abnormalities after stereotaxic injection with LV-CTSA-NEU1-GFP

Six months after the injections, we analyzed the behavior of LV-CTSA-NEU1-GFP injected, sham-injected, and control WT and *Hgsnat*^{P304L} mice using the Y-maze test to measure spatial memory, NOR test to assess short-term memory, and OF test to study activity and anxiety levels. Previous results from our lab have shown that *Hgsnat*^{P304L} mice at six months of age show deficits in spatial memory that can be revealed by the Y-maze test [61]. In our experiments, although we saw a tendency for *Hgsnat*^{P304L} mice to show a lower percentage of alternation than the WT mice, we did not find any significant difference between the control WT mice, WT mice treated with LV-CTSA-NEU1-GFP, control *Hgsnat*^{P304L} mice, and *Hgsnat*^{P304L} mice injected with LV-CTSA-

NEU1-GFP or LV-GFP (Fig. 16). The exact reason of this discrepancy is not known. Still, we speculate that it may be caused by the experimental setup and the lower number of animals studied for each group.

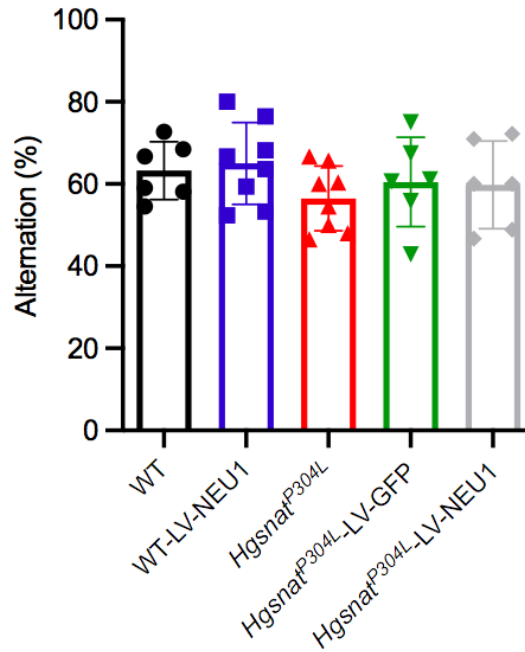


Figure 16. Y-maze test does not reveal a significant difference in the behaviour of WT and MPS IIIC mice at the age of 6 months.

Spatial memory was analyzed using the Y-maze behavioral test in six-month-old WT mice, WT mice injected with LV-CTSA-NEU1-GFP (LV-NEU1), *Hgsnat*^{P304L} mice, and *Hgsnat*^{P304L} mice injected with LV-CTSA-NEU1-GFP or LV-GFP. *Hgsnat*^{P304L} mice tend to show lower percent of successful alternations between the arms of the maze than the WT mice, but no significant difference was observed between the different groups of mice. Data show means \pm SD, $n \geq 6$. Significance was determined by the One-way ANOVA test followed by Tukey's multiple comparison test.

We performed the NOR test to analyze short-term memory as described previously [61]. Both treated and untreated WT groups showed a positive discrimination index, indicating that WT mice spent more time exploring a novel object than a familiar object (Fig.17). In contrast, for untreated and sham-treated MPS IIIC mice, the discrimination index is equal to zero, indicating that they have deficits in short-term memory. *Hgsnat*^{P304L} mice injected with LV-CTSA-NEU1-GFP show a trend for an increase in the discrimination index and novel object exploration time

compared to the untreated and sham-treated *Hgsnat*^{P304L} groups, suggesting that the injection of the LV-CTSA-NEU1-GFP improved the short-term memory (Fig.17).

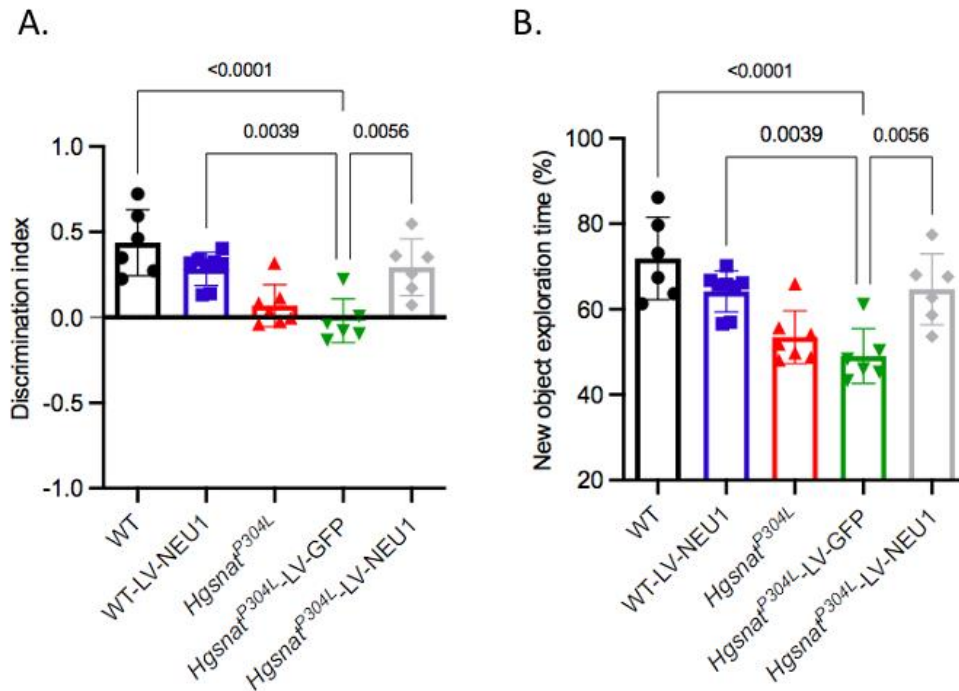


Figure 17. Improvement of the short-term memory in *Hgsnat*^{P304L} mice injected with LV-CTSA-NEU1-GFP.

A) Discrimination index and **B)** the percentage of time spent exploring the novel object were measured using the NOR test in six-month-old WT mice, WT mice injected with LV-CTSA-NEU1-GFP (LV-NEU1), *Hgsnat*^{P304L} mice, and *Hgsnat*^{P304L} mice injected with LV-CTSA-NEU1-GFP or LV-GFP. *Hgsnat*^{P304L} mice injected with LV-CTSA-NEU1-GFP tend to show an improvement in short-term memory with a higher discrimination index and time spent with the new object than control or sham *Hgsnat*^{P304L} mice. Data show means \pm SD, $n \geq 6$. Significance was determined by One-way ANOVA test followed by Tukey's multiple comparison test.

We further used the OF test to study activity and anxiety levels in treated mice. Previous studies by Pan, Taherzadeh *et al.* showed that MPS IIIC mice have hyperactivity and reduced anxiety [61]. Consistent with these results, we found that untreated and sham-treated *Hgsnat*^{P304L} mice crossed the center of the arena more frequently than the WT mice (Fig.18). Whereas untreated *Hgsnat*^{P304L} mice and sham-treated *Hgsnat*^{P304L} mice spent on average 11.69% and 7.27%, respectively, of their time in the center zone, *Hgsnat*^{P304L} mice that received a bilateral injection of

LV-CTSA-NEU1-GFP, spent on average only 3.55% of their time in the center zone (Fig.19A), showing a trend for normalization of anxiety after the treatment with the LV-CTSA-NEU1-GFP virus. Furthermore, *Hgsnat*^{P304L} mice treated with LV-CTSA-NEU1-GFP also showed a trend for a reduction in the percentage distance spent in the zone and in the number of entries to the center zone (Fig. 19B and C, respectively).

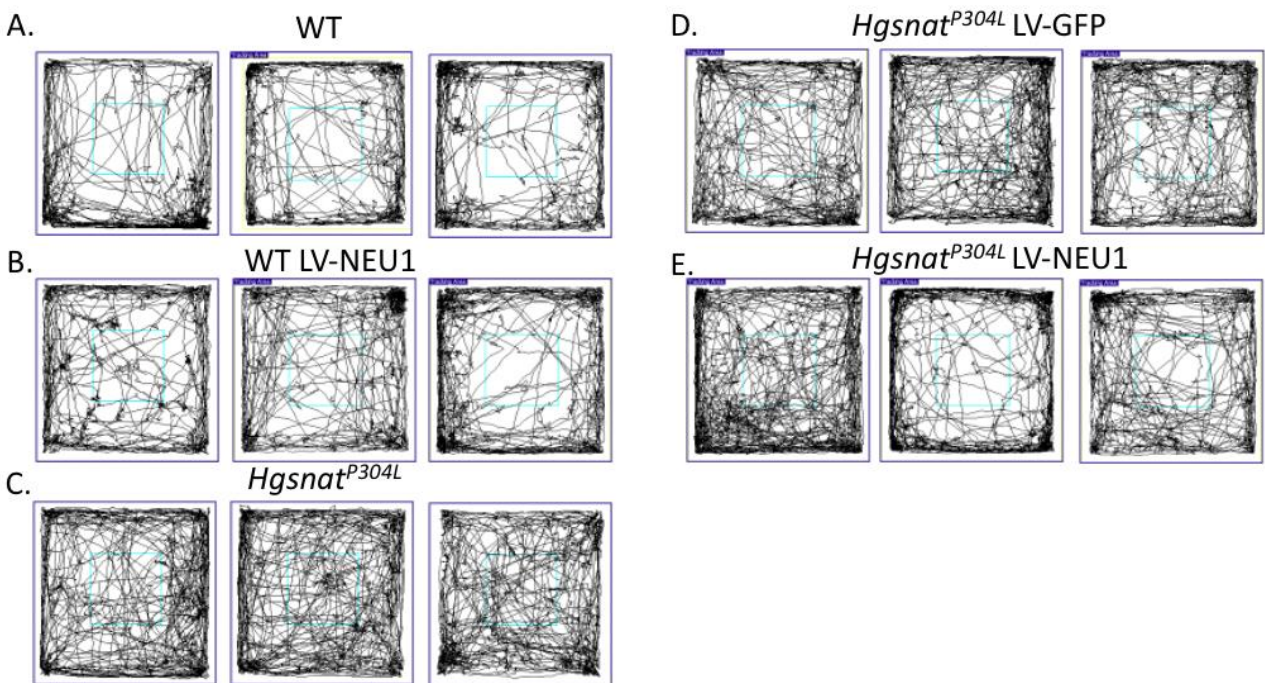


Figure 18. Trajectory traces

Representative traces of the trajectories of **A)** control WT mice, **B)** WT mice injected with LV-CTSA-NEU1-GFP (LV-NEU1), **C)** control *Hgsnat*^{P304L} mice, **D)** *Hgsnat*^{P304L} mice injected with LV-GFP, or **E)** with LV-CTSA-NEU1-GFP virus during the OF test.

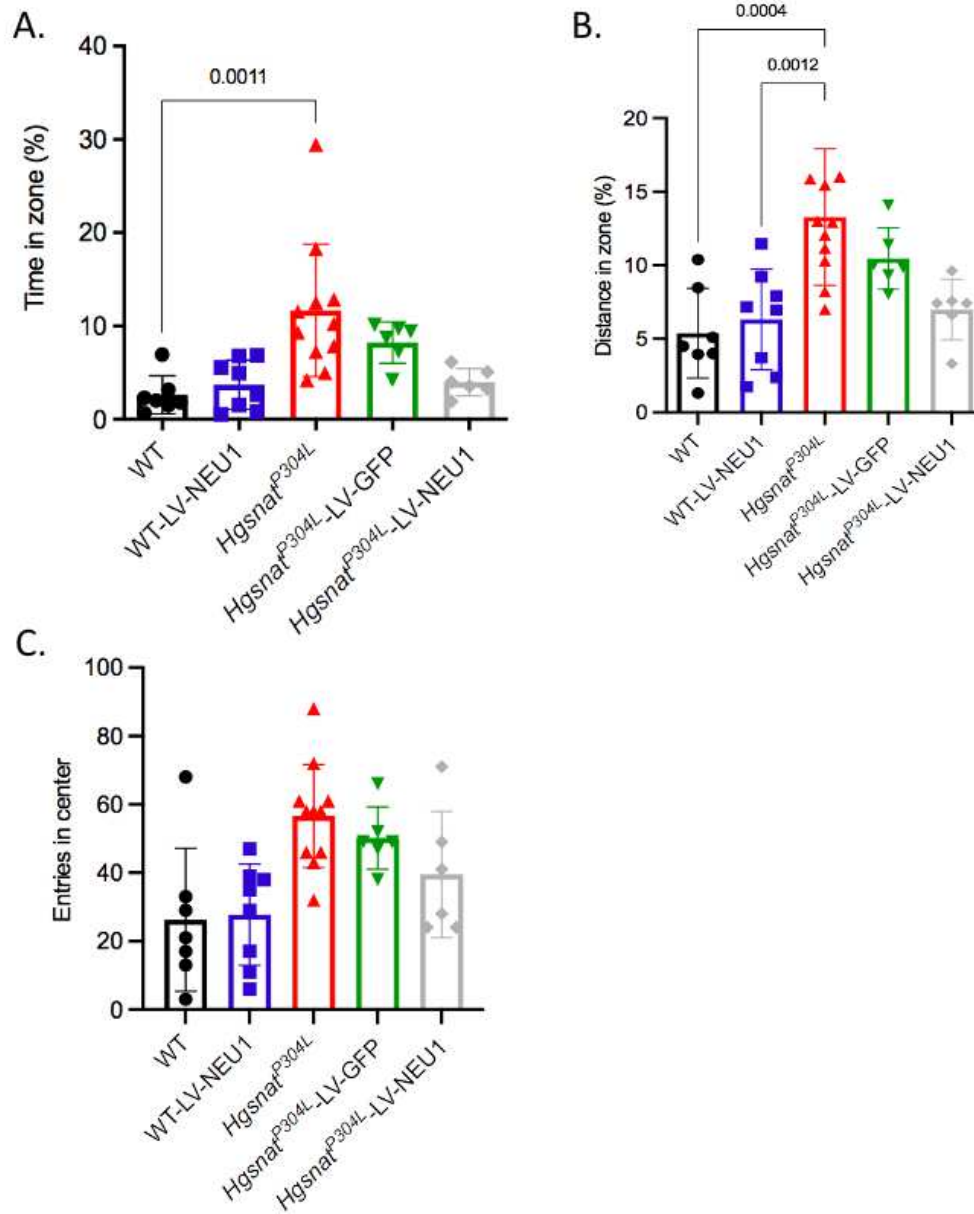


Figure 19. *Hgsnat*^{P304L} mice injected with LV-CTSA-NEU1-GFP show a trend for normalization of reduced anxiety as revealed by OF test.

A) The percentage of time spent in the center of the arena. **B)** The percentage of the distance traveled in the center zone. **C)** Number of entries to the center of the arena. *Hgsnat*^{P304L} mice injected with LV-CTSA-NEU1-GFP (LV-NEU1) showed a trend for normalization of reduced anxiety. Data show means ± SD. Significance was determined by the One-way ANOVA test followed by Tukey's multiple comparison test.

B) Distribution of the NEU1-GFP expression in the mouse brain six months post-injection

Following the behavioral tests, mice were sacrificed and perfused with PFA to fix brain sections. Sagittal brain sections were analyzed by confocal fluorescent microscopy to assess the expression of NEU1-GFP and GFP in the brain areas. Fig.20 and 21 show representative brain images of *Hgsnat*^{P304L} mice that received injections of LV-GFP and LV-CTSA-NEU1-GFP, respectively. Widespread expression of both GFP and NEU1-GFP proteins was observed in the neurons of the hippocampus, especially the granule cells of the dentate gyrus, the hilar mossy cells, and the CA2/CA3 areas (Fig.20 and 21). However, despite our attempts to deliver the virus into the cortex, we could not observe any GFP-positive cells in this area.

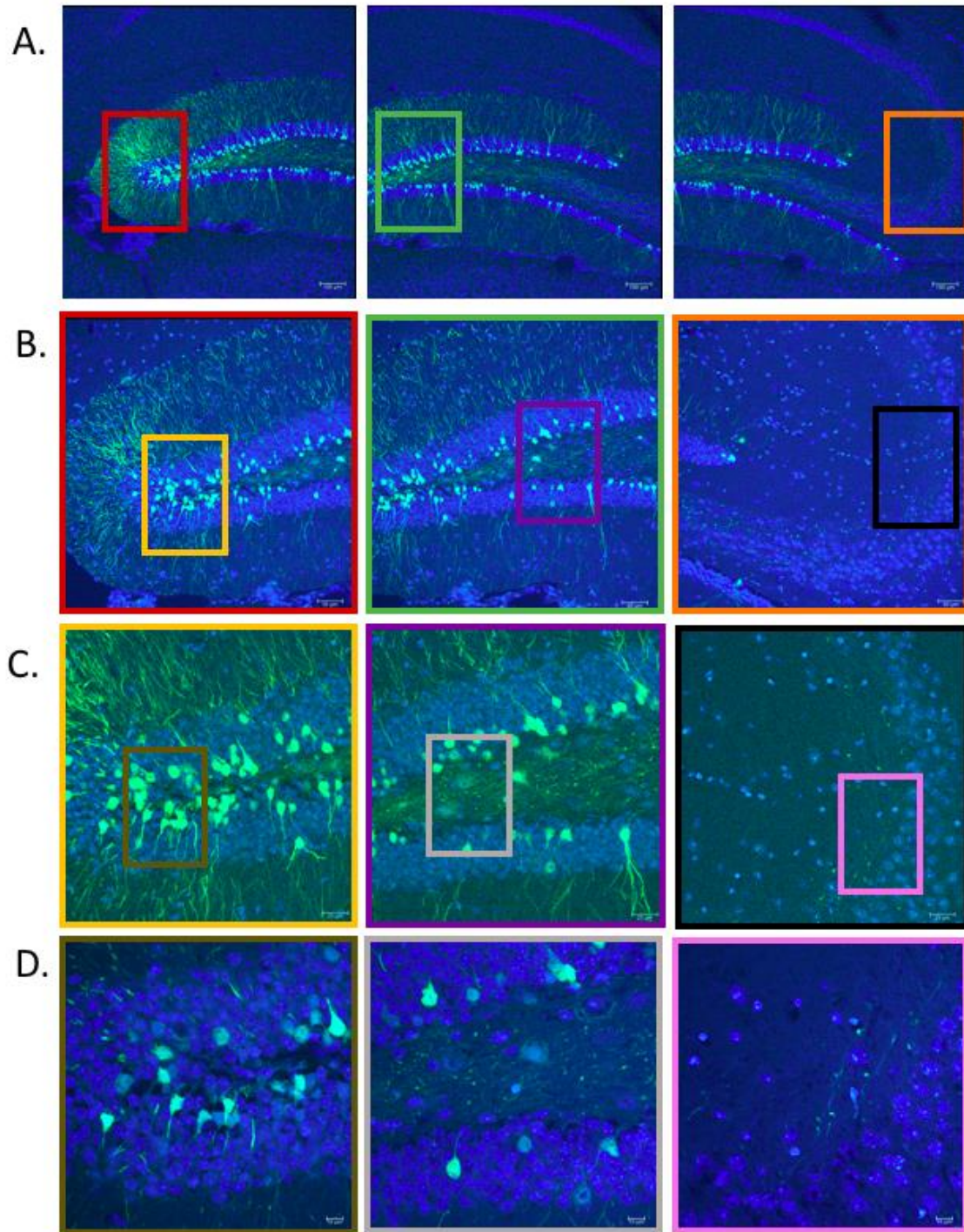


Figure 20. GFP expression in the mouse brain six months after stereotaxic injections of LV-GFP.

Viral expression was assessed six months after injecting 900 nL of the LV-GFP virus. Images were taken using 10x (**A**), 20x (**B**), 40x (**C**), and 63x (**D**) objectives. GFP-mediated fluorescence is shown in green. Nuclei were counterstained with DAPI (blue). Boxes show positions of zoomed areas.

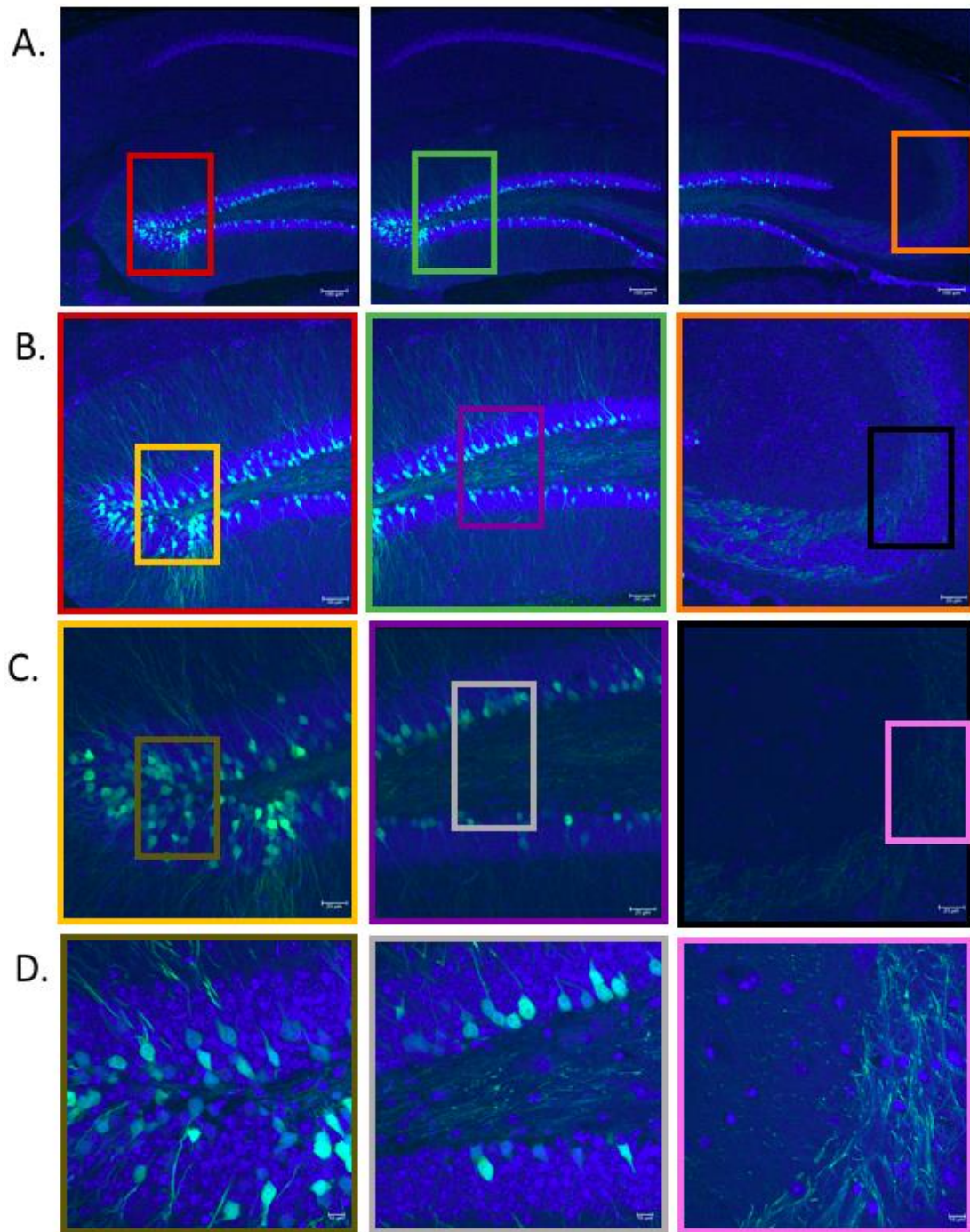
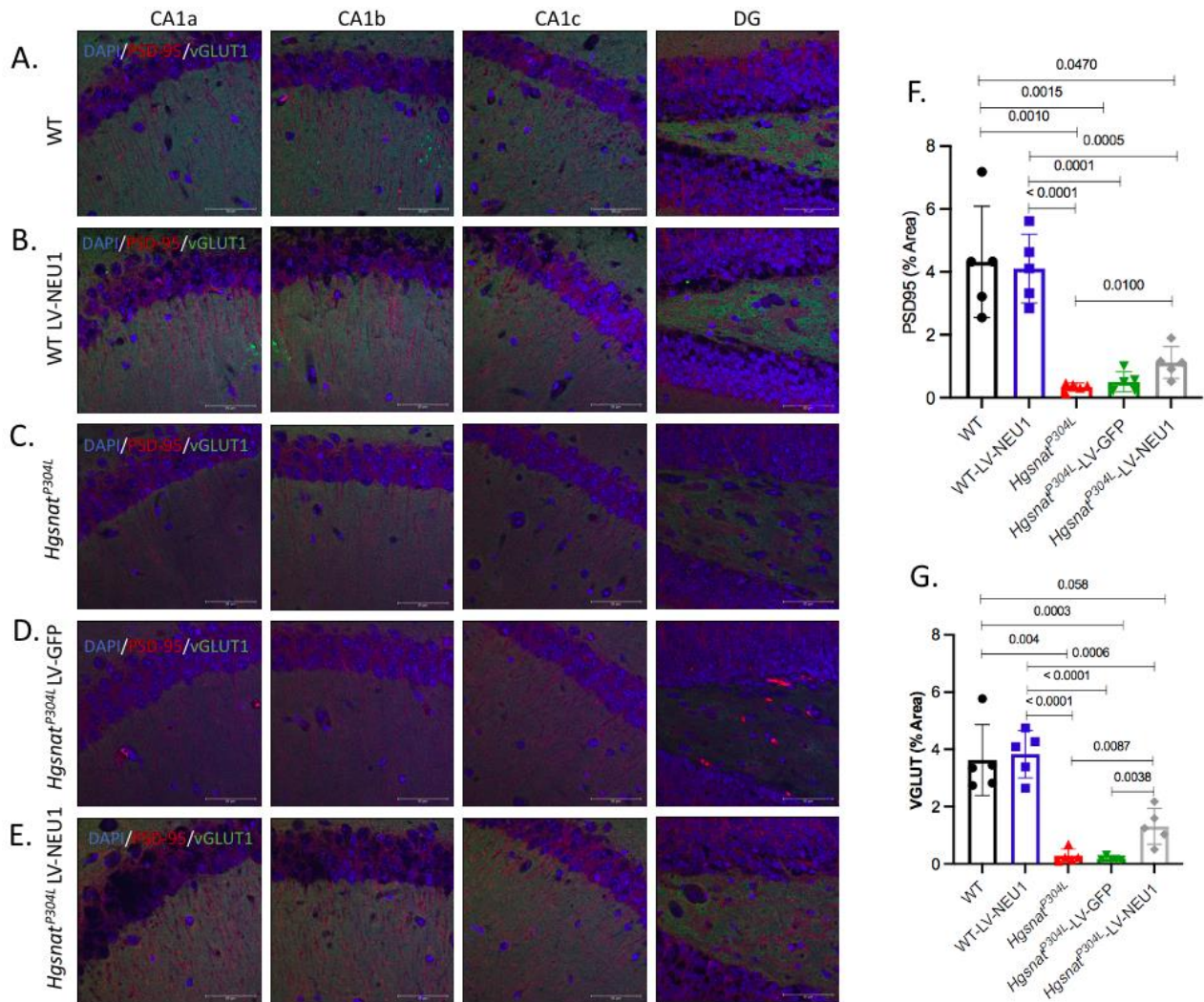


Figure 21. NEU1-GFP expression in the mouse brain six months after stereotaxic injections of LV-CTSA-NEU1-GFP.

Viral expression was assessed six months after injecting 900 nL of the LV-GFP virus. Images were taken using 10x (A), 20x (B), 40x (C), and 63x (D) objectives. GFP-mediated fluorescence is shown in green. Nuclei were counterstained with DAPI (blue). Boxes show positions of zoomed areas.

C) Stereotaxic injection of LV-CTSA-NEU1-GFP partially rescues reduction of synaptic protein markers in the hippocampus of *Hgsnat*^{P304L} mice.

To test if short-term memory improvement in *Hgsnat*^{P304L} mice injected with LV-CTSA-NEU1-GFP was associated with rescuing synaptic defects, we analyzed fixed brain slices for several synaptic protein markers, including VGLUT1, PSD-95, and Syn1, shown to be remarkably decreased in MPS IIIC mice [61]. Our current data consistently demonstrate that with previous findings, VGLUT1, PSD-95, and Syn1 puncta levels in the hippocampi of *Hgsnat*^{P304L} and the sham-treated *Hgsnat*^{P304L} mice are significantly decreased compared to WT mice. The injection of LV-CTSA-NEU1-GFP does not increase the levels of these synaptic markers in WT mice. However, treatment of *Hgsnat*^{P304L} mice with LV-CTSA-NEU1-GFP causes a significant increase in markers of glutamatergic synaptic neurotransmission, VGLUT1, and PSD-95 (Fig.22). The levels of the synaptic vesicular protein Syn1 show a non-significant trend for an increase in *Hgsnat*^{P304L} mice treated with the LV-CTSA-NEU1-GFP (Fig.23).



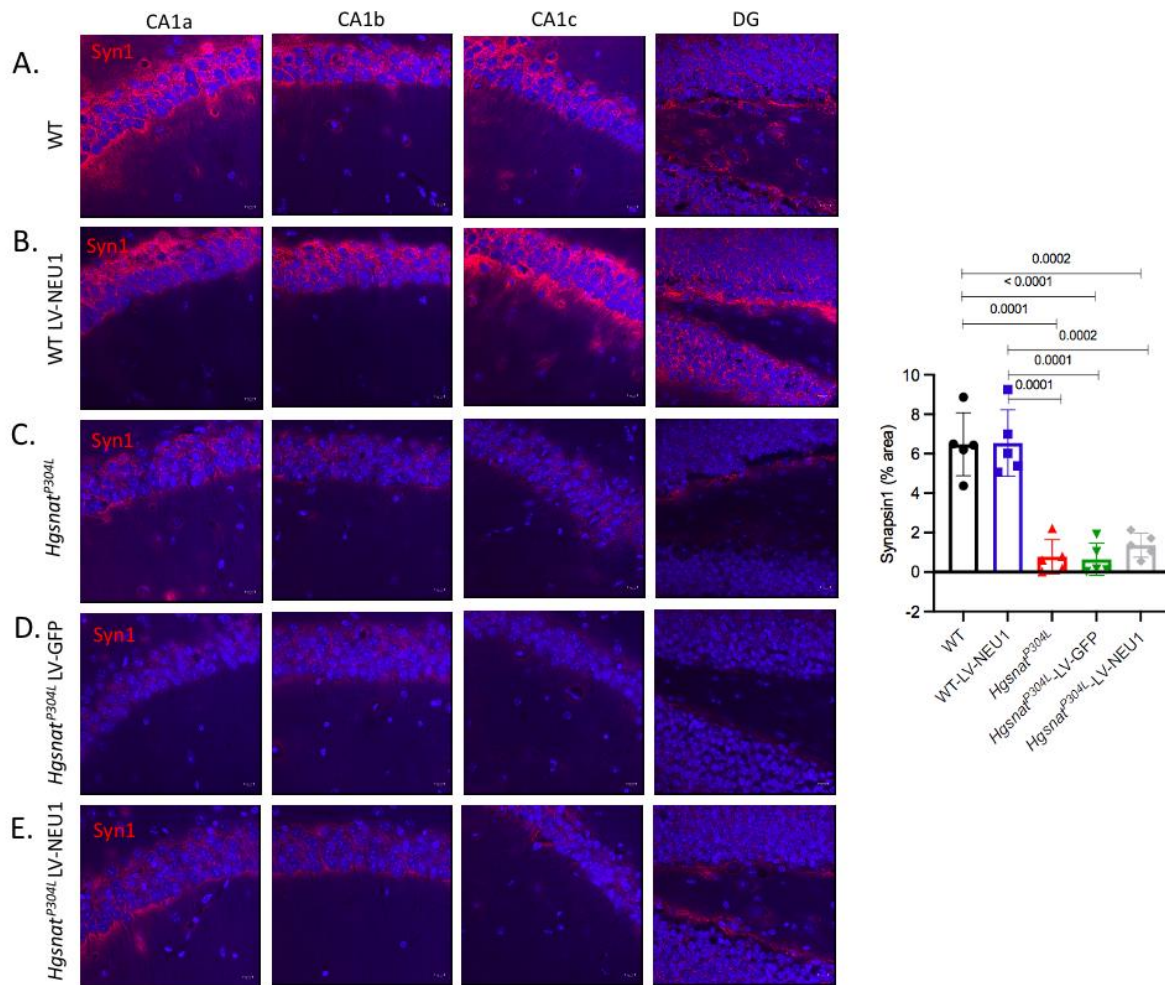


Figure 23. Levels of synaptic vesicle protein marker Syn1 show a trend for increase in the brains of *Hgsnat*^{P304L} mice injected with LV-CTSA-NEU1-GFP

Representative confocal images of four different regions of the hippocampus of **A)** WT mice, **B)** WT mice injected with LV-CTSA-NEU1-GFP (LV-NEU1), **C)** *Hgsnat*^{P304L} mice, **D)** *Hgsnat*^{P304L} mice injected with LV-GFP, and **E)** *Hgsnat*^{P304L} mice injected with LV-CTSA-NEU1-GFP. Brain sections were stained for Syn1 (red). The nuclei were counterstained with DAPI (blue). Confocal images were taken using a 63x objective, scale bar equals 50 μ m. Data on the graphs show means \pm SD, n=5. Significance was determined by unpaired t-test. DG=dentate gyrus.

The formation of amyloid plaques is known to be one of the hallmarks of MPS III [57]. Since previous publications suggested that NEU1 deficiency in the mouse brain may trigger amyloidogenesis, we analyzed whether levels of amyloid protein were reduced in *Hgsnat*^{P304L} mice that received injections of LV-CTSA-NEU1-GFP. Thus, mouse brain sections were stained with the antibody against β -amyloid precursor protein (APP) and analyzed by fluorescent confocal microscopy. Our results, however, demonstrated APP levels in the pyramidal neurons of the

hippocampus (not shown) and the SS cortex (Fig.24) of *Hgsnat*^{P304L} mice injected with LV-CTSA-NEU1-GFP were similar to those in *Hgsnat*^{P304L} and sham-treated *Hgsnat*^{P304L} groups. Finally, we also analyzed the brain slices for the levels of GM2 ganglioside, which shows secondary storage in the brains of MPS III patients and mice. We found no amelioration of this marker in *Hgsnat*^{P304L} mice treated with LV-CTSA-NEU1-GFP (Fig.25) compared with *Hgsnat*^{P304L} and sham-treated *Hgsnat*^{P304L} mice.

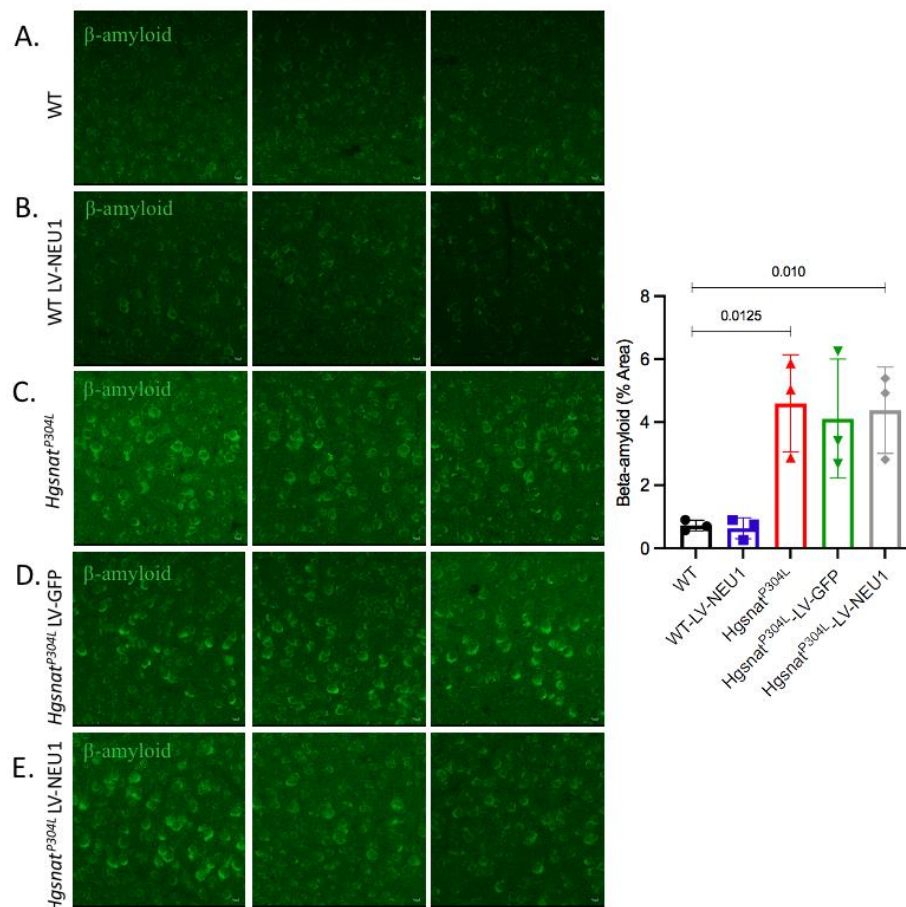


Figure 24. *Hgsnat*^{P304L} mice treated with LV-CTSA-NEU1-GFP show amyloid protein accumulation in level 4 and 5 pyramidal cortical neurons similar to that in *Hgsnat*^{P304L} and sham-treated *Hgsnat*^{P304L} mice.

Representative confocal images of the SS cortex of **A)** WT mice, **B)** WT mice injected with LV-CTSA-NEU1-GFP (LV-NEU1), **C)** *Hgsnat*^{P304L} mice, **D)** *Hgsnat*^{P304L} mice injected with LV-GFP, and **E)** *Hgsnat*^{P304L} mice injected with LV-CTSA-NEU1-GFP. Brain sections were stained with antibodies against APP (green). Confocal images were taken using a 40x objective, scale bar equals 25 μ m. Data show means \pm SD, n=5. Significance was determined by unpaired t-test.

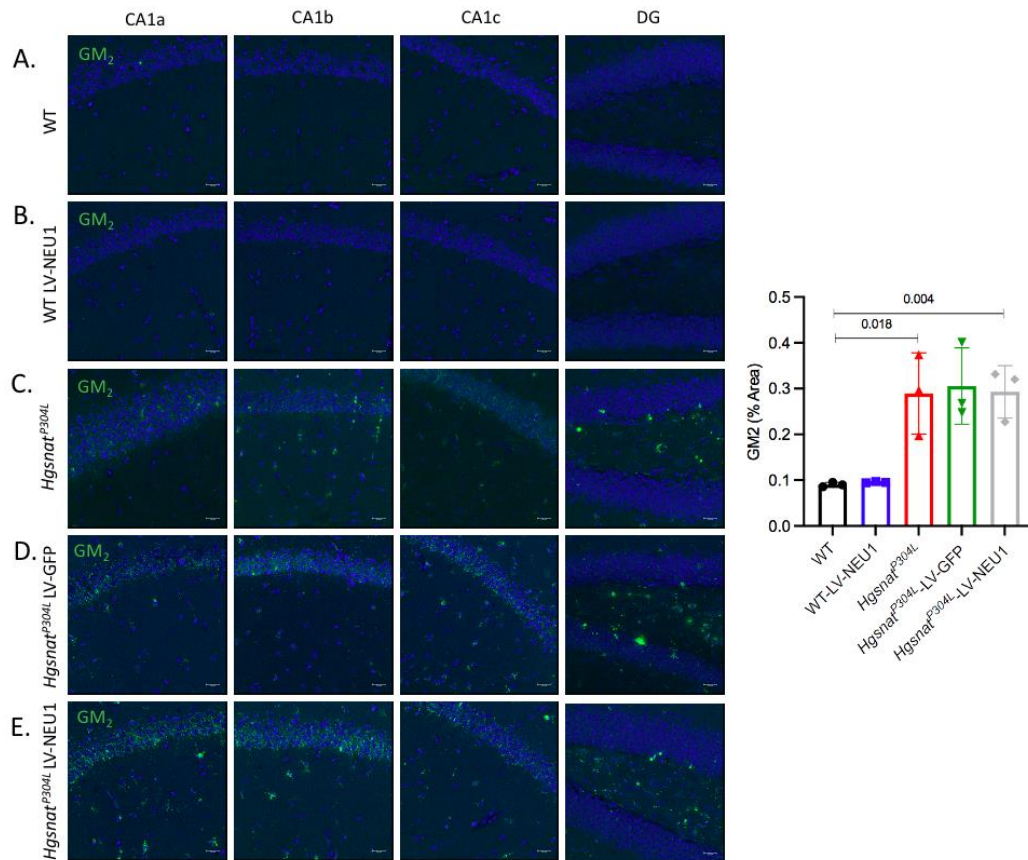


Figure 25. *Hgsnat*^{P304L} mice treated with LV-CTSA-NEU1-GFP show GM2 ganglioside accumulation in pyramidal hippocampal neurons similar to that in *Hgsnat*^{P304L} and sham-treated *Hgsnat*^{P304L} mice.

Representative confocal images of four different regions of the hippocampus of **A)** WT mice, **B)** WT mice injected with LV-CTSA-NEU1-GFP (LV-NEU1), **C)** *Hgsnat*^{P304L} mice, **D)** *Hgsnat*^{P304L} mice injected with LV-GFP, and **E)** *Hgsnat*^{P304L} mice injected with LV-CTSA-NEU1-GFP. Brain sections were stained with antibody against GM2 ganglioside (green). The nuclei were counterstained with DAPI (blue). Confocal images were taken using a 40x objective, scale bar equals 25 μ m. Data show means \pm SD, n=3. Significance was determined by unpaired t-test. DG=dentate gyrus.

Aim 5. No amelioration of synaptic defects in human iPSC-derived cultured cortical MPS IIIA neurons transduced with LV-CTSA-NEU1-GFP.

We used cultured cortical iPSC-derived neurons to test if the rescue of NEU1 deficiency also increases synaptic proteins PSD-95 and VGLUT1 in human Sanfilippo neurons. The induced pluripotent stem cells (iPSCs) were produced by de-differentiating cultured fibroblasts of an MPS IIIA patient and healthy control with matching sex and age as described [63] using the Sendai virus

manufactured by Life Technologies. The iPSCs lines were differentiated into forebrain committed neural progenitor cells (NPC) by dual SMAD inhibition. NPC were induced in neuronal induction media (DMEM/F12) for three weeks and analyzed by ICC to confirm expression of the endoderm markers, Nestin and PAX6, and the neuronal markers, NeuN, axonal β -tubulin III (clone TUJ1) and Syn1. All cells expressed fidelity markers Nestin/Pax6/ Tuj1/ Syn1) and the cortical specific marker T-box, brain 1 (TBR1). Fluorescence-activated cell sorting (FACS) analysis of both control and MPS IIIA lines further confirmed that >80% of cells were TBR1+ and ~72% of cells double NeuN+/ TBR1+ demonstrating a high degree of iPSCs conversion into cortical specific NPC. Increased size and abundance of LAMP2+ perinuclear puncta were detected by immunocytochemistry in MPS IIIA NPC, suggesting increased lysosomal biogenesis/lysosomal storage. Finally, the primary enzymatic defect of SGSH was confirmed at both iPSC and NPC stages. These experiments were performed by the Ph.D. candidate Travis Moore.

NEU1 activity assay revealed that the level of this enzyme in MPS IIIA NPC was drastically reduced compared to the cells obtained from a healthy control (Fig.26).

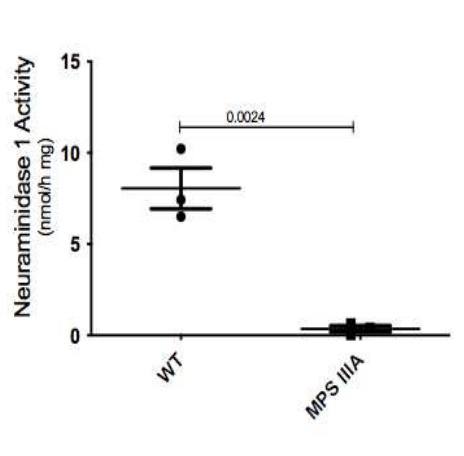


Figure 26. NEU1 activity is significantly reduced in human MPS IIIA NPC.

iPSC-derived neuronal progenitor cells from an MPS IIIA patient show reduced NEU1 activity when compared to cells from a healthy control. The data show means \pm SD, n=3, with significance determined by the unpaired t-test.

On the third day of differentiation, iPSC-derived neurons from an MPS IIIA patient were transduced with the LV-CTSA-NEU1-GFP or control LV-GFP virus at a multiplicity of infection of 10 (MOI 10) for 24 h. After three weeks in culture, the cells were fixed and analyzed by immunocytochemistry using antibodies against PSD95 and VGLUT1 (Fig. 27A). Axons were stained with antibodies against neurofilament medium-size NF-M protein and dendrites with antibodies against MAP2. Quantification of images revealed that untreated MPS IIIA and LV-GFP-transduced MPS IIIA cells have, on average, 16.1 ± 4.9 and 17.8 ± 5.9 PSD-95+ puncta per 10 μm of the axon, respectively. We did not find a significant increase of PSD-95+ puncta in MPS IIIA cells transduced with LV-CTSA-NEU1-GFP, which had on average 20.8 ± 6.2 puncta per 10 μm of the axon (Fig. 27). Healthy control cells had on average 26.7 PSD-95+ puncta per 10 μm of the axon (Fig. 27, dashed line). Similarly, VGLUT1, like PSD-95, did not show a significant increase after the transduction of MPS IIIA cells with LV-CTSA-NEU1-GFP. The average density of VGLUT1+ puncta was 12.6 ± 2.7 per 10 μm as compared to 9.9 ± 3.0 puncta per 10 μm in control MPS IIIA cells, 10.0 ± 2.7 puncta per 10 μm in MPS IIIA cells transduced with LV-GFP, or 15.1 VGLUT1+ puncta in healthy control cells (Fig. 27, dashed line). Since neuraminidase activity has also been linked to higher levels of BDNF release in response to stress [79], we also stained cells against BDNF. We did not, however, find any significant difference between the different groups of cells (Fig. 27B).

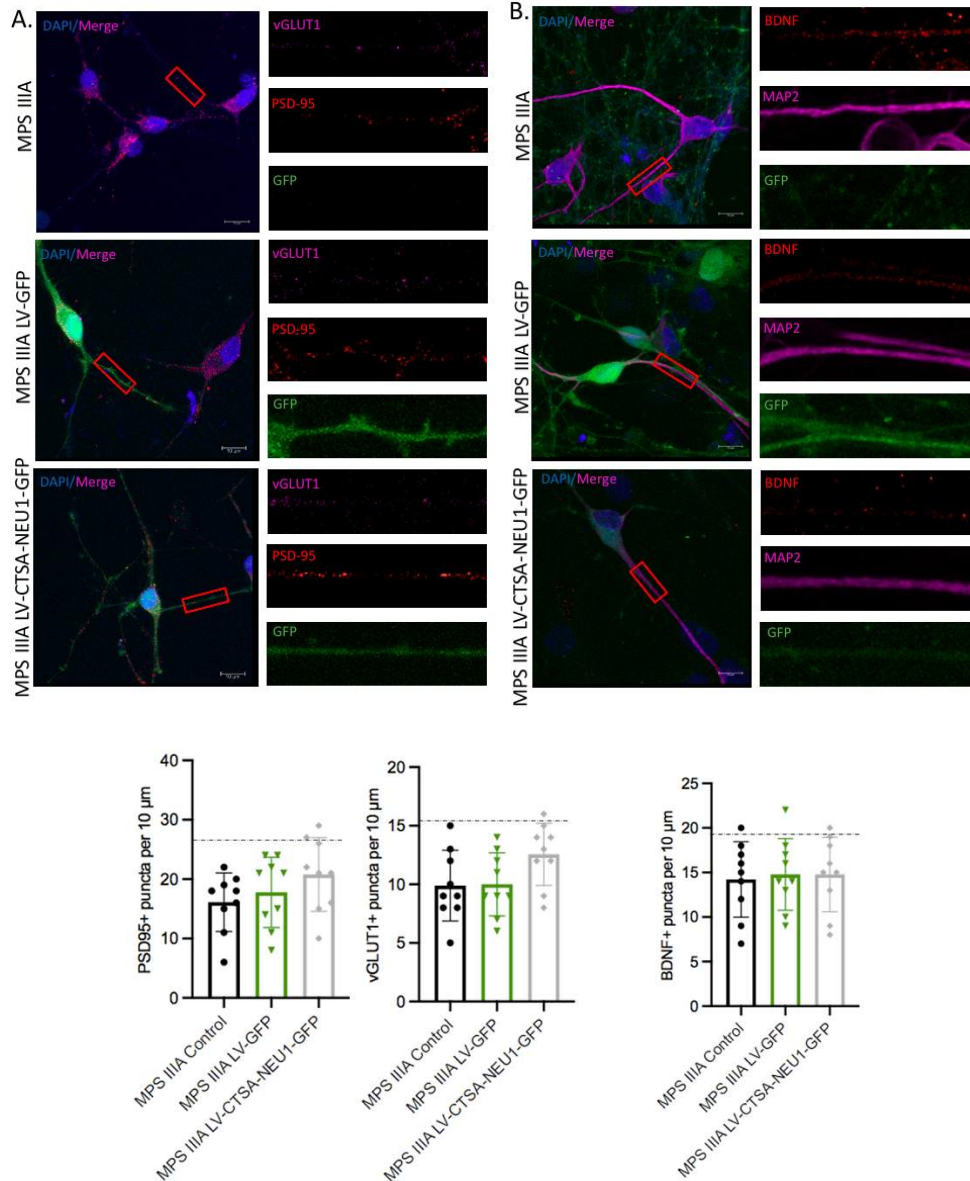


Figure 27. LV-CTSA-NEU1-GFP-transduced human cultured MPS IIIA neurons do not show amelioration of synaptic defects.

A) MPS IIIA iPSC-derived neurons transduced with LV-CTSA-NEU1-GFP do not show higher densities of PSD-95+ (red) and vGLUT1+ puncta (magenta) than control MPS IIIA cells. **B)** No difference was observed in the amount of BDNF+ puncta (red) between LV-CTSA-NEU1-GFP-transduced cells, control MPS IIIA cells, and LV-GFP-transduced cells. Dash lines represent the mean puncta value in healthy control cells. Confocal images were generated by combining 10 Z-stacks, taken at a distance of 0.5 μm using a 63x objective and 2x digital zoom. Scale bar equals 10 μm. Puncta were counted manually along the axon at 30 μm increments starting from 10 μm away from the soma and averaged to 10 μm. Graphs show means ± SD, with significance determined by the One-way ANOVA test followed by Tukey’s multiple comparison test.

CHAPTER 4

DISCUSSION

Substantial scientific evidence highlights the essential roles HS plays in the normal development of the CNS as a part of the glycan chains of proteoglycans. Heparan sulfate proteoglycans (HSPGs) have been shown to connect to various synaptic adhesion proteins during development to promote synaptic assembly and neural activity [94]. In contrast, the removal of HS chains associated with the HSPG protein core has the effect of disrupting synaptic assembly [94]. As one of the major components of the extracellular matrix (ECM), HSPGs also play key roles in maintaining the architecture of the ECM, regulating the differentiation, proliferation, and migration of cells as well as interacting with protein ligands through HS side chains during cell-cell signaling [95,96]. HS is also involved in other fundamental physiological processes such as pregnancy, feeding behavior, and embryonic development [97, 98]. Despite the diverse functions that HS plays in the CNS, the accumulation of free undegraded HS oligomers that occurs in neurological MPS diseases has been proposed to play a crucial role in neurodegenerative processes in the CNS. From inducing widespread neuroinflammation through interactions with the TLR4 and MyD88, promoting the formation of protein aggregates, or interacting with tau proteins, the accumulation of HS was shown to contribute to neurodegeneration through multiple pathways [66,67,99]. The present study reveals a novel pathophysiological pathway associated with the accumulation of HS. We demonstrate that the storage of HS in the lysosomes causes a secondary deficiency of NEU1, which could be one of the potential causes of synaptic defects documented in most neurological MPS.

Our data show that unlike other lysosomal enzymes, which activity is increased in the cells with lysosomal storage because of increased lysosomal biogenesis, the total acidic neuraminidase

activity is reduced in the brain and visceral organs of MPS IIIC mice. Since NEU2 has a neutral pH optimum and is mainly expressed in the placenta and testis [47], we speculated that this result reflects a reduction in the expression of one (or several) of the three remaining neuraminidases, NEU1, 3, or 4. We further confirmed that NEU1 was the isoenzyme showing the secondary deficiency in the tissues of MPS IIIC mice by conducting enzymatic assays in the presence of the NEU3 and NEU4 inhibitor, C9-4BPT-DANA. We further analyzed the levels of NEU1 activity and the NEU1 protein in the different brain regions of MPS IIIC mice. We found a correlation between the levels of HS storage and NEU1 reduction. Surprisingly, the kidney of MPS IIIC mice did not show a decrease in NEU1 activity, and this could be related to a less severe accumulation of HS in this organ. While the liver and the brain showed widespread intracellular storage, lysosomal storage was less evident in the kidney, which had relatively low levels of stored HS [68]. Similarly, when we stained different brain sub-regions of MPS IIIC mice against NEU1 and HS, we found that NEU1 was not deficient in the olfactory bulb, an area in which HS was not accumulated.

To determine if there was a causal relationship between HS storage and NEU1 deficiency, we treated cultured cells with different concentrations of exogenous HS purified from the urine of MPS IIIC patients and measured NEU1 activity in the treated and untreated cells. For this experiment, we used cultured bone marrow-derived macrophages (BMDM) because these cells are known to endocytose exogenous HS, internalize it in the lysosomes and partially degrade the polymer by reducing the polymer length [69]. We have chosen to use HS isolated from MPS IIIC patients' urine which contains high levels of partially digested HS oligomers similar to those accumulated in the brain microglia and neurons [101]. This provides an advantage over the use of

purified commercial HS since it models better the situation in the brain [70]. Our data revealed a reduction of NEU1 activity in the cells treated with HS that was proportional to HS levels in the culture medium. In contrast, when the primary genetic defect and the storage of HS in the brain of MPS IIIC mice is corrected by gene therapy with the AAV-HGSNAT vector that encodes for the wild-type HGSNAT enzyme, the levels of NEU1 were rescued, proving that the primary storage of HS caused NEU1 deficiency.

Previously, we also confirmed that NEU1 deficiency was due to alterations in the post-transcriptional mechanisms since the level of *Neu1* mRNA was not significantly different between our MPS IIIC mice and control WT mice [52, unpublished]. Importantly, HS also could not inhibit purified NEU1 in vivo [unpublished]. We, therefore, hypothesized that HS accumulation in the lysosomes resulted in the disruption of the NEU1 complex with CTSA, lysosomal β -galactosidase/GLB1, and N-acetyl-galactosamine-6-sulfatase/GALNS (so-called lysosomal multienzyme complex or LMC), resulting in the loss of enzymatic activity and rapid proteolytic degradation of NEU1 causing its deficiency [102]. Indeed, analysis of protein extracts of MPS IIIC mouse brains by size-exclusion chromatography, conducted in our laboratory after completing my M.Sc. project, confirmed that the LMC was disrupted [52, unpublished]. This opened a new line of investigation because the disruption of LMC in human sialidosis patients also causes rapid degradation of GLB1 and results in secondary deficiency of GALNS [103]. In the mouse galactosialidosis and MPS IIIC cells, GLB1 is not reduced [104]. Still, the most recent data from our lab confirmed lysosomal β -galactosidase deficiency in human iPSC-derived neurons of MPS IIIA patients, thus extending the effect of HS accumulation to another lysosomal enzyme.

After confirming that HS accumulation causes secondary deficiency of NEU1, my next goal was to establish whether this effect has any pathophysiological consequences in the CNS. Since NEU1 removes sialic acids and PSA from sialoglycoconjugates on neuronal surfaces during neuronal activity, and since this process was reported to be necessary for the proper formation of synapses [51], we hypothesized that the secondary NEU1 deficiency could be involved in the appearance of synaptic defects seen in neurological MPS. We thus performed stereotaxic injections of LV expressing CTSA and GFP-tagged NEU1 in the hippocampus of P18 and P19 *Hgsnat*^{P304L} mice to study the effects of overexpressing NEU1 on synaptic transmission. The advantage of stereotaxic injection is that it targets lentivirus to specific brain regions with excellent spatiotemporal control [71]. Due to high reproducibility, stereotaxic surgeries allow the infusion of lentivirus into similar areas in different mice, making inter-animal comparison plausible. In our experiments, GFP-positive and NEU1-GFP-positive cells were observed mainly in the dentate gyrus. They could be identified as the granule cells, the hilar mossy cells, and the pyramidal neurons of the CA2/CA3 areas. Immunohistochemical staining against pre- and postsynaptic markers of glutamatergic synapses, VGLUT1 and PSD-95, revealed that *Hgsnat*^{P304L} mice injected with the LV-CTSA-NEU1-GFP virus showed higher levels of both synaptic markers in the hippocampus consistent with amelioration of glutamatergic synaptic transmission. Furthermore, the number of Syn1+ puncta also showed a trend for an increase in the cells overexpressing NEU1 in the mouse brain. Similar results were observed in human iPSC-derived MPS IIIA neurons transduced with the LV-CTSA-NEU1-GFP virus.

We further tested whether the secondary NEU1 deficiency could contribute to other pathological CNS changes reported in the MPS III patients and mice, including the accumulation

of sialylated sphingolipids (gangliosides) and misfolded amyloid protein. We could not detect any reduction of the secondary storage of GM2 ganglioside in the cells overexpressing NEU1, which suggested that the NEU1 deficiency did not contribute to the impairment of ganglioside catabolism and autophagy in MPS IIIC neurons. However, our experiments neither confirmed nor rejected the link between NEU1 deficiency and amyloidogenesis. In MPS IIIC mice, the accumulation of misfolded amyloid protein occurs mainly in the level 4 and 5 pyramidal neurons of the SS cortex [61]. Despite our attempts to inject the LV in this area, we did not observe any GFP-positive cells in the cortex. Thus, although β -amyloid staining was similar in untreated *Hgsnat*^{P304L} mice and *Hgsnat*^{P304L} mice treated with LV-CTSA-NEU1-GFP, we cannot exclude that the absence of the effect was not due to the lack of NEU1 expression. In contrast, the hippocampal neurons strongly positive for GFP or NEU1-GFP did not have any APP accumulation in the first place.

A plausible explanation for the lack of infection in the SS cortex could be that our LV preferentially infected young and dividing cells. While adult neurogenesis occurs frequently in the dentate gyrus of the hippocampus, the existence of neurogenesis remains a debate in the cortex. Further experiments involving specific transduction of cortical neurons with the virus expressing NEU1-GFP should be performed to test our hypothesis on the involvement of NEU1 deficiency in amyloidogenesis.

When planning such experiments, one should also consider that a possible pitfall of using lentiviral vectors is the extent of their diffusion. In general, the inefficient viral distribution to neurons from the injection site remains one of the main obstacles associated with gene therapy for neurological diseases [reviewed in 72]. Adeno-associated viruses spread further away from the

injection site than lentiviruses due to their smaller sizes. However, the packaging capacity of AAV vectors is only limited to 4.7-5.0 kb in length [73]. To achieve the efficient overexpression of NEU1, we would need to use two different AAV vectors, one encoding for NEU1-GFP and a second vector encoding for the protective protein CTSA, which is required for the activation and stability of NEU1, instead of using one LV-CTSA-NEU1-GFP. The expression of the NEU1 would thus require co-infection of the same neuron with both vectors, which would be a much less frequent event. Therefore, we resolved to use lentiviruses instead, which also provide an advantage of a life-long expression of the transgene since it is incorporated into the genome of the host cells.

Consistent with an increase in the levels of glutamatergic synaptic proteins, we also observed an improvement in short-term memory and partial rescue of reduced anxiety in *Hgsnat*^{P304L} mice treated with LV-CTSA-NEU1-GFP. The partial improvement of behavior could directly be related to the increased NEU1 activity and amelioration in glutamatergic neurotransmission in the hippocampus. Many studies have shown substantial contributions of NEU1 in both hippocampus and memory processing developments. For instance, Sajo *et al.* reported that NEU1-dependent degradation of PSA is required for the proper lamination of granule cells [51]. Because PSA are large volume negatively charged sugar polymers, the presence of PSA on immature granule cells reduces interactions between the cells and thus facilitates their migration in the dentate gyrus. When immature granule cells reach their correct location, which is the innermost layer of the granule cell layer (GCL), NEU1 cleaves PSA from these cells, thereby terminating their migration [51]. Since granule cells are the primary recipients of inputs from the entorhinal cortex and thus are part of the first step in the information processing that ultimately leads to memory formation, we think that by increasing the NEU1 levels in the hippocampi of *Hgsnat*^{P304L} mice, we contributed to the correct lamination of granule cells. Subsequently, this

would induce the formation of synaptic connections with other hippocampal neurons, thus improving short-term memory in MPS IIIC mice. Additionally, there is substantial evidence that granule cells use glutamate as their primary neurotransmitter, consistent with an increase in the density of both excitatory markers VGLUT1 and PSD-95 [reviewed in 74].

Another possibility is that NEU1 overexpression in the hippocampus of *Hgsnat*^{P304L} mice contributes to the desialylation of neuronal cell surface during memory formation. It has been suggested that the levels of protein sialylation in the brain are not static but change dramatically during development and in response to physiological conditions [75]. It was proposed that neuraminidases, including NEU1, may be partially responsible for these changes. For instance, Minami *et al.* reported drastic induction of neuraminidase activity in the mossy fiber terminals in the dentate gyrus's hilus and CA3 regions during memory processing [75]. Moreover, the injection of a pan-neuraminidase inhibitor DANA in the hippocampus of rats caused an impairment of long-term potentiation (LTP) and increased escape latency in the Morris water maze test [75]. The importance of regulating brain protein sialylation by NEU was further demonstrated by Savotchenko *et al.* [76]. In their experiments, pharmacological downregulation of NEU activity resulted in a significant decrease in LTP, an increase in short-term depression, and an alteration of synaptic plasticity [76].

Similarly, Minami *et al.* found that NEU activity was increased on a time scale of seconds after neuronal excitation and that removing sialic acid on the neuronal surface was critical for hippocampal memory formation in a contextual fear-conditioning paradigm [77]. Since the hippocampus is also known to modulate anxiety by interacting with both cortical and subcortical

areas involved in emotion and stress responses, we propose that NEU1 overexpression in the hippocampus of *Hgsnat*^{P304L} mice contributed to the regulation of hippocampal excitability and plasticity in response to stressful conditions [78]. The clearance of PSA in the brain by NEU1 after acute stress was demonstrated by the studies of Abe *et al.*, who found that cells, including microglia and astrocytes, release NEU1 in the form of exosomes to cleave PSA in the brain in response to stressful events [79]. Their data also indicated that the release of NEU1 induces the secretion of BDNF and other neurotrophic molecules essential to cope with stress conditions [79]. Altogether, these experiments demonstrate the importance of NEU1 for regulating sialic acid and PSA levels on brain cell surfaces during neuronal activity associated with both memory formation and anxiety-related behaviors. We, therefore, stipulate that reduction in the activity of endogenous NEU1 related to HS storage in neurological MPS disorders, followed by abnormal regulation of sialic acids and PSA, can substantially modify hippocampal synaptic transmission and plasticity and thus may be the cellular correlate of behavioral and cognitive impairment.

CHAPTER 5

CONCLUSION

It is unlikely that a single mechanism can explain the whole spectrum of pathological CNS changes and deficits observed in MPS diseases. While several pathophysiological pathways associated with CNS pathology in MPS III have already been identified, our research delineates a novel mechanism explaining synaptic defects and neurodegeneration through a secondary deficit of NEU1. By implicating our first research aim, we demonstrated a correlation between HS accumulation and NEU1 deficiency in MPS IIIC disease. Results obtained in the Aim 3 expanded our understanding of the mechanics underlying NEU1 deficiency by showing that accumulating HS is a causative agent. Results obtained in Aims 2 and 4 demonstrated that NEU1 deficiency could be rescued by reducing HS storage and that overexpression of NEU1 in MPS IIIC mice partially corrects their behaviors. These aims were thus also critical in suggesting novel therapeutic interventions for diseases of the MPS spectrum.

Our main findings can be summarised as follows:

1. NEU1 activity is decreased in the brains of MPS III mice in contrast to those of other lysosomal enzymes.
2. NEU1 deficiency is caused by lysosomal storage of HS and can be rescued by reducing the primary genetic defects leading to HS storage.
3. Rescue of NEU1 deficiency by stereotaxic injections of LV-CTSA-NEU1-GFP virus in the hippocampus of MPS IIIC mice partially corrects behavioral abnormalities and deficient levels of protein markers of the glutamatergic synapse, PSD-95, and VGLUT1, linking NEU1 deficiency with synaptic deficits.

Altogether, our results show that the secondary deficiency of NEU1 in MPS diseases is associated with synaptic and behavioral defects but likely not with increased amyloidogenesis. We believe that our research establishes a relationship between HS storage and NEU1 and thus yields novel insights into MPS III pathology. Our study also may suggest additional approaches for treating this disease.

CHAPTER 6

BIBLIOGRAPHY

1. Alberts, B., Johnson, A., Lewis, J., *et al.* Transport from the Trans Golgi Network to Lysosomes. *Garland Science*. Molecular Biology of the Cell 4th edition, 2002.
2. Cooper, G. M. The Cell: A Molecular Approach. *Sunderland (MA): Sinauer Associates*. 2nd edition, 2000.
3. Bala, S., Szabo, G. TFEB, a master regulator of lysosome biogenesis and autophagy, is a new player in alcoholic liver disease. *Digestive Medicine Research*. 10.21037/dmr.2018.09.03. 2018 Sep; 1:16.
4. Settembre, C., Zoncu, R., Medina, D.L. A lysosome-to-nucleus signaling mechanism senses and regulates the lysosome via mTOR and TFEB. *The EMBO Journal*. 31: 1095-1108, 2012.
5. Staudt, C., Puissant, E., Boonen, M. Subcellular Trafficking of Mammalian Lysosomal Proteins: An Extended View. *International Journal of Molecular Sciences*. 10.3390/ijms18010047. V18, 2017.
6. Parenti, G., Medina, D.L., Ballabio, A. The rapidly evolving view of lysosomal storage diseases. *EMBO Molecular Medicine*. Volume 13, issue 2, 13: e12836, 2021.
7. Ferreira, C. R., Gahl, W.A. Lysosomal storage diseases. *Translational Science of Rare Diseases*.
8. Ballabio, A., Gieselmann, V. Lysosomal disorders: From storage to cellular damage. *BBA Molecular Cell Research*. Volume 1793, Issue 4, p. 684-696, 2009.
9. Pan, C., Nelson, M.S., Reyes, M. *et al.* Functional abnormalities of heparan sulfate in mucopolysaccharidosis-I are associated with defective biologic activity of FGF-2 on human multipotent progenitor cells. *Blood*. 106 (6): 1956–1964, 2005.
10. Tanaka, Y., Guhde, G., Eskelinen, E.L., *et al.* Accumulation of autophagic vacuoles and cardiomyopathy in LAMP-2-deficient mice. *Nature*. 406(6798):902-6, 2000.
11. Zhou, R., Yazdi, A.S., Menu, P., Tschopp, J. A role for mitochondria in NLRP3 inflammasome activation. *Nature*. 469, 221–225, 2011.
12. Platt, F.M., Boland, B., Van der Spoel, A.C. Lysosomal storage disorders: the cellular impact of lysosomal dysfunction. *The Cell Biology of Disease*. 199 (5): 723–734, 2012.
13. Pastores, G.M., Maegawa, G.H.B. Neuropathic Lysosomal Storage Disorders. *Neurologic Clinics*. 31(4):1051-7, 2013.

14. La Cognata, V., Guarnaccia, M., Polizzi, A., *et al.* Highlights on Genomics Applications for Lysosomal Storage Diseases. *Cells*. 9(8), 1902, 2020.
15. La Cognata, V., Cavallaro, S. A Comprehensive, Targeted NGS Approach to Assessing Molecular Diagnosis of Lysosomal Storage Diseases. *Genes*. 12(11):1750, 2021.
16. Tsukimura, T., Tayama, Y., Shiga, T., *et al.* Anti-drug antibody formation in Japanese Fabry patients following enzyme replacement therapy. *Molecular Genetics and Metabolism Reports*. Volume 25, 100650, 2020.
17. Jones, S.A., Breen, C., Heap, F., *et al.* A phase ½ study of intrathecal heparan-N-sulfatase in patients with mucopolysaccharidosis IIIA. *Molecular Genetics and Metabolism*. 118(3):198-205, 2016.
18. Giugliani, R., Nestrasil, I., Chen, S. *et al.* Intravenous infusion of iduronidase-IgG and its impact on the central nervous system in children with Hurler syndrome. *Molecular Genetics and Metabolism*. Volume 120, Issues 1-2, p. S55-S56, 2017.
19. Hordeaux, J., Buza, E.L., Dyer, C., *et al.* Adeno-Associated Virus-Induced Dorsal Root Ganglion Pathology. *Mary Ann Liebert publisher*. 31(15-16):808-818, 2020.
20. Barth, A., Magalhaes, T.S.P.C., Reis, A.B.R., *et al.* Early hematopoietic stem cell transplantation in a patient with severe mucopolysaccharidosis II: A 7 years follow-up. *Molecular Genetics and Metabolism Reports*. 8; 12:62-68, 2017.
21. Yamada, Y., Kato, K., Sukegawa, K., *et al.* Treatment of MPS VII (Sly disease) by allogeneic BMT in a female with homozygous A619V mutation. *Bone Marrow Transplantation*. 21, 629-634, 1998.
22. Ellgaard, L., Helenius, A. Quality control in the endoplasmic reticulum. *Nature reviews molecular cell biology*. 4, 181-191, 2003.
23. Simpson, L.W., Good, T.A., Leach, J.B. Protein folding and assembling in confined environments: Implication for protein aggregation in hydrogels and tissues. *Biotechnology Advances*. 42: 107573, 2020.
24. Parenti, G. Treating lysosomal storage diseases with pharmacological chaperones: from concept to clinics. *EMBO Molecular Medicine*. 1(5): 268–279, 2009.
25. Kishnani, P., Tarnopolsky, M., Roberts, M., *et al.* Duvoglustat HCl Increases Systemic and Tissue Exposure of Active Acid α -Glucosidase in Pompe Patients Co-administered with Alglucosidase α . *Molecular Therapy*. 25(5):1199-1208, 2017.
26. Woodard, J., Zheng, W., Zhang, Y. Protein structural features predict responsiveness to pharmacological chaperone treatment for three lysosomal storage disorders. *PLOS Computational Biology*. 17(9): e1009370, 2021.

27. Platt, F.M., Neises, G.R., Dwek, R.A., Butters, T.D. N-butyldeoxynojirimycin is a novel inhibitor of glycolipid biosynthesis. *Journal of Biological Chemistry*. 8;269(11):8362-5, 1994.
28. Mistry, P., Lukina, E., Turkia, H.B. Clinical outcomes after 4.5 years of eliglustat therapy for Gaucher disease type 1: Phase 3 ENGAGE trial final result. *Wiley American Journal of Hematology*. 96(9): 1156–1165, 2021.
29. De Ruijter, J., Valstar, M.J., Narajczyk, M., *et al.* Genistein in Sanfilippo disease: A randomized controlled crossover trial. *Annals of Neurology*. Volume 71, Issue 1, p.110-120, 2012.
30. Bigger, B.W, Begley, D.J., Virgintino, D., Pshezhetskt, A.V. Anatomical changers and pathophysiology of the brain in mucopolysaccharidosis disorders. *Molecular Genetics and Metabolism*. 125(4):322-331, 2018.
31. Van de Kamp, J.J., Niermeijer, M.F. Von Figura, K., Giesbert, M.A.H. Genetic heterogeneity and clinical variability in the Sanfilippo syndrome (types A, B, and C). *Clinical Genetics*. Volume 20, Issue 2, p. 152-160, 1981.
32. Martins, C., de Meideros, P.F.V., Leistner-Segal, S. Molecular characterization of a large group of Mucopolysaccharidosis type IIIC patients reveals the evolutionary history of the disease. *Wiley Human Mutation*. 40: 1084-1100, 2019.
33. Wijburg FA, Wegrzyn G, Burton BK, Tylki-Szymanska A. Mucopolysaccharidosis Type III (Sanfilippo Syndrome) and Misdiagnosis of Idiopathic Developmental Delay, Attention Deficit/Hyperactivity Disorder or Autism Spectrum Disorder. *Acta Paediatr*. doi: 10.1111/apa.12169, p.462-70, 2013.
34. Pará, C., Bose, P., Bruno, L. et al. Early defects in mucopolysaccharidosis type IIIC disrupt excitatory synaptic transmission. *JCI Insight*. Volume 6, Issue 15, 2021;6(15): e142073, 2021.
35. Feldhammer, M., Durand, S., Pshezhetsky, A.V. Protein Misfolding as an Underlying Molecular Defect in Mucopolysaccharidosis III Type C. *PLOS One*. Volume 4, Issue 10, 2009.
36. Wagner, V.F., Northrup, H. Mucopolysaccharidosis Type III. Gene Reviews. University of Washington, Seattle, 1993-2022.
37. Alexopoulou, A.N., Multhaupt, H.A.B., Couchman, J.R. Syndecnas in wound healing, inflammation and vascular biology. *The International Journal of Biochemistry & Cell Biology*. Volume 39, Issue 3, pages 505-528. doi.org/10.1016/j.biocel.2006.10.014, 2006.

38. Griffin, L., Gloster, T.M. The Enzymatic Degradation of Heparan Sulfate. *Protein and Peptide Letters*, 2017.
39. Freeman, C., Hopwood, J. Lysosomal degradation of heparin and heparan sulphate. *Adv. Exp. Med. Biol.* 313: 121-134, 1992.
40. Meikle, P.J., Fuller, M., Hopwood, J. Chapter 10 – Lysosomal Degradation of Heparin and Heparan Sulfate. *Chemistry and Biology of Heparin and Heparan Sulfate*. P.285-311, 2005.
41. Pshezhetsky, A.V. Lysosomal storage of heparan sulphate causes mitochondrial defects, altered autophagy, and neuronal death in the mouse model of mucopolysaccharidosis III type C. *Autophagy*. 12:6, 1059-1060, doi: 10.1080/15548627.2015.1046671, 2016.
42. Morimoto, H., Kida, S., Toden, E. Clearance of heparan sulfate in the brain prevents neurodegeneration and neurocognitive impairment in MPS II mice. *Molecular Therapy*. Volume 29, No.5, p. 1853-1861, 2021.
43. Dwyer, C.A., Scudder, S.L., Lin, Y. Neurodevelopmental Changes in Excitatory Synaptic Structure and Function in the Cerebral Cortex of Sanfilippo Syndrome IIIA Mice. *Scientific Reports*. 7: 46576, 2017.
44. Pará, C., Bose, P., Luigi, B. *et al.* Early defects in mucopolysaccharidosis type IIIC disrupt excitatory synaptic transmission. *JCL insight*. 6(15):e142073, 2021.
45. Tordo, J., O'Leary, C., Antunes, A.S.L., *et al.* A novel adeno-associated virus capsid with enhanced neurotropism corrects a lysosomal transmembrane enzyme deficiency. *Brain*. Volume 141, Issue 7, p. 2014-2031, 2018.
46. Pshezhetsky, A.V., Ashmarina, M. Lysosomal multienzyme Complex: Biochemistry, Genetics, and Molecular Pathophysiology. *Progress in Nucleic Acid Research and Molecular Biology*. 69:81-114, 2001.
47. Koseki, K., Wada, T., Hosono, M., *et al.* Human cytosolic sialidase NEU2-low general tissue expression but involvement in PC-3 prostate cancer cell survival. *Biochem. Biophys. Res. Commun.* 428, p. 142-149, 2012.
48. Wada, T., Yoshikawa, Y., Tokuyama, S. *et al.* Cloning, Expression, and Chromosomal Mapping of a Human Ganglioside Sialidase. Elsevier. Volume 261, Issue 1, 1999.
49. Seyrantepe, V., Landry, K., Trudel, S. Neu4, a Novel Human Lysosomal Lumen Sialidase, Confers Normal Phenotype to Sialidosis and Galactosialidosis Cells. *Journal of Biological Chemistry*. Volume 279, Issue 35, P37021-37029, 2004.
50. Wang, Q., Chen, Z., Peng, X. *et al.* Neuraminidase 1 Exacerbating Aortic Dissection by Governing a Pro-Inflammatory Program in Macrophages. *Frontiers in Cardiovascular Medicine*. Volume 8, 8:788645, 2021.

51. Sajo, M., Sugiyama, H., Yamamoto, H. et al. Neuraminidase-Dependent Degradation of Polysialic Acid Is Required for the Lamination of Newly Generated Neurons. *PLoS ONE*.11(1): e0146398, 2016.
52. Heon-Roberts R., Xu,T., and Pshezhetsky A.V. Secondary deficiency of neuraminidase 1 causes oversialylation of brain glycoconjugates in neurological mucopolysaccharidoses (unpublished).
53. Gowda, V.K., Srinivasan, V.M., Benakappa, N, Benakappa, A. Sialidosis Type 1 with a Novel Mutation in the Neuraminidase-1 (*NEU1*) Gene. *The Indian Journal of Pediatrics*. 84, 403-404, 2017.
54. Coppola, A., Ianniciello, M., Vanli-Yavuz, E.N., et al. Diagnosis and Management of Type 1 Sialidosis: Clinical Insights from Long-Term Care of Four Unrelated Patients. *Brain Sciences*. 10(8): 506, 2020.
55. Bonten, E.J., Arts, W., Beck, M. Novel mutations in lysosomal neuraminidase identify functional domains and determine clinical severity in sialidosis. *Human Molecular Genetics*. Volume 9, Issue 18, p. 2715-2725, 2000.
56. Ausseil, J., Desmaris, N., Bigou, S. et al. Early Neurodegeneration Progresses Independently of Microglial Activation by Heparan Sulfate in the Brain of Mucopolysaccharidosis IIIB Mice. *PLoS One*. 3(5): e2296, 2008.
57. Martins, C., Hulkova, H., Dridi, L. et al. Neuroinflammation, mitochondrial defects and neurodegeneration in mucopolysaccharidosis III type C mouse model. *Brain*. 138(2): 336–355, 2015.
58. Starkov, A.A. The role of mitochondria in reactive oxygen species metabolism and signaling. *Annals of the New York Academy of Sciences*. Volume 1147, Issue 1, p. 37-52. doi: 10.1196/annals.1427.015, 2008.
59. Zambrowicz, B.P., Abuin, A., Ramirez-Solis, R., et al. Wnk1 kinase deficiency lowers blood pressure in mice: a gene-trap screen to identify potential targets for therapeutic intervention. *PNAS*. 100(24):14109-14, 2003.
60. Hansen, G.M., Markesich, D.C., Burnett, M.B. Large-scale gene trapping in C57BL/6N mouse embryonic stem cells. *Genome Research*. (10):1670-9, 2008.
61. Pan, X., Taherzadeh, M., Bose, P., et al. Glucosamine amends CNS pathology in mucopolysaccharidosis IIIC mouse expressing misfolded HGSNAT. *Journal of Experimental Medicine*. Volume 219, No. 8, e20211860, 2022.
62. Heap, R.E., Marin-Rubio, J., Peltier, J. et al. Proteomics characterization of the L929 cell supernatant and its role in BMDM differentiation. *Life Science Alliance*. 4(6): e202000957, doi: 10.26508/lsa.202000957, 2021.

63. Chen, X., et al., NeuroEDDU protocols_iPSC culture_interactive protocol. 2019.
64. Chen, X., et al., *Induction of Dopaminergic or Cortical neuronal progenitors from iPSCs*. 2019.
65. Chen, X., et al., Generation of dopaminergic or cortical neurons from neuronal progenitors (interactive protocol). 2019.
66. Reynolds-Peterson, C., Xu, J., Zhao, N., *et al.* Heparan Sulfate Structure Affects Autophagy, Lifespan, Responses to Oxidative Stress, and Cell Degeneration in *Drosophila parkin* Mutant. *G3 Genes*. Volume 10, p. 129-141, 2020.
67. Motamedi-Shad, N., Monsellier, E., Torrassa, S., *et al.* Kinetic analysis of amyloid formation in the presence of heparan sulfate: faster unfolding and change of pathway. *Journal of Biological Chemistry*. 284(43):29921-34, 2009.
68. Bhaumik, M., Muller, V.J., Rozaklis, T., *et al.* A mouse model for mucopolysaccharidosis type IIIA (Sanfilippo syndrome). *Oxford Academic*. Volume 9, Issue 12, 1999.
69. Thomson, M. Endocytosis, partial degradation and release of heparan sulfate by elicited mouse peritoneal macrophages. *International Journal of Biological Macromolecules*. Volume 16, Issue 5, p.245-251, 1994.
70. Alexopoulou, A.N., Multhaupt, H.A.B., Couchman, J.R. Syndecnas in wound healing, inflammation and vascular biology. *The International Journal of Biochemistry & Cell Biology*. Volume 39, Issue 3, pages 505-528. doi.org/10.1016/j.biocel.2006.10.014, 2006.
71. Olivetti, P.R., Lacefield, C.O., Kellendonk, C. A device for stereotaxic viral delivery into the brains of neonatal mice. *BioTechniques*. Volume 69, No.4, p. 307-312, 2020.
72. During, M.J., Ashenden, L-M. A. Towards gene therapy for the central nervous system. *Trends in Molecular Medicine*. Volume 4, Issue 11, p. 485-493, 1998.
73. Zheng C.X., Wang, S.M., Bai, Y.H., *et al.* Lentiviral vectors and adeno-associated virus vectors: useful tools for gene transfer in pain research. *Anatomical Record (Hoboken)*. 301(5): 825–836. doi: 10.1002/ar.23723, 2018.
74. Amaral, D. G., Scharfman, H.E., Lavenex, P. The dentate gyrus: fundamental neuroanatomical organization. *Progress in Brain Research*. 163:3-22, 2007.
75. Minami, A., Saito, M., Mamada, S., *et al.* Role of Sialidase in Long-Term Potentiation at Mossy Fiber-CA3 Synapses and Hippocampus-Dependent Spatial Memory. *PLoS One*. 11(10): e0165257, 2016.

76. Savotchenko, A., Romanov, A., Isaev, D., *et al.* Neuraminidase Inhibition Primes Short-Term Depression and Suppresses Long-Term Potentiation of Synaptic Transmission in the Rat Hippocampus. *Hindawi*. Volume 2015,908190, 10 pages, 2015.
77. Minami, A., Meguro, Y., Ishibashi, S., *et al.* Rapid regulation of sialidase activity in response to neural activity and sialic acid removal during memory processing in rat hippocampus. *The Journal of Biological Chemistry*. Volume 292, No. 14, p. 5645-5654, 2017.
78. Revest, J-M., Dupret, D., Koehl, M., *et al.* Adult hippocampal neurogenesis is involved in anxiety-related behaviors. *Nature*. Volume 14, p. 959-967, 2009.
79. Abe, C., Yi, Y., Hane, M., Kitajima, K., Sato, C. Acute stress-induced change in polysialic acid levels mediated by sialidase in mouse brains. *Nature*. Scientific reports no. 9, Article number: 9950, 2019.
80. Settembre, C., Di Malta, C., Polito, V.A., *et al.* TFEB Links Autophagy to Lysosomal Biogenesis. *Science*. 332(6036), p. 1429-1433, 2013.
81. Medina, D.L, Di Paola, S., Peluso, I., *et al.* Lysosomal calcium signaling regulates autophagy via calcineurin and TFEB. *Nature Cell Biology*. 17(3), p. 288-299., 2015.
82. Gieselmann, V. What can cell biology tell us about heterogeneity in lysosomal storage diseases. *Acta Paediatrica*. Volume 94, Issue s447, p. 80-86, 2007.
83. Polgreen, L.E., Vehe, R.K., Rudser, K., *et al.* Elevated TNF- α is associated with pain and physical disability in mucopolysaccharidosis types I, II, and VI. *Molecular Genetics and Metabolism*. Volume 117, Issue 4, p.427-430, 2016.
84. Azambuja, A.S, Pimentel-Vera, L.N., Gonzalez, E.A., *et al.* Evidence for inflammasome activation in the brain of mucopolysaccharidosis type II mice. *Metabolic Brain Disease*. Volume 35, p. 1231-1236, 2020.
85. Zhou, Q-H, Baodo, R.J, Lu, J. Z., Hui E. K-W, Pardridge, W. M. Brain-penetrating IgG-iduronate 2-sulfatase fusion protein for the mouse. *Drug metabolism and Disposition*. 40 (2), p. 329-35, 2012.
86. Sevin, C., Deiva, K. Clinical Trials for Gene Therapy in Lysosomal Diseases with CNS Involvement. *Frontiers in Molecular Biosciences*. Volume 8, 2021.
87. McCafferty, E.H., Scott, L.J. Migalastat: A Review in Fabry Disease. *Drugs*. 79(5), p.543-554, 2019.
88. Amiri, M., Naim, H.Y. Miglustat-induced intestinal carbohydrate malabsorption is due to the inhibition of α -glucosidases but not β -galactosidases. *Journal of Inherited Metabolic Disease*. Volume 35, p. 949-954, 2012.

89. Yilmaz, B.S., Davison, J., Jones, S.A., Baruteau, J. Novel therapies for mucopolysaccharidosis type III. *Journal of Inherited Metabolic Disease*. Volume 44, Issue 1, p. 129-147, 2020.
90. Zelei, T., Csetneki, K., Voko, Z., Siffel, C. Epidemiology of Sanfilippo syndrome: results of a systematic literature review. *Orphanet Journal of Rare Diseases*. Volume 13, number 53, 2018.
91. Kowalewski, B., Lamanna, W.C., Lawrence, R., *et al.* Arylsulfatase G inactivation causes loss of heparan sulfate 3-O-sulfatase activity and mucopolysaccharidosis in mice. *Proceedings of the National Academy of Sciences of the United States of America*. 109(26), p. 10310-10315, 2012.
92. Khateb, S., Kowalewski, B., Bedoni, N., *et al.* A homozygous founder missense variant in arylsulfatase G abolishes its enzymatic activity causing atypical Usher syndrome in humans. *Genetics in Medicine*. Volume 20, Number 9, p.1004-1012, 2018.
93. Annunziata, I., Patterson, A., Helton, D., *et al.* Lysosomal NEU1 deficiency affects amyloid precursor protein levels and amyloid- β secretion via deregulated lysosomal exocytosis. *Nature Communications*. Volume 4, number 2734, 2013.
94. Maiza, A., Sidahmed-Adrar, N., Michel, P.P., *et al.* 3-O-sulfated heparan sulfate interactors target synaptic adhesion molecules from neonatal mouse brain and inhibit neural activity and synaptogenesis in vitro. *Scientific reports*. Volume 10, number 19114, 2020.
95. Bishop, J.R., Schuksz, M., Esko, J.D. Heparan sulphate proteoglycans fine-tune mammalian physiology. *Nature*. 446, p.1030-1037, 2007.
96. Qiao, D., Meyer, K., Mundhenke, C., *et al.* Heparan Sulfate Proteoglycans as Regulators of Fibroblast Growth Factor-2 Signaling in Brain Endothelial Cells. *The Journal of Biological Chemistry*. Volume 278, number 18, p. 16045-16053, 2003.
97. Zcharia, E., Metzger, S., Chajek-Shaul, T., *et al.* Transgenic expression of mammalian heparinase uncovers physiological functions of heparan sulfate in tissue morphogenesis, vascularization, and feeding behavior. *FASEB Journal*. (2), p.252-63, 2004.
98. Kirn-Safran, C., D'Souza, S.S., Carson, D.D. Heparan Sulfate Proteoglycans and Their Binding Proteins in Embryo Implantation and Placentation. *Seminars in Cell & Developmental Biology*. 19(2),p.187-193, 2008.
99. Zhu, Y., Gandy, L., Zhang, F., *et al.* Heparan Sulfate Proteoglycans in Tauopathy. *Biomolecules*. 12(12): 1792, 2022.
100. Pshezhetsky, A.V., Ashmarina, M. Keeping it trim: roles of neuraminidases in CNS function. *Glycoconjugate Journal*. 35: 375-386, 2018.

101. Fuller, M., Rozaklis, T., Ramsay, S.L. Disease-Specific Markers for the Mucopolysaccharidoses. *Pediatric Research*. 56, p.733-738, 2004.
102. Vinogradova, V.M., Michaud, L., Mezentsev, V.A., *et al.* Molecular mechanism of lysosomal sialidase deficiency in galactosialidosis involves its rapid degradation. *Biochemical Journal*. 330(2), p. 641-650, 1998.
103. Pshezhetsky, A.V., Potier, M. Association of N-acetylgalactosamine-6-sulfate sulfatase with the multienzyme lysosomal complex of beta-galactosidase, cathepsin A, and neuraminidase. Possible implication for intralysosomal catabolism of keratan sulfate. *Journal of Biological Chemistry*. 271(45), p. 28359-65, 1996.
104. Seyrantepe, V., Canuel, M., Carpentier, S., *et al.* Mice deficient in Neu4 sialidase exhibit abnormal ganglioside catabolism and lysosomal storage. *Human Molecular Genetics*. 17(11), p. 1556-68, 2008.